HHS Public Access

Author manuscript

Chem Soc Rev. Author manuscript; available in PMC 2020 October 07.

Published in final edited form as:

Chem Soc Rev. 2019 October 07; 48(19): 5140–5176. doi:10.1039/c9cs00011a.

Anisotropic nanomaterials for shape-dependent physicochemical and biomedical applications

Lijiao Yang[a,b], **Zijian Zhou**[b], **Jibin Song**[a], **Xiaoyuan Chen**[b]

[a]MOE Key Laboratory for Analytical Science of Food Safety and Biology, College of Chemistry, Fuzhou University, Fuzhou 350108, P. R. China

[b]Laboratory of Molecular Imaging and Nanomedicine, National Institute of Biomedical Imaging and Bioengineering, National Institutes of Health, Bethesda, MD 20892, USA

Abstract

This review is a systematic understanding of the mechanism of shape-dependent effect on nanoparticles (NPs) for elaborating and predicting their properties and applications based on the past two decades of research. Recently, the significance of shape-dependent physical chemistry and biomedicine has drawn ever increasing attention. While there has been a great deal of efforts to utilize NPs with different morphologies in these fields, so far researches are largely localized in particular materials, synthetic methods, or biomedical applications, and ignored the interactional and interdependent relationships of these areas. This review is a comprehensive description of shape for NPs from theory, synthesis, property to application. We figure out the roles that shape play in the properties of different kinds of nanomaterials together with physicochemical and biomedical applications. Through systematical elaboration of these shape-dependent impacts, better utilization of nanomaterials with diverse morphologies would be realized and definite strategies would be expected for breakthroughs in these fields. In addition, we proposed some critical challenges and open problems that need to be addressed in nanotechnology.

Graphical Abstract

jibinsong@fzu.edu.cn, shawn.chen@nih.gov.

Conflicts of interest

The authors declare no competing financial interest.

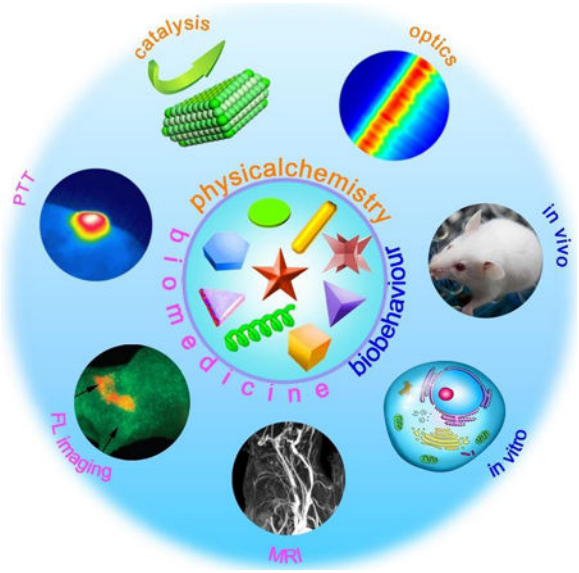

1. Introduction

The shape or anisotropy is known to be intertwined with many parameters, which has a considerable effect on physical, chemical and physiological characteristics of nanoparticles (NPs).[1–3] Precise control of their morphology impacts profoundly on regulating them as desired for various physicochemical and biomedical employments. As far, numerous nanomaterials in clinical use or research in the laboratory are of spherical shape. Whereas, in the recent two decades, there is also a fast development of NPs with anisotropic morphologies for various applications (Figure 1).[4–13] A number of well-designed strategies have been undertaken to utilize NPs with different morphologies, such as regulating anisotropic shape to tailor their optical and catalytic characteristics.[14–17] On the other hand, shape engineered materials are also widely used in biomedical field such as fluorescence imaging,[18, 19] magnetic resonance imaging,[20] and photothermal therapy.[21] Meanwhile, shape factors influence cytotoxicity,[22, 23] uptake,[24, 25] target,[26] biodistribution and pharmacokinetics of NPs.[27–29] For *in vivo* studies, anisotropic NPs are usually used to improve tumor targeting due to their prolonged circulation time and altered biological fate.[30, 31]

The most attractive point about nanotechnology origins from the possibility to precisely engineer its physical, chemical and biological properties. Changes of structural parameters such as shape and size typically alter the chemistry and structure of NPs, which could be controlled to achieve desired behaviors in physicochemical properties and biological applications.[32, 33] However, at present, the great majority of systems are spherical due to their convenience in synthesis and a lack of full understanding of their structure-activity relationships in morphology. As researchers, we should envision that the future NPs in physical chemistry and nanomedicine could be engineered as we expect and have a definite form that follows their function. It is essential to establish intrinsic correlation of these well characterized NPs with various anisotropic shapes and their physicochemical and biomedical

performances through the bridge of chemical structure and biological effect, by which foreseeable insights and unambiguous strategies can be achieved. With these insights, we could develop nanomaterials as desired through a rational design instead of trial-and-errors.

In this review, we summarize the past two decades of studies on NPs-based materials with different shapes in physicochemical and biomedical applications, *e.g.*, optics, catalysis, imaging, or therapy, with a specific focus on the impact of shape. We give a systematic statement around these NPs from mechanism, synthesis, property to application. Their biological behaviors, such as toxicity, uptake, and target are discussed as well.

To date, specific kinds of materials, synthetic methods, or biomedical applications have been studied in lots of researches and a huge volume of published data were produced on these topics. However, their interactional and interdependent relationships are ignored, integrating them together is rather challenging due to the interdisciplinary nature. Herein, we are concerned with different shaped NPs and mainly divide them into several parts: (1) theoretical mechanisms of shape-dependent effects, (2) primary synthetic approaches of anisotropic NPs, (3) physicochemical and (4) biomedical applications, (5) shape induced biological behaviors. Several principles are raised to help design future NPs. Moreover, some critical challenges and open questions that need to be addressed are proposed.

2. Mechanisms of the shape-dependent properties

The shape influences many related physical, chemical and physiological factors of NPs, thus differentiate in their physicochemical (such as catalytic and optical), biomedical, and biological performance.[34] A systematic understanding of the mechanism of shape-dependent effect on NPs is essential to predict their properties and explore their applications.

Fully harnessing the power of anisotropic shaped nanocatalysts requires a detailed understanding of the intrinsic essence of their enhanced performance at the atomic level, which in turn requires a fundamental knowledge of their geometric and electronic structures. Metal NPs with different morphologies and structures endow them with various optical properties and applications in photonics.[35] The main theoretical mechanism is that the adsorption energy of adsorbents and the activation energy of reactions on different metal facets are discrepant due to their different surface atomic and electronic structures.[36] Therefore, the activity for many optical procedures can be modulated and optimized by trimming the anisotropic shapes and exposing facets. In addition, metallic nanostructures supporting surface plasmon resonances with collective excitations of the conduction electrons exhibit unique optical properties.[37] Modifying their structures or geometric parameters is a convenient way to tailor surface plasmon resonance properties for specific applications.[38, 39] The plasmon resonance depends strongly on particle length and shape. The dipole plasmon resonance gradually red shifts as the length-to-width ratio increases. For instance, the color of gold NPs in colloidal dispersions can vary from blue to red as the particle becomes more oblate.[40] When the polarization is chosen to be along the minor axis, there is a second resonance arises that plasmon resonance has blue shifts as the particle becomes more oblate. The color and optical properties of metal NPs stem from localized surface plasmons, anisotropic shapes such as rods have an additional absorption peak and

possess quite different characteristics. In consequence, metal NPs with different shapes and aspect ratios exhibit distinct localized surface plasmonic resonance (LSPR) and surface enhanced Raman spectra (SERS) properties.[41, 42] Nanomaterials also have size and shape dependent nonlinear optical properties,[43] and the shape effects can be separated from the localized surface plasmon wavelength by comparing the solution with a similar linear extinction at the laser excitation wavelength.[44]

In most cases, catalytic behavior highly depends on the shape of the catalyst, since nanocatalysts with different anisotropic shapes could exhibit different selectivities and/or activities.[45–47] One account for such shape dependence of catalytic property essentially originates from the differences in geometric structure and electronic state of catalyst atoms associated with distinctive crystallographic surfaces.[48] As a result, catalysts based on NPs with different crystallographic shapes usually display quite different catalytic performances even for the same catalytic reaction.[49, 50] Meanwhile, another reason is that shape with different anisotropy tunes the fraction of atoms of the topmost surface layer of a NP, the proportions of atoms at corner and edge of a particle, and the specific surface area of a catalyst. Adsorption energy and activation barrier depend greatly on the local structure on the reactive surface of NPs with anisotropic shapes. The surface structure of catalyst affects the stability of reaction intermediates and the activation energy of surface chemical reactions in two distinct ways. One is the electronic effect, the difference in local electronic structures due to the surface metal atoms in different environments. The other geometrical effect originates from the fact that various surface geometries provide different configurations for the molecule bonding. They offer atoms with electronic structures different from close-packed surfaces and meantime offer new configurations of surface atoms. But as a function of the reaction energy for different surface geometries, they act different in the transition state energy for chemical reaction on surface, for instance, CH_4 dissociation and NO dissociation.[51–53] Moreover, the structure sensitivity and reactivity of different facets, which translates directly into the dependence of the rate and selectivity of supported catalysts on size, morphology, and defect density of anisotropic NPs. The distribution of coordination sites (edge, terrace, kink, or corner sites) is dependent on the shape of metal NPs. Various coordination sites could exhibit quite different properties of coordination chemistry toward reactants, intermediates and products (Figure 2)[54].

The morphology plays an important role in the biomedical applications of NPs. NPs with various shapes show diverse adaptabilities in fluorescence imaging (for instance, metal sulfides and $NaGdF_4$) and photothermal therapy (*e.g.*, Au NPs) due to their different optical performances. The shape plays a significant role in fluorescence imaging because the Stokes shift highly depends on the aspect ratio of nanocrystals.[55, 56] Fluorescent NPs can absorb and convert the energy into radiation of visible light,[57] trimming their geometrical shape of nanostructures will generate a shift in the scattering and the photoluminescence (PL) spectra.[58] Anisotropic NPs with a relatively large size and small surface ratio and thus little surface defects, have high sensitivity and selectivity because of the static quenching and the inner filter effect.[59] Moreover, the enhancement of the PL yield is ascribed to anisotropic NP plasmons, especially to the augment of scattering or absorption cross sections.[60] Furthermore, the upconversion quenching also can be tuned with surface defects by adjusting of size and shape.

On the other hand, morphology is pivotal for contrast abilities of iron oxide NPs in magnetic resonance imaging as the theory that it influences the effective radius and the local field inhomogeneity of the magnetic core, the surface-area to volume ratio together with the gradient of stray field under an external applied magnetic field.[61] Magnetic NPs with distinct shapes generate non-uniform spatial stray fields under the background field owing to the anisotropic characters of magnetic dipole interactions.[62] The magnetic relaxation, and the dephasing and efficient diffusion processes of the water protons in nearby area, which are affected with local gradients of the stray field by shortening the spin−spin relaxation time.[61, 63] The geometrical shape plays an important role in the spatial distribution (intensity, direction, and gradient) of the magnetic stray field.[64] The NPs with large shape anisotropy has high intensity and spatial non-uniformity of the stray field, and produces great influence on water proton diffusion and dephasing. Therefore, the morphology largely determines the gradient of stray field and the effective radius, which finally affects the transverse relaxation rate. In the spin−lattice relaxation process of water proton, the exposed metal ions on the surface can provide an efficient chemical exchange for protons and thus accelerate the relaxation process.[65] Consequently, the longitudinal relaxivity of NPs has a positive correlation with the surface-area-to-volume ratio and the occupancy rate of effective metal ions on exposed surfaces. In addition, these principles could serve as guidelines for the design of nanomaterial-based agents for sensitive and accurate diagnosis or therapy in the clinic.

Changes in the shape or geometry of NPs can alter the pharmacokinetics and biodistribution of the agent, which in turn alters the toxicological profile.[66] The amount and rate of phagocytosis of particles are determined by the radius of curvature where particles contact the surface of a cell. Hence anisotropic NPs are likely to be taken up by cells because their high aspect ratio can lead to more contacts with the cell surface. The shape-independent mechanisms for *in vitro* and *in vivo* behaviors are as follows. *In vitro* toxicity is greatly influenced by type of NP material, degree of particle uptake, and the *in vitro* model used. NPs with very high aspect ratio can mediate some pro-inflammatory or cytotoxic effects and induce frustrated phagocytosis in professional phagocytotic cells. Meanwhile, anisotropic particles increase the potential of targeting ligands to interact with receptors on cell surface, and this increased valency leads to higher cellular targeting. For *in vivo* behavior, anisotropic NPs have prolonged circulation time due to flow alignment in circulation and thus could improve *in vivo* tumor targeting compared to their spherical counterparts.[15] The geometry or anisotropy of NPs also has a remarkable effect on their *in vivo* biodistribution behavior, such as discoidal NPs mainly localize in the lungs/heart and larger anisotropic NPs are prone to accumulate in the spleen.

3. Synthetic approaches

Synthesizing precisely shaped nanostructures is of primary importance because the nanometer-scale structural details of anisotropic shapes can significantly affect their properties. NPs with numerous morphologies and dimensions could be accomplished *via* various routes and reaction conditions such as temperature, concentration of precursor, or capping agent.[67] In other words, the synthetic approach could change the anisotropic shape

which has an important impact on altering their anisotropic effects. In this section, we hence mainly summarized the synthetic methods of NPs with common anisotropic morphologies.

3.1 Surface coordination

Partial synthetic methods that enable precise control over NP morphology require agents such as small molecules to force growth of NP in a particular direction by coordinating with the surface metal atoms.[54, 68] Therefore, there is a strong relevance between surface coordination and the shape-controlled synthesis. The coordination of small molecule ligands on metal surfaces has inspired numerous experimental and theoretical studies for noble metal NPs.[69] For instance, CO prefers to coordinate on Pd{111} facets in bridge and hollow modes.[70] By simply introducing CO as the surface confining agent, ultrathin Pd nanosheets with Pd{111} facets as their main exposed face were easily obtained.[71–73] Besides, ultrathin Rh nanosheets enclosed by Rh{111} basal planes[74], Pt nanocubes with Pt{100} facets[75, 76] and Au nanowires[77] (Figure 3a) were also formed when CO was introduced in the synthesis. When CO and H_2 were used simultaneously, single-crystalline Pd tetrapods enclosed by {111} facets were obtained (Figure 3b).[78] In addition to CO and H_2, many other small molecules regulating the surface structures and shapes of metal nanocrystals have been demonstrated. Yang *et al.* reported that NO_2 binding contributes to prepare nanocrystals with more Pd{111} facets exposed due to the stabilization effect of NO_2 on Pd{111} facets (Figure 3c).[79] Moreover, the coordination of amine on low coordinated metal site provides an effective strategy to prepare concave Pt NPs with {411} high-index facets (Figure 3d).[80]

A significant numbers of syntheses of NPs with various morphologies need other capping agents (*e.g.*, certain species of ions or polymers).[81] The absorbing or binding of capping agent would protect specific facets or significantly reduce the surface energies of facets, thus leading to the confined growth in a particular direction. For instance, halide, such as cetyltrimethylammonium bromide, has been well-documented as a critical factor to control the shape of various NPs.[82–84] Similarly, Rh nanocubes, Pd nanocubes and nanowires, were synthesized owing to the selective binding of halides on Pd/Rh{100}.[85–87] Whereas in another case, octapod iron oxide NPs were successfully fabricated by the special selectivity of chloride anions capping rather than other halide ions.[88]

A variety of reagents can be altered to change the shape of the NPs in the synthesis process. Besides halides, the concentration of Au salt, silver nitrate, and ascorbic acid can be adjusted to gain Au nanospheres, pentagonal twinned Au nanorods, and trisoctahedral Au NPs (Figure 4).[89] The initial gold seed is generally formed by the reduction of gold salt (*e.g.*, $HAuCl_4$) by a reducing agent, together with a weak binding ligand (such as citrate or cetyltrimethylammonium bromide, CTAB). The size or morphology of the Au NPs can be firstly tuned by the anisotropic shaped seeds with the using of capping agents, such as CTAB-stabilized cuboctahedra Au NPs, citrate-stabilized pentagonally twinned Au NPs, or silver nitrate-utilized Au nanorods (Figure 4I). Other capping reagents can be employed as synthetic handles and interact synergistically to direct the shape-controlled growth of NPs, including the halide counterion (Cl^-, Br^-, I^-), the relative concentrations of Au salt/silver nitrate/ascorbic acid, and the concentration of the surfactant (Figure 4II). Hence a number of

anisotropic Au products were prepared, such nanospheres, single-crystalline rods (aspect ratios of 3.5−15), and trisoctahedral structures (Figure 4III a–e).

This growth approach for the synthesis of gold NPs can also been extended to other related metals, such as copper and silver, or even platinum and palladium. The only principal difference among these growth approaches applied to obtain different anisotropic nanocrystals is the compositions of the growth solution. Moreover, this method can also be further extended to evaluate and screen the facet selectivity of a given capping agent. For instance, Zeng *et. al* realized control of the shapes of silver nanocrystals with different capping agents.[9] The binding of citrate to {111} facets is stronger than that of {100} facets of face-centered cubic Ag. In the presence of sodium citrate, the growth rate of {111} facets is slower than that of {100} facets during a seeded growth process. Therefore, {100} facets will gradually disappear while {111} facets will become dominant, eventually leading to the formation of Ag octahedrons. However, on the contrary, PVP binds more strongly to {100} than the {111} facets, thus reducing the growth rate along [100] direction. It makes the {111} facets disappear faster than the {100} facets, resulting in nanocubes and nanobars. Jin and co-workers reported the shape-controlled synthesis of copper NPs in an aqueous solution with glucose as a reducing agent and hexadecylamine as a capping agent.[90] It is also demonstrated that the formation of a class of highly faceted planar lanthanide fluoride nanocrystals (nanoplates and nanoplatelets) resulting from the patchy coverage of ligands around the nanoplate edges.[91]

Meanwhile, the effect of various polymeric capping agents were investigated, such as Tween 80, Tween 20 and PEG on the shape and size of $YbVO_4/NiWO_4$ nanocomposites.[92] The cations of oleate salts, hydrion, sodium, potassium, and dibutylammonium were found to have great influence on the shape in the synthesis of iron oxide NPs by using iron(III) oleate, and hence the spherical, cubic, and bipyramidal iron oxide NPs were obtained.[93, 94] In a similar manner, monodisperse octahedral iron oxide NPs were obtained by using oleylamine as a stabilizer and reducing agent.[95] Besides, Liu *et al.* experimentally verified the co-existence and different roles of oleate anions (OA) and molecules (OAH) in the crystal formation, the control over the ratio of OA to OAH can be employed to directionally inhibit, promote or etch the crystallographic facets of $NaYF_4$ NPs (Figure 5).[96] With such programmable additive and subtractive engineering, fabricating NPs with a variety of anisotropic shapes can be implemented.

3.2 Physical parameters

Physical parameter such as pH and temperature have important impacts on the shapes or anisotropy of NPs, since they influence the crystal nucleus formation and the growth or evolution of particles directly. Recently, the significance of pH has been realized and the manipulation of NPs by tuning pH is reported.[97–101] Xue and Mirkin found that the silver nanoprism could be tuned by different pH values in the photochemical synthesis.[102] In this case, the excellent control over nanoprism with an edge length of fixed 10-nm thickness were implemented with appropriate pH regulation. Li *et al.* reported that pH value varies the morphologies of $LaCO_3OH$ microcrystals in the growth (Figure 6).[103] The nucleation and then the crystal formed after the dissolution of $CO(NH_3)_2$ which was used as the carbon

source. Then a selective adsorption of OH^- on the crystal took place at different pH values. Finally, the multiform products were formed due to this preferential growth direction of the $LaCO_3OH$ crystal. Their shape undergone changes from elliptical nanoflakes (pH = 2) to rhombic microplates (pH = 7), and then to sandwichlike microspindles (pH = 10).

The temperature plays an important role in the thermodynamic control in solution phase, which is a simple and effective strategy that is easily achieved during an experiment. As a result, the thermodynamic control has been widely applied for the shape-controlled synthesis of nanocrystals.[104–106] The hexagonally closely packed (hcp) ruthenium hourglass nanocrystals can be achieved by the shape control from thermodynamic growth.[107] Li and Peng reported the temperature effects of the shape-controlled synthesis of colloidal CdSe quantum disks.[108] They found that a proper temperature range (approximately 140 to 250 °C) is needed for the successful synthesis of CdSe quantum disks. Because the up-temperature limit is dictated by the close packing of hydrocarbon chains in fatty acids, and the low-temperature limit is related to the reactivity of initial materials. Likewise, Guo *et al.* reported the shape-controlled synthesis of SnTe nanostructures by regulating the temperature.[109] The shapes are tunable from highly monodisperse nanocubes to nanorods with varied aspect ratios, and eventually to long and straight nanowires (Figure 7). They discovered that the reaction at high temperature fast forms thermodynamically favored nanocubes, while low temperature leads to elongated particles. The distinction of growth and shape-focusing is likely due to the interparticle ripening differences at various temperatures.

Meanwhile, the kinetic parameter is equally important and well explored to control the shape. Taking the shape growth of a cubic seed as an example, the newly formed atoms should be deposited onto the corners owing to the high energy of these sites (Figure 8).[110] The adatoms can deposit onto the corner sites or diffuse to different surfaces. The growth pathway thereby the shape of the product has a strong dependence on the rates for atom deposition and surface diffusion (*i.e.*, $V_{deposition}/V_{diffusion}$), which leads to four different geometrical shapes in the end.

3.3 Seed growth

Seed-mediated growth is a powerful and versatile means for the preparation of anisotropic nanocrystals.[111–114] The vast enchantment of this method stems from the fact that nucleation and growth steps are separated, hence allowing an astonishing degree of control over the shape and aspect ratio, which could influence the properties of nanocrystals and determine their performance in various applications.[115–117]

The seed-mediated synthesis approach includes two main strategies, homogeneous and heterogeneous growth. If the seed crystal and the final crystal are composed of the same metal, then it is a homoepitaxial process, and the diverse morphologies of NPs can be expanded with endless possibilities by applying seeds with controllable internal structures. This approach is exploited by most of groups to obtain metal nanostructures with precise control over the size and aspect ratio. For instance, Zhang *et al.* recently demonstrated that Ag nanocubes with controllable edge lengths of 30–200 nm can be achieved by using cubic single crystalline as seed.[118] While penta-twinned Au NPs, with preselected morphology (nanorods, bipyramids, and decahedra) and aspect ratios, were formed by using small

conventional Au seeds (Figure 9a–d).[119] The thermal treatment induces both growth and twin formation of the traditional NP seed. Keeping all other parameters constant, the aspect ratio for each type could be readily tuned by simply varying the concentration of thermally treated seed. Consequently, these grown penta-twinned NPs with different shapes were obtained. Similarly, triangular Au nanoplates were produced by oriented attachment of spherical Au seeds (Figure 9e).[120] Spherical Au seed particles were produced within a few hours after irradiation. The contact between seeds led to oriented attachment at the correct crystallographic alignment, resulting in the flake structures. Then the aggregation of these small flakes with additional seeds forms polycrystalline plates by adding H_2O_2. Ultimately, the triangular crystalline Au plates were formed by the recrystallization of these polycrystalline plates and the continued attachment of seeds at the edges. In another case, Au nanobipyramids (NBPs) were produced from decahedral Au seeds due to the overgrowth on penta-twinned decahedra (Figure 9f–m).[121] The penta-twinned decahedral Au seeds are critical to the formation of NBPs because the free-defect overgrowth of the penta-twinned NBPs could be easily accomplished on these decahedral seeds with penta-twinned structures. In the overgrowth, {100} facets with relatively high surface free energy were selectively adsorbed by protecting agents or Ag-based species. As a consequence, the selective deposition on {111} along ⟨110⟩ occurs fast, which generates one dimensional NBP. Meanwhile, the production of NBPs is mainly determined by the molar ratio of Au^{3+} and Au seeds. NBPs with a yield higher than 90% was realized when the ratio ranged from 8 to 10. Moreover, these prepared NBPs exhibited excellent SERS performance in virtue of many present tips, hotspots, edges, and steps on their surfaces. The homogeneity and quality of the seeds in these methods make it easier to supervise the shape evolution throughout the growth process, and guarantee a common mode for all seeds involved to afford uniform products.

If the seed and the objective crystal consist of different metals, it is then a heterogeneous procedure (Figure 10a).[122] This approach is used in the synthesis of penta-twinned Cu nanorods with controllable aspect ratios, the uniform Pd decahedral seeds lead to the heterogeneous nucleation and determine the growth of Cu along the fivefold axis to form nanorods.[123] It was also certified that the ultrathin Pt shell could be formed on the surface of a Pd concave cube as the seed by introducing $PtCl_4^{2-}$ to accomplish the deposition of Pt atoms (Figure 10b).[124] Another type of seed-mediated growth approach is a two-step process for growing the shell of CdSe/CdS core/shell nanorods, which combines an first established fast-injection based step to create initial elongated shell and a second slow-injection growth of the core.[125]

In addition to metal nanostructures,[126] many metal oxides could be prepared in seed-mediated methods. The size and shape control of spinel ferrite nanocrystals could be accomplished by this way.[127, 128] Anatase TiO_2 nanorod antennas can be produced from a rhombic core *via* a nonaqueous colloidal seed-mediated growth method.[129] Systematic studies on the growth mechanism in this work reveal that the formation of nanorods and core-antenna nanocrystals based on the seeds involves an epitaxial growth process with specific orientational preference (Figure 11).

3.4 Template mediated process

Template-mediated method has been well developed as a facile and general route to synthesize NPs, because it can choose an appropriate template to manipulate both the size and shape of the resulting structures.[130, 131] The commonly used templates consist of porous template,[132–135] surface mask template,[136–139] biological and organic template,[140–143] and solution-phase template, *etc.*[144–146] For instance, the syntheses with solution-phase template, including metallic or dielectric core template,[147–149] sacrificial template (*e.g.*, galvanic replacement or Kirkendall effect)[150–152] and colloidal template, have been applied for developing phase-separated heterogeneous morphologies. In the Au-Pd-Ag hollow nanostructure, the removal of silver is dominated by galvanic replacement in the formation of the binary Pd-Ag structure at the beginning. Later the gaps around these cavities were formed, then it was finally governed by the Kirkendall effect with the adding of the gold salt (Figure 12)[153]. The disparity between fluxes of gold and silver produced a net flux of vacancies in the surface and the center because the diffusion speed of silver in gold is faster than that of gold in silver. Gu *et al.* observed the nucleation of Ag domains on Fe_3O_4 NPs templates after ultrasonic emulsification.[154] Ultrasonication offers necessary energy to mix the organic and aqueous phases and allows NPs to self-assemble at the liquid-liquid interface in the microemulsion. Due to the partial coverage or unstable nature of surfactant molecules on NPs, few Fe(II) sites on the surface act as the catalytic center for the reduction of Ag^+ and the Ag NP seed. Once the silver nucleation sites formed, the subsequent reduction of Ag^+ will proceed at these sites and then Fe_3O_4-Ag heterodimers are obtained. Similarly, Sun *et al.* synthesized the dumbbell-like Au|Fe_3O_4 nanostructures by the decomposition of iron pentacarbonyl, $Fe(CO)_5$, onto the surface of Au templates followed by oxidation under air with precursors in 1-octadecene.[155] Another example is CdTe tetrapod-shaped NPs can be employed as colloidal template to prepare nanorods through site selective modification.[156] The tetrapods partially coated with a protective polymer layer and deposited on a silicon surface, leaving an exposed arm. After decoration with Au NPs in a site selective fashion, this modified arm were readily broken off from the tetrapods and released from the substrate, yielding CdTe nanorods.

On the other hand, the biological and organic templates,[157] consisting of DNA,[158, 159] peptides and peptide assemblies,[160, 161] proteins,[162, 163] viruses and microorganisms,[164] lipid assemblies and other synthetic supramolecular structures, micelles and emulsions, dendrimers, carbon nanotubes,[165] have also been tried. For example, soft templates like micelles and reverse microemulsions, have been used to prepare NPs composed of alloys, metal oxides, inorganic molecules, and noble metals like Ag.[166] The surfactant molecules with amphiphilic groups, can form a well-defined structure such as hollow sphere, due to the hydrophobic end only binds with organic solvent and hydrophilic head only binds with water.[34]

3.5 Other approaches

In addition to the above main synthetic approaches of anisotropic NPs with different morphologies, there are still a number of other routes that have been tested. For instance, the strategy based on a general phase transfer and separation mechanism usually occurred at the interfaces of the liquid, solid and solution phases for noble metal, magnetic/dielectric NPs,

rare-earth NPs, semiconducting NPs, organic optoelectronic semiconducting and conducting polymer NPs.[167] Another research reported the shape control of cubic, cuboctahedral, and octahedral $CuCu_2O$ core-shell NPs on Si(100) could be completed by one-step electrodeposition without capping agent and template.[168] The unique shape of NPs is obtained by the synthesis with physical or biological parameter applied, such as light-mediated synthesis or biomolecule introduced preparation, which could be found in plasmon-mediated synthesis of triangular core–shell nanoprisms from Au seeds,[169] silver triangular bipyramids,[170] heterometallic nanorods and icosahedra.[171] Zhang *et al.* reported a facile method to synthesize five-fold twinned, starfish-like rhodium nanocrystals in a polyol system by eliminating oxidative etching with a chloride-free precursor (Figure 13).[172] The Rh nanocrystals with five branched arms were realized in high yields due to the use of $[\{(CF_3COO)_2Rh\}_2]$ instead of Na_3RhCl_6 as a precursor to exclude Cl^- ions from the reaction system.

4. Physicochemical applications

How to regulate the anisotropic shape of metal-based NPs is a linchpin to regulate their physicochemical characteristics, such as optical and catalytical properties. NPs with different anisotropies usually exhibit quite discrepant activity or selectivity in optical reaction. The shape of NPs affects greatly in catalytic performance owing to the diversity in geometric structure and electronic state of the catalyst atoms, together with their different crystallographic surfaces.

4.1 Optical application

Controlling the shape of metal NPs allows us to control their optical properties and applications in Raman, fluorescence or near-infrared luminescence. For example, noble metal NPs (Au, Ag) interact with UV-vis light through the excitation of localized surface plasmon resonance (LSPR), which is highly sensitive to the shape of the nanostructures.[173, 174] Targeted shape of metal NPs can be synthesized by controlling the surface sites or undergoing a seed-mediated growth process. Compared with spherical nanostructures, anisotropic shapes such as Au@Ag core-shell nanocubes were prepared by the use of single-crystal spherical Au nanocrystallites as seeds, with cetyltrimethylammonium chloride (CTAC, better than CTAB) as the capping agent and ascorbic acid as the reductant.[174] The nanocubes with controllable edge lengths can be finely tuned by varying the ratio of $AgNO_3$ precursor to Au seeds. When the edge length was over 20 nm, the LSPR spectra only showed characteristic features of pure Ag nanocubes and displayed a continuous red-shift with the increasing size. When the edge length continued raising, a split of LSPR peak appeared due to the corners of the nanocubes are sharper than those of the smaller spherical or cubic ones. This method could be applied to systematically investigate the influence on the LSPR properties of the anisotropic core-shell nanocrystals, and obtain the critical edge lengths or shell thickness for the plasmon excitation.

4.1.1 Raman scattering—Plasmonic nanostructures is of paramount importance because the structural details can significantly influence their plasmonic properties.[175–178] Precisely structured nanocrystals with anisotropic shape of corner sharpness compared with

spheres can provide highly plasmonic signal generation and SERS enhancement.[179, 180] The shape effect in SERS of anisotropic NPs (such as Ag and Au) is an electromagnetic enhancement, which is owing to a shift of the localized surface plasmon resonances.[181, 182] It modifies the local field enhancements on the particle surface compared with that of a sphere. SERS enhancement can be magnified at the tip of elongated metal NPs when the excitation is polarized along long axis.[183] This tip or corner effect, is also called the "lightning rod effect", which can result in large electric field and Raman enhancement near the sharp surface or at the sharp ends of the NPs. Hence the spatial anisotropy is ascribed to strong optical scattering and plasmon concentration at corners and edges of nanostructures.[184] Compared to nanospheres with smooth surfaces, another factor which plays a vital role in SERS is the "hot spots" in the surface due to the presence of sharp edges or active rough surfaces.[185] The degree of localization at the hot spot is an intrinsic property of the shape or aspect ratio of the particle,[186] which can be traced back to that the magnitude of the induced dipole is affected by the shape. The high Raman signals enhancement is attributed to that more intense local electromagnetic fields generate at the hot spots, which make them more effective Raman scattering than nanospheres.[185, 187]

Among these controlled shaped nanostructures, gold nanocrystals are most commonly employed due to their unique plasmonic properties and Raman scattering properties. Au NPs with the desired cube shape of highly controlled corner sharpness can scatter light in a steadily reproducible manner, and the quantitative SERS enhancement factors for the dimers are very narrowly distributed (Figure 14a).[188] Particularly, the enhancement factors of 72 nm sharp-cornered Au NC dimers have a distribution within one order of magnitude. It is proved that hexoctahedral Au nanocrystals enclosed exclusively by high-index {321} facets exhibit more enhanced plasmonic properties and higher SERS activities than normal spherical ones (Figure 14b).[189] In addition, branched Au/Pd bimetallic NCs exhibit much better plasmonic properties and SERS activities than spherical Au/Pd NPs (Figure 14c).[190] Moreover, Au nanorods showed red-shifted LSPR spectra with increased aspect ratios,[191–194] and would shift their LSPR peaks to shorter wavelengths with Ag shell coating.[195, 196] For other nanomaterials such as Ag NPs, anisotropic nanocrystals showed enhanced SERS signals compared with their spherical ones.[118] The SERS signal extracted from a single Ag nanocube strongly depends on laser polarization. Compared with isotropic sphere, the intensity of the SERS signal of a cube with the laser polarization along the face diagonal is much stronger than that of the SERS signal along the edge. This phenomenon is caused by the difference in near-field distribution over the surface of a nanocube under different polarization directions. This systematical comparison and investigation of LSPR and SERS properties could also shed light on the design of the best substrate for SERS.

4.1.2 Fluorescence imaging—The anisotropy or geometric shape of NPs is considerably significant for their applications in fluorescence imaging. Quantum dots (QDs) for fluorescence imaging are the most representative candidates among all fluorescent nanomaterials because of their broad excitation spectra, narrow fluorescence emission bands, and resistance to photobleaching. The PL intensity and wavelength in QDs can be tuned mainly by engineering their size, shape, and composition.[197–199] Size-dependent fluorescence properties are generally found in typical 2−10 nm semiconductor QDs.[200, 201]

With decreasing size of QDs, the energy gap expands between the top of the valence band and the bottom of the conduction band, and this increase in energy associated with exciton generation/recombination brings a blue shift in both absorbance and PL spectra.[202] Tailoring composition can be achieved by forming core/shell structures which is divided into three types based upon the band alignment of valence and conduction bands between their constituent materials.[203, 204] For instance, Cd-based type II QDs exhibit near-IR emission due to electron−hole recombination across the core/shell interface,[205] and Cd-free type II QDs with PL colors changing by simply varying the shell thickness.[206] Adding a shell can also improve the PL quantum yield.[207] Another method of trimming composition is doping by adding another metal or tuning the ratios of metal precursors to alter the PL peak.[208, 209] In addition, the intensity of the emission can be engineered by adjusting pH,[210, 211] and the PL wavelength can be fabricated by varying the synthetic temperature.[212]

The shape effect in controlling the fluorescence property of semiconductor QDs have attracted the researchers' interests in these years. For example, the synthesis and fluorescence imaging of tetrahedral InP and CdTe/CdSe core/shell QDs were systematically studied.[213, 214] Quantum rods (QRs) are brighter probes than QDs since the Stokes shift is greatly dependent on the aspect ratio (length/diameter) of rod.[55, 56] Meanwhile, the color control is achievable by tuning the diameter, which governs the band gap energy of QDs.[215] With the increase of width or length, the emission peak moves to lower energy, and the position of emission peak depends more sensitively on the width than on the length. The reason for this is that the band gap is chiefly determined by the lateral confinement which plays a vital role even in long rods. Likewise, it was reported that CdSe QRs emitted light that was linearly polarized towards the c-axis of the crystals and the degree of polarization rests with the aspect ratio of the NPs.[216] Yong *et al.* reported CdSe/CdS/ZnS QRs as targeted optical probes for live cell fluorescence imaging.[217] In this paper, transferrin (Tf) was conjugated onto CdSe/CdS/ZnS QRs for targeted delivery, confocal and two-photon imaging proved that the receptor-mediated uptake of the bioconjugates into the HeLa cells (Figure 15). In addition, Deng and co-workers found that manganese-doped zinc sulfide quantum crystals with a rod shape have tunable dual-color and multiphoton emissions.[218] As reported, in addition to the effect of Mn^{2+} doping levels, as the increase of QR diameters from QR1 to QR7 with different aspect ratios, the relative intensity of the blue bands to orange bands decreases, which is mainly attributed to the enhancement of orange emission intensity, while the intensity change of blue emission is negligible.

Shape also plays a significant role in determining the optoelectronic properties of graphene quantum dots (GQDs).[219] The emission of GQDs can be widely tuned from deep ultraviolet to near-infrared by its shape of the carbon network.[220] A pristine armchair-edged GQD (arranged in rectangle shape) emits red fluorescence (670 nm) in toluene,[221, 222] which is attributed to the transition from ground state to excited singlet state.[223] While GQD in triangular shape emits red fluorescence at 748 nm and shows the absorption maximum at 591 nm.[221, 224] Moreover, Shan *et al.* also discovered the hidden effect of particle shape and criteria for evaluating the upconversion luminescence of lanthanide doped nanophosphors (Figure 16).[225]

4.1.3 Near-infrared luminescence—Near-infrared (NIR) luminescence is commonly found in fluorescence imaging and bioimaging.[226–228] Most of previous studies focused on the size and metal doping of NPs for NIR luminescence,[229–231] whereas, a few studies noticed the considerable effect of shape on luminescence.[232–234] Besides the conventional metal-based NIR luminescence, such as QDs and upconversion NPs, Li *et al.* realized the morphology-tailoring of a red AIEgen from pristine nanorods to nanospheres for NIR fluorescence imaging by encapsulating quinoline-malononitrile-2 (QM-2) into hybrid micelles.[235] This nanostructure exhibits great promise in NIR imaging due to its good solubility in aqueous systems, the uniform diameter of about 30 nm, an increased fluorescence brightness with a large Stokes shift of 190 nm, and the strongly enhanced photostability (Figure 17).

4.2 Catalytic application

Nanocatalysis is undergoing an explosive growth. Researchers have reported striking novel catalytic properties for nanocatalysts compared to their bulk counterparts, including significantly enhanced reactivities and selectivities.[236, 237] Many studies elucidate the factors that tremendously affect the catalytic performance of metal NPs such as their size, shape, or interaction with their support.[238] However, these preceding parameters are not independent, for instance, size and support of NPs decide the most stable shape of NPs, which makes the analysis more complicated. Among these aspects, the shape-dependent effect in catalysis attracts increasing attention in recent years. It has been verified that the exposed crystal faces, determined by the morphology of catalyst NPs, considerably affects the catalytic behavior. The surface structure of exposed crystal face has a critical effect on the adsorption energy, reaction energy and activation barrier. Nanocatalysts with various anisotropic shapes often expose several different facets, together with other types of sites such as edges or corners. In a reactive environment, the reactants and products are able to induce other facets or completely new structures to be exposed. Undercoordinated sites at edges and corners are commonly particularly important for the catalysis. On the other hand, the potential energy diagram for surface reactions usually depends greatly on the surface structures of facets. For example, comparing the potential energy diagram for CO dissociation on different Ni facets, steps on the surface interact closely with the final product.[239] The dissociation barrier is also considerably lower, which means that not all sites on a nanoparticle contribute equally to the catalytic activity. Any process involving dissociation can be strongly favored at defects and the edges or corners of anisotropic particles.

4.2.1 Photocatalysis—NP-based photocatalysis is one of the most promising procedures in the sustainable making of organic pollutant degradation, clean energy sources, and hydrogen production from water splitting or carbon dioxide reduction.[240–242] The exposed facets associated with shapes play a crucial role in the photocatalytic activity of NPs, which is due to the preferential flow of photogenerated carriers to the specific facets. Recently, the fascinating shape-dependent photocatalytic activity of titanium dioxide crystal facets has attracted enormous interest.[243–248] To improve the photocatalytic activity, previous reports mainly focus on increasing the surface area of high-energy exposed facets such as {001} and {100}.[249] Whereas, Roy and coworkers demonstrated that the presence of both the high-energy {001} oxidative and low-energy {101} reductive facets in an optimum

ratio is equally important for efficient charge separation and photocatalytic activity enhancement (Figure 18a).[250] Another research also convinced that the co-exposed {001} and {101} facets of anatase TiO_2 are significant for the photocatalytic activity for CO_2 reduction into CH_4.[251] They proposed the "surface heterojunction" concept based on the density functional theory (DFT) calculations to explain the photocatalytic performance differences (Figure 18b). These uniform TiO_2 NPs can find potential applications in dye-sensitized solar cells and also hydrogen generation through water splitting.

In addition, zinc oxide is an important semiconductor that has been widely applied in photocatalysis, whereas morphology control is an important approach to improve its photocatalytic performance. The ZnO tetrapods with different morphologies (nanoplates, nanorods) exhibit strong photocatalytic activities against methylene blue.[252] Mesoporous and hexagon shaped ZnO nanodisks with exposed specific polar facets exhibit enhanced photovoltaic performance in QD sensitized solar cells.[253] Anisotropic nanoplatelets can be used to engineer the heterojunction band structure and greatly improve the photocatalytic properties in a wide range by raising charge separation.[254] ZnO rods/reduced graphene oxide composites showed high photocatalytic performances for efficient sunlight-driven photocatalysis, and the high specific surface of ZnO rods is one of the important reasons.[255] Other anisotropic structures of metal oxides, such as Bi_2O_3 hierarchical nanostructures, also show excellent photocatalytic capabilities.[256]

It has also been reported that Ag and Au NPs with controlled geometry can affect the rate of photochemical reaction of adsorbed molecules.[257–259] The shape and facet effects are also momentous for photocatalytic properties of single-crystalline Ag_3PO_4 crystals. Ag_3PO_4 rhombic dodecahedrons with only {110} facets exhibit much higher activities than that of cubes bounded entirely by {100} facets for the degradation of organic contaminants, which may be mainly ascribed to the higher surface energy of {110} facets than that of {100} facets (Figure 18c–f).[260] Besides the above NPs, shape induced (spherical, sheets and rods) differences of photocatalytic activity also exist in CdS nanostructures for photodegradation of methylene blue dye under UV irradiation.[261] In addition, high photocatalysis and visible light-induced charge retention are found with hybrid CdSe-Au nanodumbbells.[262]

4.2.2 Electrocatalysis—It is borne in mind that the catalytic reactivity of NPs increases proportionally with the number of metal atoms on the surface.[263] Because of the massive surface area of NP dispersions, increasing their anisotropy can lead to a marked change in their catalytic activity. For example, Pt NPs of various shapes showed enhanced and selective catalytic performances over spherical NPs.[264–266] Researches have explored a number of strategies to control the shape of Pt-based catalysts to obtain enhanced catalytic properties, including the yield of high-index facets and design of controlled architectures (*e.g.*, textured, core-shell, or dendritic structure).[47] Pd nanocrystals show structure-sensitive catalytic properties as well,[45, 267–269] with the maximum current density of the formic acid oxidation increased in the order of octahedrons < truncated octahedrons < cuboctahedrons < truncated cubes < cubes, confirming that catalytic rate on Pd{100} was faster than that on Pd{111}.[270] Taking into account their similar trend of anodic potential, Pd nanocubes with slightly truncated corners are the best catalyst for the oxidation of formic acid.

Electrochemical reduction of CO_2 provides great potential for intermittent renewable energy storage. Liu and colleagues reported a predominant shape-dependent electrocatalytic reduction of CO_2 to CO on triangular silver nanoplates (Tri-Ag-NPs).[271] Tri-Ag-NPs showed an enhanced current density, considerably higher selectivity and significantly improved energy efficiency, together with a considerable durability compared with those of similarly sized Ag NPs and bulk Ag (Figure 19). Additionally, CO can be detected at an ultralow onset potential, indicating the excellent catalytic activity and superiority of Tri-Ag-NPs toward CO_2RR. Density functional theory calculations (DFT) calculations revealed that the enhanced electrocatalytic activity and high selectivity of Tri-Ag-NPs at an ultralow overpotential is a consequence of the shape-controlled triangular structure, which provides both the optimum edge-to-corner ratio and the predominant Ag{100} facet. The above studies provide promising approaches to trim catalytic activity and selectivity of metal nanocatalysts *via* producing optimal facets and edge sites of specified shapes.

5. Biomedical applications

5.1 Fluorescence imaging

Fluorescence (and phosphorescence) based imaging has found particular interests and probably is one of the most widespread methods in various biomedical applications.[272–275] The acquisition of fluorescence imaging usually is with the aid of fluorescent probes or nanomaterials, like semiconductor-nanoprobes (silicon-based nanostructures,[276–278] carbon dots,[279] semiconducting SWNTs and semiconducting sulfides[280]) and Au NPs,[281] which can absorb and convert certain types of energy into radiation of visible light.[57] As a result, trimming the morphology will contribute much to the fluorescence properties of the NPs-based probes. Among all kinds of fluorescent nanomaterials, QDs[282–284] for visible light imaging and rare earth materials for upconversion bioimaging are the main representative and attractive candidates.

5.1.1 Visible light imaging—Fluorescent QDs are ideal fluorescence probes due to their narrow fluorescence line widths, shape (or size) tunable emission, photostability, and excitation with a single wavelength.[285–288] Compared with spherical QDs, QRs with anisotropy could offer some superior properties such as larger absorption cross sections, faster radiative decay rates, linearly polarized emissions, more substantial Stokes shifts, and capability of functionalization at different sites with multiple binding moieties. These unique characteristics enable QRs promising materials with a wide range of applications, from biomedical imaging and biosensors to nanodevices. Yong *et al.* demonstrated that the tumor targeting and imaging in live animals could be achieved with functionalized semiconductor quantum nanocrystals with a rod shape.[289] The highly luminescent CdSe/CdS/ZnS QRs can be successfully applied for targeted tumor fluorescence imaging, which is owing to conjugated cyclic RGD peptide binding to the $\alpha_V\beta_3$ integrins overexpressed in tumor vasculature. Hence, the optical imaging showed tumor sites in virtue of the accumulation of QR probes after systemic injection (Figure 20). *In vivo* tumor detection and cytotoxicity studies showed no adverse effects, indicating no toxicity in the cellular and tissue levels of functionalized QRs. As a result, they could be utilized as bright, photostable, and biocompatible luminescent probes for the early diagnosis of cancer. Likewise, another report

suggested that the water-dispersible, noncytotoxic QRs in luminescence bioimaging can be fulfilled using silica-coating.[290] It is also reported that dumbbell-shaped carbon quantum dots/Au NPs nanohybrid can be utilized as an efficient ratiometric fluorescent probe for sensing Cd^{2+} ions and L-ascorbic acid.[291] The high sensitivity and selectivity of this dumbbell-shaped NPs ascribes to the static quenching and the inner filter effect. The addition of Cd^{2+} causes the formation of cubic aggregates, results in fast and complete fluorescence quenching of Au NCs. While in the presence of L-ascorbic acid, the above quenched sensor recovers gradually. Besides fluorescent QDs, it is reported that biocompatible Au nanoclusters (or Au dimers) with appropriate surface capping agent could also be employed as fluorescence contrast agents for live cell imaging.[60, 292] The improvement of the photoluminescence yield is attributed to nanoparticle plasmons, particularly to the increase of scattering or absorption cross sections. Adjusting the shape or geometry of Au nanostructures allows a redshift in both the scattering and the photoluminescence spectra.

Besides metal-based NPs,[293, 294] the shape effects also exist in organic nanostructures. Shao *et al.* reported that the micro/nanoaggregates with controlled morphologies (from rod to sphere) fabricated from organic quinoline–malononitrile (QM) derivatives can realize desirable far-red and NIR fluorescence and tumor-targeted bioimaging.[295] The biocompatible QM nanoprobes are shape-tailored and preferable for cell-tracking and tumor-targeted bioimaging (Figure 21). Similarly, another study demonstrated the shape effect on aggregation-induced emission (AIE) probes for *in vivo* imaging by tuning their morphologies.[296]

5.1.2 Upconversion bioimaging—Upconversion luminescence (UCL) is a nonlinear optical process, which usually converts NIR photons to short-wavelength emission.[58] Recent advances in nanotechnology have promoted the development of upconversion nanomaterials as potential candidates of fluorescent probes for biomedical applications.[297] In this area, it was found that anisotropic shaped NPs showed numerous applications for upconversion bioimaging.[298–300] For example, lanthanide-doped $NaGdF_4$ nanorods with multicolor photoluminescence[301] and hexagonal-phase $NaYF_4$:Yb,Er/Tm nanocrystals with controllable shape and upconversion fluorescence have been reported.[302] The $NaYF_4$:Yb^{3+}/Er^{3+}/Tm^{3+} nanoplates, nanospheres, and nanoellipses showed strong upconversion fluorescence and emitted varied fluorescence. The nanoplates showed stronger upconversion fluorescence emission compared to nanospheres and nanoellipses. It is possible that the nanoplates have a relatively large size and small surface and thus little surface defects, which are usually fluorescence quenchers. In addition, Murray *et al.* reported $NaYF_4$-based spheres, nanorods, nanoplates, and nanoprisms and their tunable upconversion emissions.[59] Besides engineering the dopant concentration, tuning the size or shape of anisotropic upconversion NPs is also an effective way to alter the upconversion luminescence. With increased size, both the total intensity of emission and the intensity ratio of green to red emission of $NaYF_4$:Yb/Er NPs increased. This phenomenon can be attributed to the fact that the upconversion quenching caused by surface defects and ligands becomes more important with the decrease in size. On the other hand, the as-synthesized $NaYF_4$:Yb/Ce/Ho spherical NPs and hexagonal nanoplates both displayed dominant red

emission under the 980 nm excitation, but their total intensities of emission were much weaker than NPs with other shapes. These NPs hold great potential for the employment in biomedicine as fluorescent labels or imaging probes.

Zeng and co-workers achieved dual-modal X-ray and upconversion bioimaging by administering ligand-free $NaLuF_4$:Gd/Yb/Er nanorods.[303] In this work, the $NaLuF_4$:Gd/Yb/Er nanorods exhibited enhanced visualization of blood vessels for *in vivo* synergistic X-ray imaging and UCL bioimaging of nude mice compared with that without nanorods (Figure 22). The nanorods also have excellent paramagnetism that can be employed as potential contrast agent for magnetic resonance imaging. These results indicate that the UCL nanorods could be utilized as promising candidates for angiography imaging and disease diagnosis. In addition, a series of core-shell UCL nanostructures are widely used in upconversion bioimaging as well.[304–307]

5.2 Magnetic resonance imaging

Magnetic resonance imaging (MRI) has been extensively employed among numerous clinical diagnostic techniques during the past two decades due to its safety and high spatial resolution for soft tissues.[308–310] MRI in some clinical trials require the use of contrast agents (CAs), which can accelerate the proton relaxation process of nearby water molecules under an external magnetic field, enhance the contrast between the detected region and background, and thus improve the sensitivity and accuracy.[311–313] There are mainly three types of CAs, namely, T_1 positive CAs for T_1 imaging (*e.g.*, Gd chelates, paramagnetic Gd_2O_3, MnO or $NaGdF_4$ nanomaterials),[314–318] T_2 negative CAs for T_2 imaging (*e.g.*, superparamagnetic IO, $ZnFe_2O_4$ and Fe_5C_2 NPs),[319–322] and T_1-T_2 CAs (*e.g.*, EuIO, GdIO NPs)[323–325] for T_1-T_2 dual modal imaging. Among them, the shape (morphology) plays a vital role in influencing T_1 or T_2 contrast enhancement effects in T_1 and T_2 imaging.[326–328]

5.2.1 T_1 imaging—Conventional paramagnetic (*e.g.*, Gd^{3+} or Mn^{2+}) complexes-based T_1 CAs are small molecules that are renal cleared within a few minutes, while NP-based T_1 CAs could avoid this short circulation time.[329, 330] Researchers can tailor the shapes of NP-based CAs to meet the biological requirements for optimizing T_1 imaging. For example, Gd(III)-nanodiamond conjugates enable contrast enhancement for MRI compared to other agents.[331] Ultrathin manganese oxide nanoplates exhibited strong MR contrast enhancement for *in vivo* T_1 imaging derived from the large quantity of manganese ions exposed on the surface.[332] Likewise, MnO nanotubes with more surface manganese ion density also showed larger r_1 value compared to traditional manganese oxide nanospheres.[333, 334] In a similar manner, Zhou *et al.* reported higher-performance T_1 relaxivity of IO plates (Figure 23a–d)[335] and GdIOP nanoplates (Figure 23e–g)[336] compared to spheres ascribing to high ratios of surface metal (Fe or Gd) ions, which is a result of the geometrical shape confinement. Hence, the shape influences the T_1 contrast effect due to the surface to volume ratio, because the exposed metal ions on the surface may provide efficient chemical exchange for protons and thus accelerate the T_1 relaxation process. This theory is further demonstrated according to systematic and theoretical analyses of longitudinal relaxivities of ferrite oxides with different shapes (Figure 23h).[337] In this work, the longitudinal relaxivity has positive

correlations with surface-area to volume ratio and occupancy rate of effective metal ions on exposed surfaces of magnetic NPs.

5.2.2 T_2 imaging—The magnetic resonance signal in transverse relaxation process can be modulated with magnetic NPs in T_2 imaging. Besides size,[338] composition,[339–341] and surface functionalization,[62, 63] the shape also plays a critical role in determining the contrast abilities for T_2 imaging. For T_2 CAs, superparamagnetic IO establish a local perturbed dipolar field to shorten proton relaxation and increase signal difference of tissue and surrounding background. The local field inhomogeneity under an external magnetic field can be further elevated by artificially involving NPs with anisotropic geometries and shapes.[342] For example, Zhao *et al.* reported that iron oxide NPs with octapod shape display an ultrahigh transverse relaxivity, and dramatically enhance the sensitivity of T_2 imaging for early stage detection of cancer, due to the large effective radius and local field inhomogeneity of the magnetic core than the spheres (Figure 24a,b).[88] This octapod shape was also well exploited in subsequent studies, such as ZnIO NPs[343, 344] and CoIO NPs[345], all these samples have high sensitivity and accuracy for sensitive CE-MRI. Furthermore, Yang *et al.* showed that magnetic ferrite oxide NPs with heterogeneous shapes (sphere, plate, tetrahedron, rhombohedron, and octapod, in Figure 24c) generate distinct stray fields and gradients under background field, affect the speed of efficient dephasing and diffusion process of surrounding protons, determine effective radii together with saturated magnetizations of particle, and finally affect transverse relaxation rates and *in vivo* liver and tumor T_2-weighted imaging performance (Figure 24 d–i).[337]

5.3 Photothermal therapy

Killing tumor cells by photothermal therapy relies on hyperthermia, which is a condition that cells are subjected to heat (above 42 °C) for tens of minutes. It will cause irreversible damage to the cells due to destruction of cell membranes and/or denaturing of proteins.[346, 347] Nanomaterials such as Au NPs can absorb and convert electromagnetic energy into heat by photothermal effect[348, 349] and have high tumor specificity due to their ability to accumulate in tumor site through passive targeting and/or active targeting enabled by ligands.[350]

Shape also has a profound effect on Au NPs-based application in photothermal therapy. West and Halas proved the selective photothermal ablation of SKBR3 breast cancer cells of Au nanorods conjugated with anti-HER2 antibody.[351] Li *et al.* demonstrated the effective photothermal ablation of melanoma tumors by applying melanocyte-stimulating hormone conjugated hollow Au nanospheres.[352] Song *et al.* reported ultrasmall Au nanorod vesicles have an enhanced tumor accumulation and fast excretion from the body for cancer therapy.[353] These Au nanorods vesicles could accomplish rapid excretion from the body due to the degradation into small nanorods by hydrolysis of the coated PLGA, enhanced photothermal properties by the strong interparticle plasmonic coupling, prominent tumor accumulation and high photothermal cancer therapy efficacy (Figure 25). In another case, glutathione-responsive self-assembled Au NPs could be applied for enhanced tumor imaging and imaging-guided photothermal therapy with a nanowreath shape, which caused improved photothermal properties compared to Au seeds and/or thick Au nanoring with smooth

surface due to the presence of Au branches, small junctions, and central holes in Au nanowreaths.[354] In this work, the GSH-responsive self-assembled magnetic Au nanowreaths have a NIR absorption, resulting in strong photoacoustic signal and effective photoablation of tumor for imaging-guided photothermal therapy.

Besides the discussed materials, Kim *et al.* utilized golden carbon nanotubes as multimodal photoacoustic and photothermal high-contrast molecular agents.[355] Li and co-workers reported CuTe nanocrystal with different shapes (nanocubes, nanoplates, and nanorods) that have different plasmonic properties as photothermal agents.[356] Morphology of polymer nanovehicle also plays a significant role. It was reported that molecular bottlebrush-based unimolecular micelle with tunable morphologies including sphere, rod, worm or core-shell structures, could offer different bio-behaviors and effects on inhibiting tumor growth for photothermal cancer therapy.[21]

6. Biological behaviours

Shape factors (morphology, geometry or anisotropy) of NPs have an influence on particle-cell interactions. For instance, the radius of curvature is crucial in determining the amount and rate of particle phagocytosis. Anisotropic geometry also influences the *in vitro* behaviors like cytotoxicity, cell uptake and *in vivo* behaviors, such as biocompatibility, targeting ability, biodistribution and clearance of NPs.

6.1 *In vitro* behaviours

6.1.1 Cytotoxicity—The NPs-mediated cytotoxicity is known to be affected by several factors, cell surface, colloidal stability, particle uptake and other physicochemical factors.[357] The anisotropy or geometry can influence the quantity of particles ingested. Too high ratio of NPs uptake could disrupt cellular functions and bring about adverse cytotoxic effect, which induces excessive endocytosis and results in oxidative stress-mediated mitochondrial damage.[358]

Though the relationships between cytotoxicity and shapes are not obvious,[359, 360] their correlation does exist in many studies indeed. For example, investigations of the toxicity of mesoporous silica nanorods claimed shape-dependent cytotoxicity in A549 human lung epithelial cells and RAW 264.7 murine macrophages.[361] Hemolysis assay indicated that the hemolytic activity is geometry-dependent for bare SiO_2. Hamilton *et al.* studied the cytotoxicity of TiO_2 NPs with different aspect ratios using primary mouse C57BL/6 lung macrophages, and found a higher cytotoxicity for larger nanofibers among the tested spherical, short and long nanofibers.[362] In this work, the long nanofibers incubated with alveolar macrophages led to the release of cathepsin B (a lysosomal protease) and the disruption of the lysosomal membrane, resulting in drastically increased levels of interleukin-1 and interleukin-18, suggesting the particle length-dependent inflammatory response. Similarly, Stoehr *et al.* indicated the cytotoxicity of high aspect ratio silver NPs in A549 cells, silver nanowires showed shape-dependent toxicity compared to nanospheres (Figure 26).[363] Another report suggested the high aspect ratios of carbon nanotubes cause frustrated phagocytosis and result in inflammation and systemic effects.[364] Additionally,

geometry or anisotropy of NPs can also affect cytoskeletal organization,[365–368] induce disruption of lipid bilayers and cytotoxic and pro-inflammatory responses.

6.1.2 Shape-dependent cell uptake—The cell uptake of NPs has attracted considerable attention, one reason is that NPs could be applied as vehicles for intracellular drug delivery. It is well-known that cell uptake of NPs is determined by an intricate interplay of physicochemical properties like shape, size, and surface functionalization, and the effect of shape is extensively investigated in recent years. For instance, Xie *et al.* reported the shape effect on cellular uptake of methylpolyethylene glycol coated Au NPs in the forms of stars, rods, and triangles by RAW264.7 cells.[369] The efficiency of cellular uptake from low to high follows the order of stars, rods, and triangles. Their results demonstrated that shape can modulate the cellular uptake of NPs, and different shapes were inclined to undergo various endocytosis pathways in different proportions. Similarly, shape dependence of Au NPs uptake into mammalian cells were demonstrated between rods with different aspect ratios and spheres.[370]

Another report investigated the uptake behaviors of fluorescently labeled spherical and non-spherical NPs with equal volume by qualitative and quantitative analysis.[25] Uptake of NPs in MSC and HeLa cells have a negative correlation between aspect ratio and uptake rate, showing non-spherical NPs with less cellular uptake than the spherical counterparts (Figure 27). This phenomenon can be attributed to the larger average curvature radius of non-spherical particles. In a similar report, shape and orientation matter for the cellular uptake of non-spherical NPs were studied, providing systematic understanding for membrane wrapping of NPs, viruses, and bacterial forms.[24] Stable endocytic states with small and high wrapping fraction is favorable for rod-like NPs, a submarine mode is tended for high aspect ratios and round tips, and a rocket mode is likely for small aspect ratios and flat tips. In addition, Wang *et al.* have also shown that the DNA-functionalized nanoflowers can be readily taken by cells.[371]

The findings in these studies will give implications in the chemical design of NPs in biomedical applications (*e.g.*, tuning intracellular delivery rates), and provide useful guidelines for the design of NPs for drug delivery.

6.2 *In vivo* behaviours

6.2.1 Biocompatibility—Conventional problems of biocompatibility of NPs *in vivo* stem from the fact that toxicity is influenced by particle physicochemical properties like shape effects. Inhalation of high aspect ratio fibers leads to frustrated phagocytosis of pulmonary macrophages, which can result in poor biocompatibility such as asbestosis, bronchogenic carcinoma, pleural fibrosis, mesothelioma, and pleural plaque formation.[364, 372] Compared to traditional spherical NPs, long fibers also cause more recruitment of polymorphonuclear leukocytes, exotic body giant cells, and other pathology. For example, after injection into the peritoneal cavity of female C57BL/6 mice with carbon nanotubes of various lengths, granulomatous inflammation was found through histological analysis of diaphragms.[373] However, other reports suggested that systemic toxicity caused by intravenous administration of high aspect ratio CNT is not palpable, acute systemic toxicity

could be mitigated with proper coatings like PEG/phospholipid.[374–376] Similarly, intravenous injection of PEGylated carbon nanotubes showed no significant toxicity in nude mice.[377] The long-term biocompatibility is tied to particle biodistribution, *in vivo* fate *(i.e.*, excretion), and degradation, and these will be discussed in latter parts in this review.

6.2.2 Targeting ability—NPs generally distribute throughout the body after intravenous injection, thus optimizing factors such as particle shape can help particles accumulate or target to the sites where need to be introduced. NPs have been considered as ideal tools on nanotechnology platforms to deliver drugs for cancer therapy due to their ability to target tumors by passive or active targeting (small molecule, aptamer or antibody targeting).[378] The nonspecific targeting mechanism relies on the "enhanced permeability and retention" (EPR) of NPs that are allowed to enter the tumor interstitial space due to the enhanced permeability of the tumor vasculature and the suppressed lymphatic filtration.[379, 380] Whereas, shape of particle still in part dictates the passive particle localization at tumor sites despite the mechanism of EPR effect.

For example, Kolhar *et al.* demonstrated that rod shaped NPs exhibit higher specific and lower nonspecific accumulation at the target tissue compared to their spherical ones.[381] Mathematical modeling of particle–surface interactions reveals that the higher specificity and avidity of nanorods generated from the balance of polyvalent interactions, which promotes adhesion, entropic losses and shear–induced detachment. The shape–specific tissue accumulation and shape–induced enhancement of vascular targeting is also observed in brain and lungs for NPs coupled with anti–intracellular adhesion molecules and anti–transferrin receptor antibodies (Figure 28).

Targeted delivery of therapeutic agents in the vascular compartment is a significant issue for treating hemorrhage, thrombosis, and atherosclerosis. Platelets have an inherent ability of vascular injury site-directed margination, site-specific adhesion, and amplification of injury site-specific aggregation, and these functions can be tuned by their shapes. In this regard, Anselmo *et al.* fabricated platelet-like NPs (PLNs) to target vascular injuries and enable hemostatic functions with the biochemical and biophysical designs such as mimicking shape and surface biology.[382] The PLNs displayed enhanced surface-binding compared with their spherical and rigid discoidal counterparts, together with site-selective adhesion and platelet-aggregation properties. *In vivo* studies indicated that PLNs targeted at the wound site and led to ~65% reduction in bleeding time, effectively attained the hemostatic functions of natural platelets (Figure 29).

Another example is Au NPs (20 nm spheres, 40 nm spheres, 40 nm cubes, and 36 nm × 10 nm rods) have been investigated as effective vaccine adjuvants *in vivo* for West Nile virus. In this work the shape played a role in enhancing immune response *via* different cytokine pathways.[383] Moreover, Chauhan *et al.* reported that nanorods exhibited superior transport and distribution into mammary tumors to nanospheres of similar plasma half-life *in vivo*.[384] The nanorods with the smallest diameter or longest aspect ratio showed the highest concentration of doxorubicin in tumor and lower amounts in spleen, liver, and lungs due to the more effective escape of NPs from the reticuloendothelial system with a smaller

diameter. Likewise, filomicelle-paclitaxel showed significant inhibition of tumor growth in mice bearing A549 xenograft tumors compared to spherical paclitaxel NPs or free drug.[385]

6.2.3 Biodistribution and clearance—Understanding how shape affects the biodistribution of intravenously injected NPs is of fundamental importance for the rational design of delivery systems. There have been numerous studies of the *in vivo* biodistribution behaviours of anisotropic NPs. Huang *et al.* reported the biodistribution of silica NPs in mice post intravenous administration,[386] short nanorods with an aspect ratio of 1.5 accumulated more in the liver whereas long nanorods with an aspect ratio of 5 localized more in the spleen. Yu *et al.* investigated the mucosal penetration of mesoporous silica spheres and rods, and the rod-shaped silica NPs were shown to penetrate and accumulate more in small intestines compared to spherical ones.[387] The shape advantage for nanorods than spheres are dictated by the porosity of the mucus as well as the shape-induced diffusion of anisotropic nanorods.

Another study investigated the organ distribution of spherical, quasi-hemispherical, cylindrical and discoidal silicon NPs after intravenous injection into MDA-MB-231 tumor bearing female mice.[388] Cylindrical NPs were deposited at a larger extent in the liver, while discoidal NPs were observed to accumulate significantly more in the lungs and heart than the cylindrical, hemispherical, or spherical NPs, which may be because of the margination propensity of discoidal particles resulting in the accumulation of NPs on vascular walls. Likewise, plate-like Au doped NPs were also shown to accumulate in heart and lungs (Figure 30).[389] In another similar research, Godin *et al.* confirmed that discoidal mesoporous silica NPs accumulated up to five times more than spherical counterparts with a similar diameter in breast tumors.[390] NPs can also accumulate in hair follicles or skin folds after transporting through the stratum corneum. Transfollicular delivery of ovalbumin by using polymeric NPs could bring about a significant cellular and humoral immune response without compromising the stratum corneum barrier.[391–393]

Investigating the circulation time *in vivo* and clearance of NPs with the consideration of the shape affect is significant for their biomedical applications. It appears that NPs with higher aspect ratios prolong circulation time *in vivo*. It was reported that filamentous micelles made from amphiphilic block copolymers had significantly longer circulation time than that of their spherical ones.[394] Other reports further supported this result that higher aspect ratio NPs hold longer circulation time.[395] For instance, Au nanorods persisted significantly more in circulation compared to spherical NPs.[396] This is due to the extension by the flow and accumulation next to the vessel walls for larger particles with high aspect ratios, together with the uniform radial distribution and limited near-wall accumulation for smaller particles.[394, 397] The clearance of NPs with anisotropic shapes is incomparably complicated when it comes to different morphologies, such as discoidal/plate-like NPs are also shown to accumulate in heart and lungs due to margination under flow.[388, 389] Some of them appear to be similarly governed by diameter (or length) in circulation. While most of particulate matters will be trapped and cleared by the reticuloendothelial system (RES), NPs with high aspect ratio tend to be filtered out by the spleen, when the particles are larger than 200 nm.[398–400] NPs with diameter between 15 and 200 nm tend to accumulate and be cleared by the liver, which has a large coverage of the majority of anisotropic NPs.[401] And small NPs less

than 10 nm can reach various organs by crossing the tight endothelial junctions and be rapidly cleared *via* glomerular filtration by the kidneys and excreted to the urine.[402–404] Evidence also suggests that some high aspect ratio NPs can also be filtered *via* the kidneys when the cross-sectional diameter is small enough to pass through the glomerular pore.[405]

7. Summary and Prospects

Initially, anisotropic NPs attracted interests from scientific communities due to their fascinating catalytic, optical, electrical, or magnetic properties. Subsequently, it was discovered that distinctive shapes of these NPs could potentially dictate their various applications as well as interactions with single cells and ultimately whole organisms. This review summarizes the most recent researches on anisotropic NPs-based materials in their specific physicochemical and biomedical applications, including optics, catalysis, imaging, and therapy. A systematic understanding of these NPs from mechanism, synthesis, property to application as well as their *in vitro* and *in vivo* biological behaviors are discussed. We have witnessed a fairly remarkable progress in manipulating anisotropic NPs for their exciting potential physicochemical and biomedical applications in the last two decades. Despite these incredible accomplishments, anisotropic NPs still face lots of major challenges that need to be addressed before they can be eventually employed in industrial or biomedical applications.

For the synthesis, as the literatures with regard to fabrication of anisotropic NPs reported in this review continue to expand, the basis for experimental design is evolving from empirical rules towards well-established scientific theory. Delicate control has been achieved, nevertheless, there is still a long way to go to plenarily understand all the complexities involved in this charming science. For example, the scale up production of anisotropic NPs is one of the major challenges as many anisotropic nanomaterials were only realized at a lab scale. Actually, many different kinds of shaped NP addressed in this review could not be facilely scaled up such as the preparation of octopods with a good magnetite crystal structure. Although it is obviously important to make efforts to scale up synthesis of NPs, therapeutic gains from such anisotropic materials and costs of these endeavors must be taken into account. Therefore, there should be focuses on economical and comprehensive designs as well as efforts towards the scalable production of anisotropic NPs in the future.

For catalysis and optics, catalyst NP with unique shape exposes one or one group of specific crystallographic surface. This crystallographic surface consists of certain surface atoms with specific electronic state and induced shape-dependent catalytic performance, which has been well-demonstrated in literature. It should be notable that the shape-dependent catalytic performance on nanocatalyst is commonly related to different coordination environment of catalyst atoms on facets, resulting in definite activity and selectivity. Anisotropy can also impart particular optical property and enhance the imaging capability of material, for instance, SERS sensing with gold nanostars. These unique optical characteristics with anisotropic NPs provide strategies for further developments in ultrasensitive imaging.

For biobehaviour and biomedicine, we should keep in mind that fundamental studies on the shape effect in the NP-biological interaction is incomplete to date. Particularly for the

uptake, anisotropic NPs are preferentially endocytosed by most cell types when the diameter is larger than 100 nm, while at smaller scales the consequence of shape on the uptake of NPs is contentious. It appears that NPs with high aspect ratios are favorably endocytosed compared with other shapes, whereas, the different surface chemistry has a disproportionately stronger effect. More characterization data, such as colloidal stability and polydispersity, may explain the contradictions in previously published reports in some way. Although the question that how shape impacts the *in vitro* and *in vivo* behaviors has no simple answer in this review, it is encouraging that there are several principles can guide the design of future NPs for biomedical applications. Researchers can take full advantage of these findings to manufacture NPs for fluorescence imaging, photothermal therapy and MRI. However, we must be aware of that there is also an overdependence on recording final outcomes to show the successful utility of NPs for biomedical applications. Many researches did not perform full pharmacokinetics and biodistribution analyses of the administered anisotropic NPs, nor did they confirm that NPs actually target the cells of tissues or tumors *in vivo*.

Finally, we hope this review will not only give researchers a more comprehensive understanding of anisotropic NPs and their characteristic properties or applications, but also provide necessary insights, full thinking, and directional strategies for designing their own experiments, as well as open new horizons for scientists in the future physicochemical and biomedical applications.

Acknowledgements

This research was supported by National Natural Science Foundation of China (NSFC) projects (Grant number: 201874024), and the intramural research program of the National Institute of Biomedical Imaging and Bioengineering (NIBIB), National Institutes of Health (NIH).

References:

1. Pedone D, Moglianetti M, De Luca E, Bardi G and Pompa PP, Chem. Soc. Rev, 2017, 46, 4951–4975. [PubMed: 28696452]
2. Zhou W, Gao X, Liu D and Chen X, Chem. Rev, 2015, 115, 10575–10636. [PubMed: 26114396]
3. Fan Z and Zhang H, Acc. Chem. Res, 2016, 49, 2841–2850. [PubMed: 27993013]
4. Shen L, Yu L, Wu HB, Yu X-Y, Zhang X and Lou XW, Nat. Commun, 2015, 6, 6694. [PubMed: 25798849]
5. Wall MA, Harmsen S, Pal S, Zhang L, Arianna G, Lombardi JR, Drain CM and Kircher MF, Adv. Mater, 2017, 29.
6. Liao H-G, Jiang Y-X, Zhou Z-Y, Chen S-P and Sun S-G, Angew. Chem, 2008, 47, 9100–9103. [PubMed: 18925592]
7. Liu H, Li W, Shen D, Zhao D and Wang G, J. Am. Chem. Soc, 2015, 137, 13161–13166. [PubMed: 26414170]
8. Chen S, Wang ZL, Ballato J, Foulger SH and Carroll DL, J. Am. Chem. Soc, 2003, 125, 16186–16187. [PubMed: 14692749]
9. Zeng J, Zheng Y, Rycenga M, Tao J, Li Z-Y, Zhang Q, Zhu Y and Xia Y, J. Am. Chem. Soc, 2010, 132, 8552–8553. [PubMed: 20527784]
10. Bu L, Zhang N, Guo S, Zhang X, Li J, Yao J, Wu T, Lu G, Ma J-Y, Su D and Huang X, Science, 2016, 354, 1410. [PubMed: 27980207]
11. Zhou Z, Zhu X, Wu D, Chen Q, Huang D, Sun C, Xin J, Ni K and Gao J, Chem. Mater, 2015, 27, 3505–3515.

12. Yin X-L, Li L-L, Jiang W-J, Zhang Y, Zhang X, Wan L-J and Hu J-S, ACS Appl. Mater. Interfaces, 2016, 8, 15258–15266. [PubMed: 27237623]
13. Zhao N, Wei Y, Sun N, Chen Q, Bai J, Zhou L, Qin Y, Li M and Qi L, Langmuir, 2008, 24, 991–998. [PubMed: 18173292]
14. Rodríguez-Lorenzo L, de la Rica R, Álvarez-Puebla RA, Liz-Marzán LM and Stevens MM, Nat. Mater, 2012, 11, 604. [PubMed: 22635043]
15. Kinnear C, Moore TL, Rodriguez-Lorenzo L, Rothen-Rutishauser B and Petri-Fink A, Chem. Rev, 2017, 117, 11476–11521. [PubMed: 28862437]
16. Rodríguez-Lorenzo L, Álvarez-Puebla RA, de Abajo FJG and Liz-Marzán LM, J. Phys. Chem. C, 2010, 114, 7336–7340.
17. Dondapati SK, Sau TK, Hrelescu C, Klar TA, Stefani FD and Feldmann J, ACS Nano, 2010, 4, 6318–6322. [PubMed: 20942444]
18. Peiris PM, Toy R, Doolittle E, Pansky J, Abramowski A, Tam M, Vicente P, Tran E, Hayden E, Camann A, Mayer A, Erokwu BO, Berman Z, Wilson D, Baskaran H, Flask CA, Keri RA and Karathanasis E, ACS Nano, 2012, 6, 8783–8795. [PubMed: 23005348]
19. Fan Z, Senapati D, Singh AK and Ray PC, Mol. Pharm, 2013, 10, 857–866. [PubMed: 23110457]
20. Lacroix L-M, Frey Huls N, Ho D, Sun X, Cheng K and Sun S, Nano Lett, 2011, 11, 1641–1645. [PubMed: 21417366]
21. Li H, Liu H, Nie T, Chen Y, Wang Z, Huang H, Liu L and Chen Y, Biomaterials, 2018, 178, 620–629. [PubMed: 29602561]
22. Pietuch A, Schneider D, Rother J, Sunnick E, Rosman C, Pierrat S, Sönnichsen C, Wegener J and Janshoff A, Nanotoxicology, 2011, 5, 254–268. [PubMed: 21050076]
23. Heng BC, Zhao X, Tan EC, Khamis N, Assodani A, Xiong S, Ruedl C, Ng KW and Loo JS-C, Arch. Toxicol, 2011, 85, 1517–1528. [PubMed: 21656222]
24. Dasgupta S, Auth T and Gompper G, Nano Lett, 2014, 14, 687–693. [PubMed: 24383757]
25. Florez L, Herrmann C, Cramer JM, Hauser CP, Koynov K, Landfester K, Crespy D and Mailänder V, Small, 2012, 8, 2222–2230. [PubMed: 22528663]
26. Huang X, Peng X, Wang Y, Wang Y, Shin DM, El-Sayed MA and Nie S, ACS Nano, 2010, 4, 5887–5896. [PubMed: 20863096]
27. Carnovale C, Bryant G, Shukla R and Bansal V, Prog. Mater. Sci, 2016, 83, 152–190.
28. Chu Z, Zhang S, Zhang B, Zhang C, Fang C-Y, Rehor I, Cigler P, Chang H-C, Lin G, Liu R and Li Q, Sci. Rep, 2014, 4, 4495. [PubMed: 24675513]
29. Tian F, Clift MJ, Casey A, Pino P. d., Pelaz B, Conde J, Byrne HJ, Rothen-Rutishauser B, Estrada G, Fuente J. M. d. l. and Stoeger T, Nanomedicine, 2015, 10, 2643–2657. [PubMed: 26377045]
30. Wang H, Feng J, Liu G, Chen B, Jiang Y and Xie Q, Nanomed. Nanotechnol. Biol. Med, 2016, 12, 881–891.
31. Albanese A, Tang PS and Chan WCW, Annu. Rev. Biomed. Eng, 2012, 14, 1–16. [PubMed: 22524388]
32. Pelaz B, Alexiou C, Alvarez-Puebla RA, Alves F, Andrews AM, Ashraf S, Balogh LP, Ballerini L, Bestetti A, Brendel C, Bosi S, Carril M, Chan WCW, Chen C, Chen X, Chen X, Cheng Z, Cui D, Du J, Dullin C, Escudero A, Feliu N, Gao M, George M, Gogotsi Y, Grünweller A, Gu Z, Halas NJ, Hampp N, Hartmann RK, Hersam MC, Hunziker P, Jian J, Jiang X, Jungebluth P, Kadhiresan P, Kataoka K, Khademhosseini A, Kopeček J, Kotov NA, Krug HF, Lee DS, Lehr C-M, Leong KW, Liang X-J, Ling Lim M, Liz-Marzán LM, Ma X, Macchiarini P, Meng H, Möhwald H, Mulvaney P, Nel AE, Nie S, Nordlander P, Okano T, Oliveira J, Park TH, Penner RM, Prato M, Puntes V, Rotello VM, Samarakoon A, Schaak RE, Shen Y, Sjöqvist S, Skirtach AG, Soliman MG, Stevens MM, Sung H-W, Tang BZ, Tietze R, Udugama BN, VanEpps JS, Weil T, Weiss PS, Willner I, Wu Y, Yang L, Yue Z, Zhang Q, Zhang Q, Zhang X-E, Zhao Y, Zhou X and Parak WJ, ACS Nano, 2017, 11, 2313–2381. [PubMed: 28290206]
33. Shi J, Kantoff PW, Wooster R and Farokhzad OC, Nat. Rev. Cancer, 2016, 17, 20. [PubMed: 27834398]
34. Burda C, Chen X, Narayanan R and El-Sayed MA, Chem. Rev, 2005, 105, 1025–1102. [PubMed: 15826010]

35. Maier SA, Brongersma ML, Kik PG, Meltzer S, Requicha AAG and Atwater HA, Adv. Mater, 2001, 13, 1501–1505.
36. Yin AX, Liu WC, Ke J, Zhu W, Gu J, Zhang YW and Yan CH, J. Am. Chem. Soc, 2012, 134, 20479–20489. [PubMed: 23181397]
37. Butet J, Thyagarajan K and Martin OJF, Nano Lett, 2013, 13, 1787–1792. [PubMed: 23458149]
38. Halas NJ, Lal S, Chang W-S, Link S and Nordlander P, Chem. Rev, 2011, 111, 3913–3961. [PubMed: 21542636]
39. Prodan E, Radloff C, Halas NJ and Nordlander P, Science, 2003, 302, 419–422. [PubMed: 14564001]
40. Kelly KL, Coronado E, Zhao LL and Schatz GC, The Journal of Physical Chemistry B, 2003, 107, 668–677.
41. Xia Y, Xiong Y, Lim B and Skrabalak SE, Angew. Chem. Int. Ed, 2009, 48, 60–103.
42. Tao AR, Habas S and Yang P, Small, 2008, 4, 310–325.
43. Ray PC, Chem. Rev, 2010, 110, 5332–5365. [PubMed: 20469927]
44. Hua Y, Chandra K, Dam DHM, Wiederrecht GP and Odom TW, J. Phys. Chem. Lett, 2015, 6, 4904–4908. [PubMed: 26595327]
45. Zhang H, Jin M, Xiong Y, Lim B and Xia Y, Acc. Chem. Res, 2013, 46, 1783–1794. [PubMed: 23163781]
46. Narayanan R and El-Sayed MA, J. Phys. Chem. B, 2005, 109, 12663–12676. [PubMed: 16852568]
47. Wang YJ, Zhao N, Fang B, Li H, Bi XT and Wang H, Chem. Rev, 2015, 115, 3433–3467. [PubMed: 25871490]
48. Cao S, Tao FF, Tang Y, Li Y and Yu J, Chem. Soc. Rev, 2016, 45, 4747–4765. [PubMed: 27276189]
49. Chen J, Lim B, Lee EP and Xia Y, Nano Today, 2009, 4, 81–95.
50. Yan Y, Du JS, Gilroy KD, Yang D, Xia Y and Zhang H, Adv. Mater, 2017, 29.
51. Fernández EM, Moses PG, Toftelund A, Hansen HA, Martínez JI, Abild-Pedersen F, Kleis J, Hinnemann B, Rossmeisl J, Bligaard T and Nørskov JK, Angew. Chem. Int. Ed, 2008, 47, 4683–4686.
52. Nørskov JK, Bligaard T, Hvolbæk B, Abild-Pedersen F, Chorkendorff I and Christensen CH, Chem. Soc. Rev, 2008, 37, 2163–2171. [PubMed: 18818819]
53. Falsig H, Shen J, Khan TS, Guo W, Jones G, Dahl S and Bligaard T, Top. Catal, 2014, 57, 80–88.
54. Liu P, Qin R, Fu G and Zheng N, J. Am. Chem. Soc, 2017, 139, 2122–2131. [PubMed: 28085260]
55. Li L-S, Walda J, Manna L and Alivisatos AP, Nano Lett, 2002, 2, 557–560.
56. Mokari T and Banin U, Chem. Mater, 2003, 15, 3955–3960.
57. Ntziachristos V, Nat. Methods, 2010, 7, 603. [PubMed: 20676081]
58. Gai S, Li C, Yang P and Lin J, Chem. Rev, 2014, 114, 2343–2389. [PubMed: 24344724]
59. Ye X, Collins JE, Kang Y, Chen J, Chen DT, Yodh AG and Murray CB, Proc. Natl. Acad. Sci. U. S. A, 2010, 107, 22430–22435. [PubMed: 21148771]
60. Polavarapu L, Manna M and Xu QH, Nanoscale, 2011, 3, 429–434. [PubMed: 20944843]
61. Carroll MR, Woodward RC, House MJ, Teoh WY, Amal R, Hanley TL and St Pierre TG, Nanotechnology, 2010, 21, 035103.
62. Tromsdorf UI, Bigall NC, Kaul MG, Bruns OT, Nikolic MS, Mollwitz B, Sperling RA, Reimer R, Hohenberg H, Parak WJ, Forster S, Beisiegel U, Adam G and Weller H, Nano Lett, 2007, 7, 2422–2427. [PubMed: 17658761]
63. Hao R, Xing R, Xu Z, Hou Y, Gao S and Sun S, Adv. Mater, 2010, 22, 2729–2742. [PubMed: 20473985]
64. Laurent S, Forge D, Port M, Roch A, Robic C, Vander Elst L and Muller RN, Chem. Rev, 2008, 108, 2064–2110. [PubMed: 18543879]
65. Hancock RD and Martell AE, Chem. Rev, 1989, 89, 1875–1914.
66. Chan WCW, Acc. Chem. Res, 2017, 50, 627–632. [PubMed: 28945418]
67. Sun Y and Xia Y, Science, 2002, 298, 2176–2179. [PubMed: 12481134]

68. Owen J, Science, 2015, 347, 615–616. [PubMed: 25657234]
69. Chen M, Wu B, Yang J and Zheng N, Adv. Mater, 2012, 24, 862–879. [PubMed: 22252856]
70. Rose MK, Mitsui T, Dunphy J, Borg A, Ogletree DF, Salmeron M and Sautet P, Surf. Sci, 2002, 512, 48–60.
71. Huang X, Tang S, Mu X, Dai Y, Chen G, Zhou Z, Ruan F, Yang Z and Zheng N, Nat. Nanotechnol, 2010, 6, 28. [PubMed: 21131956]
72. Pan Y-T, Yin X, Kwok KS and Yang H, Nano Lett, 2014, 14, 5953–5959. [PubMed: 25198201]
73. Yin X, Liu X, Pan Y-T, Walsh KA and Yang H, Nano Lett, 2014, 14, 7188–7194. [PubMed: 25369350]
74. Zhao L, Xu C, Su H, Liang J, Lin S, Gu L, Wang X, Chen M and Zheng N, Adv. Sci, 2015, 2, 1500100.
75. Wu B, Zheng N and Fu G, Chem. Commun, 2011, 47, 1039–1041.
76. Chen G, Tan Y, Wu B, Fu G and Zheng N, Chem. Commun, 2012, 48, 2758–2760.
77. Kang Y, Ye X and Murray CB, Angew. Chem, 2010, 122, 6292–6295.
78. Dai Y, Mu X, Tan Y, Lin K, Yang Z, Zheng N and Fu G, J. Am. Chem. Soc, 2012, 134, 7073–7080. [PubMed: 22468699]
79. Habas SE, Lee H, Radmilovic V, Somorjai GA and Yang P, Nat. Mater, 2007, 6, 692. [PubMed: 17618289]
80. Huang X, Zhao Z, Fan J, Tan Y and Zheng N, J. Am. Chem. Soc, 2011, 133, 4718–4721. [PubMed: 21405136]
81. Niu Z and Li Y, Chem. Mater, 2013, 26, 72–83.
82. Personick ML and Mirkin CA, J. Am. Chem. Soc, 2013, 135, 18238–18247. [PubMed: 24283259]
83. Sun SB, Yuan D, Xu Y, Wang AF and Deng ZT, ACS Nano, 2016, 10, 3648–3657. [PubMed: 26886173]
84. Meyns M, Iacono F, Palencia C, Geweke J, Coderch MD, Fittschen UEA, Gallego JM, Otero R, Juarez BH and Klinke C, Chem. Mater, 2014, 26, 1813–1821.
85. Zhang Y, Grass ME, Kuhn JN, Tao F, Habas SE, Huang W, Yang P and Somorjai GA, J. Am. Chem. Soc, 2008, 130, 5868–5869. [PubMed: 18399628]
86. Carrasquillo A, Jeng J-J, Barriga RJ, Temesghen WF and Soriaga MP, Inorg. Chim. Acta, 1997, 255, 249–254.
87. Huang X, Zhang H, Guo C, Zhou Z and Zheng N, Angew. Chem. Int. Ed, 2009, 48, 4808–4812.
88. Zhao Z, Zhou Z, Bao J, Wang Z, Hu J, Chi X, Ni K, Wang R, Chen X, Chen Z and Gao J, Nat. Commun, 2013, 4, 2266. [PubMed: 23903002]
89. Lohse SE, Burrows ND, Scarabelli L, Liz-Marzán LM and Murphy CJ, Chem. Mater, 2013, 26, 34–43.
90. Jin M, He G, Zhang H, Zeng J, Xie Z and Xia Y, Angew. Chem. Int. Ed, 2011, 50, 10560–10564.
91. Ye X, Chen J, Engel M, Millan JA, Li W, Qi L, Xing G, Collins JE, Kagan CR, Li J, Glotzer SC and Murray CB, Nat. Chem, 2013, 5, 466. [PubMed: 23695627]
92. Pourmasoud S, Sobhani-Nasab A, Behpour M, Rahimi-Nasrabadi M and Ahmadi F, J. Mol. Struct, 2018, 1157, 607–615.
93. Kovalenko MV, Bodnarchuk MI, Lechner RT, Hesser G, Schaffler F and Heiss W, J. Am. Chem. Soc, 2007, 129, 6352–6353. [PubMed: 17472378]
94. Park J, An K, Hwang Y, Park J-G, Noh H-J, Kim J-Y, Park J-H, Hwang N-M and Hyeon T, Nat. Mater, 2004, 3, 891. [PubMed: 15568032]
95. Zhang L, Wu J, Liao H, Hou Y and Gao S, Chem. Commun, 2009, 4378–4380.
96. Liu D, Xu X, Du Y, Qin X, Zhang Y, Ma C, Wen S, Ren W, Goldys EM, Piper JA, Dou S, Liu X and Jin D, Nat. Commun, 2016, 7, 10254. [PubMed: 26743184]
97. Kim M-S, Lim S, Chaudhari NK, Fang B, Bae T-S and Yu J-S, Catal. Today, 2010, 158, 354–360.
98. Shimazaki Y, Kobayashi Y, Yamada S, Miwa T and Konno M, J. Colloid Interface Sci, 2005, 292, 122–126. [PubMed: 16039660]
99. Abedini A, Daud AR, Abdul Hamid MA, Kamil Othman N and Saion E, Nanoscale Res. Lett, 2013, 8, 474. [PubMed: 24225302]

100. Rusnaeni N, Purwanto WW, Nasikin M and Hendrajaya L, J. Appl. Sci, 2010, 10, 2899–2904.
101. Fang B, Chaudhari NK, Kim MS, Kim JH and Yu JS, J. Am. Chem. Soc, 2009, 131, 15330–15338. [PubMed: 19795863]
102. Xue C and Mirkin CA, Angew. Chem. Int. Ed, 2007, 46, 2036–2038.
103. Li G, Peng C, Zhang C, Xu Z, Shang M, Yang D, Kang X, Wang W, Li C, Cheng Z and Lin J, Inorg. Chem, 2010, 49, 10522–10535. [PubMed: 20961121]
104. Singh B and Dempsey E, ECS J. Solid State Sci. Technol, 2012, 1, M25–M32.
105. Sheng W, Lee SW, Crumlin EJ, Chen S and Shao-Horn Y, J. Electrochem. Soc, 2011, 158, B1398–B1404.
106. Chandan A, Hattenberger M, El-kharouf A, Du S, Dhir A, Self V, Pollet BG, Ingram A and Bujalski W, J. Power Sources, 2013, 231, 264–278.
107. Watt J, Yu C, Chang SL, Cheong S and Tilley RD, J. Am. Chem. Soc, 2013, 135, 606–609. [PubMed: 23268702]
108. Li Z and Peng X, J. Am. Chem. Soc, 2011, 133, 6578–6586. [PubMed: 21476585]
109. Guo S, Fidler AF, He K, Su D, Chen G, Lin Q, Pietryga JM and Klimov VI, J. Am. Chem. Soc, 2015, 137, 15074–15077. [PubMed: 26545157]
110. Xia Y, Xia X and Peng HC, J. Am. Chem. Soc, 2015, 137, 7947–7966. [PubMed: 26020837]
111. Tsung CK, Kou X, Shi Q, Zhang J, Yeung MH, Wang J and Stucky GD, J. Am. Chem. Soc, 2006, 128, 5352–5353. [PubMed: 16620101]
112. Nikoobakht B and El-Sayed MA, Chem. Mater, 2003, 15, 1957–1962.
113. Jana NR, Gearheart L and Murphy CJ, Adv. Mater, 2001, 13, 1389–1393.
114. Chen L, Huang B, Qiu X, Wang X, Luque R and Li Y, Chem. Sci, 2016, 7, 228–233. [PubMed: 28758001]
115. Xia Y, Gilroy KD, Peng HC and Xia X, Angew. Chem. Int. Ed, 2017, 56, 60–95.
116. Pietrobon B, McEachran M and Kitaev V, ACS Nano, 2009, 3, 21–26. [PubMed: 19206244]
117. Sun Y, Yin Y, Mayers BT, Herricks T and Xia Y, Chem. Mater, 2002, 14, 4736–4745.
118. Zhang Q, Li W, Moran C, Zeng J, Chen J, Wen LP and Xia Y, J. Am. Chem. Soc, 2010, 132, 11372–11378. [PubMed: 20698704]
119. Sanchez-Iglesias A, Winckelmans N, Altantzis T, Bals S, Grzelczak M and Liz-Marzan LM, J. Am. Chem. Soc, 2017, 139, 107–110. [PubMed: 28009166]
120. Tangeysh B, Moore Tibbetts K, Odhner JH, Wayland BB and Levis RJ, Nano Lett, 2015, 15, 3377–3382. [PubMed: 25844894]
121. Zhou G, Yang Y, Han S, Chen W, Fu Y, Zou C, Zhang L and Huang S, ACS Appl. Mater. Interfaces, 2013, 5, 13340–13352. [PubMed: 24245552]
122. Gilroy KD, Yang X, Xie S, Zhao M, Qin D and Xia Y, Adv. Mater, 2018, 30, 1706312.
123. Luo M, Ruditskiy A, Peng H-C, Tao J, Figueroa-Cosme L, He Z and Xia Y, Adv. Funct. Mater, 2016, 26, 1209–1216.
124. S. R. Lee, J. Park, K. D. Gilroy, X. Yang, L. Figueroa-Cosme, Y. Ding and Y. Xia, ChemCatChem, 2016, 8, 3082–3088.
125. Coropceanu I, Rossinelli A, Caram JR, Freyria FS and Bawendi MG, ACS Nano, 2016, 10, 3295–3301. [PubMed: 26885562]
126. Weiner RG, DeSantis CJ, Cardoso MB and Skrabalak SE, ACS Nano, 2014, 8, 8625–8635. [PubMed: 25133784]
127. Sun S, Zeng H, Robinson DB, Raoux S, Rice PM, Wang SX and Li G, J. Am. Chem. Soc, 2004, 126, 273–279. [PubMed: 14709092]
128. Song Q and Zhang ZJ, J. Am. Chem. Soc, 2004, 126, 6164–6168. [PubMed: 15137781]
129. Liu Y, Tang A, Zhang Q and Yin Y, J. Am. Chem. Soc, 2015, 137, 11327–11339. [PubMed: 26301334]
130. Martin CR, Science, 1994, 266, 1961–1966. [PubMed: 17836514]
131. Thomas A, Goettmann F and Antonietti M, Chem. Mater, 2008, 20, 738–755.
132. Lee W, Ji R, Gösele U and Nielsch K, Nat. Mater, 2006, 5, 741. [PubMed: 16921361]

133. Wu Y, Livneh T, Zhang YX, Cheng G, Wang J, Tang J, Moskovits M and Stucky GD, Nano Lett, 2004, 4, 2337–2342.
134. Wu Y, Cheng G, Katsov K, Sides SW, Wang J, Tang J, Fredrickson GH, Moskovits M and Stucky GD, Nat. Mater, 2004, 3, 816. [PubMed: 15502836]
135. Xia Y, Yang P, Sun Y, Wu Y, Mayers B, Gates B, Yin Y, Kim F and Yan H, Adv. Mater, 2003, 15, 353–389.
136. Lee MH, Lin JY and Odom TW, Angew. Chem. Int. Ed, 2010, 49, 3057–3060.
137. Fredriksson H, Alaverdyan Y, Dmitriev A, Langhammer C, Sutherland DS, Zäch M and Kasemo B, Adv. Mater, 2007, 19, 4297–4302.
138. Henzie J, Lee MH and Odom TW, Nat. Nanotechnol, 2007, 2, 549. [PubMed: 18654366]
139. Yang JC, Gao H, Suh JY, Zhou W, Lee MH and Odom TW, Nano Lett, 2010, 10, 3173–3178. [PubMed: 20698633]
140. Chen CL and Rosi NL, Angew. Chem. Int. Ed, 2010, 49, 1924–1942.
141. George J and Thomas KG, J. Am. Chem. Soc, 2010, 132, 2502–2503. [PubMed: 20136136]
142. Guli M, Lambert EM, Li M and Mann S, Angew. Chem, 2010, 122, 530–533.
143. Carter CJ, Ackerson CJ and Feldheim DL, ACS Nano, 2010, 4, 3883–3888. [PubMed: 20552994]
144. Jones MR, Osberg KD, Macfarlane RJ, Langille MR and Mirkin CA, Chem. Rev, 2011, 111, 3736–3827. [PubMed: 21648955]
145. Gunawidjaja R, Peleshanko S, Ko H and Tsukruk VV, Adv. Mater, 2008, 20, 1544–1549.
146. Lee J, Govorov AO, Dulka J and Kotov NA, Nano Lett, 2004, 4, 2323–2330.
147. Li JF, Huang YF, Ding Y, Yang ZL, Li SB, Zhou XS, Fan FR, Zhang W, Zhou ZY, Wu DY, Ren B, Wang ZL and Tian ZQ, Nature, 2010, 464, 392. [PubMed: 20237566]
148. Lu CL, Prasad KS, Wu HL, Ho JA and Huang MH, J. Am. Chem. Soc, 2010, 132, 14546–14553. [PubMed: 20873739]
149. Wu X, Redmond PL, Liu H, Chen Y, Steigerwald M and Brus L, J. Am. Chem. Soc, 2008, 130, 9500–9506. [PubMed: 18578529]
150. Xia X, Wang Y, Ruditskiy A and Xia Y, Adv. Mater, 2013, 25, 6313–6333. [PubMed: 24027074]
151. Wang Z, Luan D, Li CM, Su F, Madhavi S, Boey FY and Lou XW, J. Am. Chem. Soc, 2010, 132, 16271–16277. [PubMed: 20973538]
152. Skrabalak SE, Chen J, Sun Y, Lu X, Au L, Cobley CM and Xia Y, Acc. Chem. Res, 2008, 41, 1587–1595. [PubMed: 18570442]
153. Gonzalez E, Arbiol J and Puntes VF, Science, 2011, 334, 1377–1380. [PubMed: 22158813]
154. Gu H, Yang Z, Gao J, Chang CK and Xu B, J. Am. Chem. Soc, 2005, 127, 34–35. [PubMed: 15631435]
155. Yu H, Chen M, Rice PM, Wang SX, White RL and Sun S, Nano Lett, 2005, 5, 379–382. [PubMed: 15794629]
156. Liu H and Alivisatos AP, Nano Lett, 2004, 4, 2397–2401.
157. Bai H, Xu K, Xu Y and Matsui H, Angew. Chem. Int. Ed, 2007, 46, 3319–3322.
158. Keren K, Krueger M, Gilad R, Ben-Yoseph G, Sivan U and Braun E, Science, 2002, 297, 72–75. [PubMed: 12098693]
159. Keren K, Berman RS, Buchstab E, Sivan U and Braun E, Science, 2003, 302, 1380–1382. [PubMed: 14631035]
160. Tan YN, Lee JY and Wang DI, J. Am. Chem. Soc, 2010, 132, 5677–5686. [PubMed: 20355728]
161. Slocik JM and Naik RR, Adv. Mater, 2006, 18, 1988–1992.
162. Kasyutich O, Ilari A, Fiorillo A, Tatchev D, Hoell A and Ceci P, J. Am. Chem. Soc, 2010, 132, 3621–3627. [PubMed: 20170158]
163. Leroux F, Gysemans M, Bals S, Batenburg KJ, Snauwaert J, Verbiest T, Van Haesendonck C and Van Tendeloo G, Adv. Mater, 2010, 22, 2193–2197. [PubMed: 20225183]
164. Balci S, Noda K, Bittner AM, Kadri A, Wege C, Jeske H and Kern K, Angew. Chem. Int. Ed, 2007, 46, 3149–3151.
165. Eisele DM, Berlepsch HV, Bottcher C, Stevenson KJ, Vanden Bout DA, Kirstein S and Rabe JP, J. Am. Chem. Soc, 2010, 132, 2104–2105. [PubMed: 20104895]

166. Cushing BL, Kolesnichenko VL and O'Connor CJ, Chem. Rev, 2004, 104, 3893–3946. [PubMed: 15352782]
167. Wang X, Zhuang J, Peng Q and Li Y, Nature, 2005, 437, 121. [PubMed: 16136139]
168. Radi A, Pradhan D, Sohn Y and Leung KT, ACS Nano, 2010, 4, 1553–1560. [PubMed: 20166698]
169. Xue C, Millstone JE, Li S and Mirkin CA, Angew. Chem. Int. Ed, 2007, 46, 8436–8439.
170. Zhang J, Li S, Wu J, Schatz GC and Mirkin CA, Angew. Chem. Int. Ed, 2009, 48, 7787–7791.
171. Langille MR, Zhang J and Mirkin CA, Angew. Chem. Int. Ed, 2011, 50, 3543–3547.
172. Zhang H, Xia X, Li W, Zeng J, Dai Y, Yang D and Xia Y, Angew. Chem, 2010, 122, 5424–5428.
173. Linic S, Christopher P, Xin H and Marimuthu A, Acc. Chem. Res, 2013, 46, 1890–1899. [PubMed: 23750539]
174. Ma Y, Li W, Cho EC, Li Z, Yu T, Zeng J, Xie Z and Xia Y, ACS Nano, 2010, 4, 6725–6734. [PubMed: 20964400]
175. Linic S, Christopher P and Ingram DB, Nat. Mater, 2011, 10, 911–921. [PubMed: 22109608]
176. Butet J, Brevet PF and Martin OJ, ACS Nano, 2015, 9, 10545–10562. [PubMed: 26474346]
177. Albella P, Garcia-Cueto B, Gonzalez F, Moreno F, Wu PC, Kim TH, Brown A, Yang Y, Everitt HO and Videen G, Nano Lett, 2011, 11, 3531–3537. [PubMed: 21848270]
178. Song J, Wu B, Zhou Z, Zhu G, Liu Y, Yang Z, Lin L, Yu G, Zhang F, Zhang G, Duan H, Stucky GD and Chen X, Angew. Chem. Int. Ed, 2017, 56, 8110–8114.
179. Zhang H and Govorov AO, J. Phys. Chem. C, 2014, 118, 7606–7614.
180. Yang M, Alvarez-Puebla R, Kim HS, Aldeanueva-Potel P, Liz-Marzan LM and Kotov NA, Nano Lett, 2010, 10, 4013–4019. [PubMed: 20738117]
181. Li W, Zamani R, Rivera Gil P, Pelaz B, Ibáñez M, Cadavid D, Shavel A, Alvarez-Puebla RA, Parak WJ, Arbiol J and Cabot A, J. Am. Chem. Soc, 2013, 135, 7098–7101. [PubMed: 23647089]
182. Talley CE, Jackson JB, Oubre C, Grady NK, Hollars CW, Lane SM, Huser TR, Nordlander P and Halas NJ, Nano Lett, 2005, 5, 1569–1574. [PubMed: 16089490]
183. Boyack R and Le Ru EC, Phys. Chem. Chem. Phys, 2009, 11, 7398–7405. [PubMed: 19690711]
184. Zhu Z, Meng H, Liu W, Liu X, Gong J, Qiu X, Jiang L, Wang D and Tang Z, Angew. Chem. Int. Ed, 2011, 50, 1593–1596.
185. Fan W, Lee YH, Pedireddy S, Zhang Q, Liu T and Ling XY, Nanoscale, 2014, 6, 4843–4851. [PubMed: 24664184]
186. Liu W, Zhu Z, Deng K, Li Z, Zhou Y, Qiu H, Gao Y, Che S and Tang Z, J. Am. Chem. Soc, 2013, 135, 9659–9664. [PubMed: 23742128]
187. Kundu S, J. Mater. Chem. C, 2013, 1, 831–842.
188. Park JE, Lee Y and Nam JM, Nano Lett, 2018, 18, 6475–6482. [PubMed: 30153413]
189. Hong JW, Lee SU, Lee YW and Han SW, J. Am. Chem. Soc, 2012, 134, 4565–4568. [PubMed: 22364220]
190. Zhang L-F, Zhong S-L and Xu A-W, Angew. Chem, 2013, 125, 673–677.
191. Ye X, Jin L, Caglayan H, Chen J, Xing G, Zheng C, Doan-Nguyen V, Kang Y, Engheta N, Kagan CR and Murray CB, ACS Nano, 2012, 6, 2804–2817. [PubMed: 22376005]
192. Jana NR, Gearheart L and Murphy CJ, J. Phys. Chem. B, 2001, 105, 4065–4067.
193. Chen H, Shao L, Li Q and Wang J, Chem. Soc. Rev, 2013, 42, 2679–2724. [PubMed: 23128995]
194. Chang WS, Ha JW, Slaughter LS and Link S, Proc. Natl. Acad. Sci. U. S. A, 2010, 107, 2781–2786. [PubMed: 20133646]
195. Qu Y, Cheng R, Su Q and Duan X, J. Am. Chem. Soc, 2011, 133, 16730–16733. [PubMed: 21961900]
196. Okuno Y, Nishioka K, Kiya A, Nakashima N, Ishibashi A and Niidome Y, Nanoscale, 2010, 2, 1489–1493. [PubMed: 20820740]
197. Vanmaekelbergh D, van Vugt LK, Bakker HE, Rabouw FT, de Nijs B, van Dijk-Moes RJA, van Huis MA, Baesjou PJ and van Blaaderen A, ACS Nano, 2015, 9, 3942–3950. [PubMed: 25844664]

198. Jiang P, Zhu C-N, Zhang Z-L, Tian Z-Q and Pang D-W, Biomaterials, 2012, 33, 5130–5135. [PubMed: 22484042]
199. Zhang B, Wang Y, Yang C, Hu S, Gao Y, Zhang Y, Wang Y, Demir HV, Liu L and Yong K-T, Phys. Chem. Chem. Phys, 2015, 17, 25133–25141. [PubMed: 26349413]
200. Xu G, Zeng S, Zhang B, Swihart MT, Yong K-T and Prasad PN, Chem. Rev, 2016, 116, 12234–12327. [PubMed: 27657177]
201. Li L, Pandey A, Werder DJ, Khanal BP, Pietryga JM and Klimov VI, J. Am. Chem. Soc, 2011, 133, 1176–1179. [PubMed: 21207995]
202. Mirzaei J, Reznikov M and Hegmann T, J. Mater. Chem, 2012, 22, 22350–22365.
203. Deutsch Z, Avidan A, Pinkas I and Oron D, Phys. Chem. Chem. Phys, 2011, 13, 3210–3219. [PubMed: 21229166]
204. Acharya KP, Nguyen HM, Paulite M, Piryatinski A, Zhang J, Casson JL, Xu H, Htoon H and Hollingsworth JA, J. Am. Chem. Soc, 2015, 137, 3755–3758. [PubMed: 25746140]
205. Kim S, Fisher B, Eisler H-J and Bawendi M, J. Am. Chem. Soc, 2003, 125, 11466–11467. [PubMed: 13129327]
206. Bang J, Park J, Lee JH, Won N, Nam J, Lim J, Chang BY, Lee HJ, Chon B, Shin J, Park JB, Choi JH, Cho K, Park SM, Joo T and Kim S, Chem. Mater, 2010, 22, 233–240.
207. Chen C-W, Wu D-Y, Chan Y-C, Lin CC, Chung P-H, Hsiao M and Liu R-S, J. Phys. Chem. C, 2015, 119, 2852–2860.
208. Cooper JK, Gul S, Lindley SA, Yano J and Zhang JZ, ACS Appl. Mater. Interfaces, 2015, 7, 10055–10066. [PubMed: 25893312]
209. Chen B, Zhong H, Zhang W, Tan Z. a., Li Y, Yu C, Zhai T, Bando Y, Yang S and Zou B, Adv. Funct. Mater, 2012, 22, 2081–2088.
210. Liu Y-S, Sun Y, Vernier PT, Liang C-H, Chong SYC and Gundersen MA, J. Phys. Chem. C, 2007, 111, 2872–2878.
211. Chen G, Roy I, Yang C and Prasad PN, Chem. Rev, 2016, 116, 2826–2885. [PubMed: 26799741]
212. Cassette E, Pons T, Bouet C, Helle M, Bezdetnaya L, Marchal F and Dubertret B, Chem. Mater, 2010, 22, 6117–6124.
213. Kim K, Yoo D, Choi H, Tamang S, Ko JH, Kim S, Kim YH and Jeong S, Angew. Chem. Int. Ed, 2016, 55, 3714–3718.
214. Kim S, Lim YT, Soltesz EG, De Grand AM, Lee J, Nakayama A, Parker JA, Mihaljevic T, Laurence RG, Dor DM, Cohn LH, Bawendi MG and Frangioni JV, Nat. Biotechnol, 2003, 22, 93. [PubMed: 14661026]
215. Li L.-s., Hu J, Yang W and Alivisatos AP, Nano Lett, 2001, 1, 349–351.
216. Peng X, Manna L, Yang W, Wickham J, Scher E, Kadavanich A and Alivisatos AP, Nature, 2000, 404, 59. [PubMed: 10716439]
217. Yong KT, Qian J, Roy I, Lee HH, Bergey EJ, Tramposch KM, He S, Swihart MT, Maitra A and Prasad PN, Nano Lett, 2007, 7, 761–765. [PubMed: 17288490]
218. Deng Z, Tong L, Flores M, Lin S, Cheng JX, Yan H and Liu Y, J. Am. Chem. Soc, 2011, 133, 5389–5396. [PubMed: 21405017]
219. Yang H, Ku KH, Shin JM, Lee J, Park CH, Cho H-H, Jang SG and Kim BJ, Chem. Mater, 2016, 28, 830–837.
220. Sk MA, Ananthanarayanan A, Huang L, Lim KH and Chen P, J. Mater. Chem. C, 2014, 2, 6954–6960.
221. Yan X, Cui X, Li B and Li L.-s., Nano Lett, 2010, 10, 1869–1873. [PubMed: 20377198]
222. Zhao M, Yang F, Xue Y, Xiao D and Guo Y, ChemPhysChem, 2014, 15, 950–957. [PubMed: 24590822]
223. Mueller ML, Yan X, McGuire JA and Li L.-s., Nano Lett, 2010, 10, 2679–2682. [PubMed: 20575573]
224. Schumacher S, Phys. Rev. B, 2011, 83, 081417.
225. Shan J, Uddi M, Wei R, Yao N and Ju Y, J. Mater. Chem. C, 2010, 114, 2452–2461.

226. Shi J, Sun X, Zheng S, Li J, Fu X and Zhang H, Biomaterials, 2018, 152, 15–23. [PubMed: 29078137]
227. Chen H, Zhang J, Chang K, Men X, Fang X, Zhou L, Li D, Gao D, Yin S, Zhang X, Yuan Z and Wu C, Biomaterials, 2017, 144, 42–52. [PubMed: 28822291]
228. Lu H, Mack J, Yang Y and Shen Z, Chem. Soc. Rev, 2014, 43, 4778–4823. [PubMed: 24733589]
229. Zeng JH, Su J, Li ZH, Yan RX and Li YD, Adv. Mater, 2005, 17, 2119–2123.
230. Mai HX, Zhang YW, Si R, Yan ZG, Sun LD, You LP and Yan CH, J. Am. Chem. Soc, 2006, 128, 6426–6436. [PubMed: 16683808]
231. Liu Y, Tu D, Zhu H and Chen X, Chem. Soc. Rev, 2013, 42, 6924–6958. [PubMed: 23775339]
232. Chen G, Qiu H, Prasad PN and Chen X, Chem. Rev, 2014, 114, 5161–5214. [PubMed: 24605868]
233. Chen D, Yu Y, Huang F, Huang P, Yang A and Wang Y, J. Am. Chem. Soc, 2010, 132, 9976–9978. [PubMed: 20593808]
234. Li CX, Quan ZW, Yang PP, Yang J, Lian HZ and Lin J, J. Mater. Chem, 2008, 18, 1353–1361.
235. Li Y, Shao A, Wang Y, Mei J, Niu D, Gu J, Shi P, Zhu W, Tian H and Shi J, Adv. Mater, 2016, 28, 3187–3193. [PubMed: 26917199]
236. Zhou ZY, Tian N, Li JT, Broadwell I and Sun SG, Chem. Soc. Rev, 2011, 40, 4167–4185. [PubMed: 21552612]
237. Zhou K and Li Y, Angew. Chem. Int. Ed, 2012, 51, 602–613.
238. Li Y, Liu Q and Shen W, Dalton Trans, 2011, 40, 5811–5826. [PubMed: 21373704]
239. Andersson MP, Abild-Pedersen F, Remediakis IN, Bligaard T, Jones G, Engbæk J, Lytken O, Horch S, Nielsen JH, Sehested J, Rostrup-Nielsen JR, Nørskov JK and Chorkendorff I, J. Catal, 2008, 255, 6–19.
240. Tong H, Ouyang S, Bi Y, Umezawa N, Oshikiri M and Ye J, Adv. Mater, 2012, 24, 229–251. [PubMed: 21972044]
241. Cao S, Low J, Yu J and Jaroniec M, Adv. Mater, 2015, 27, 2150–2176. [PubMed: 25704586]
242. Zhang L, Jia Y, Wang S, Li Z, Ji C, Wei J, Zhu H, Wang K, Wu D, Shi E, Fang Y and Cao A, Nano Lett, 2010, 10, 3583–3589. [PubMed: 20715803]
243. Armstrong AR, Armstrong G, Canales J, García R and Bruce PG, Adv. Mater, 2005, 17, 862–865.
244. Yang HG, Liu G, Qiao SZ, Sun CH, Jin YG, Smith SC, Zou J, Cheng HM and Lu GQ, J. Am. Chem. Soc, 2009, 131, 4078–4083. [PubMed: 19249825]
245. Awazu K, Fujimaki M, Rockstuhl C, Tominaga J, Murakami H, Ohki Y, Yoshida N and Watanabe T, J. Am. Chem. Soc, 2008, 130, 1676–1680. [PubMed: 18189392]
246. Li YF and Liu ZP, J. Am. Chem. Soc, 2011, 133, 15743–15752. [PubMed: 21879719]
247. Dinh CT, Nguyen TD, Kleitz F and Do TO, ACS Nano, 2009, 3, 3737–3743. [PubMed: 19807108]
248. Chen X and Mao SS, Chem. Rev, 2007, 107, 2891–2959. [PubMed: 17590053]
249. Dai Y, Cobley CM, Zeng J, Sun Y and Xia Y, Nano Lett, 2009, 9, 2455–2459. [PubMed: 19438191]
250. Roy N, Sohn Y and Pradhan D, ACS Nano, 2013, 7, 2532–2540. [PubMed: 23448713]
251. Yu J, Low J, Xiao W, Zhou P and Jaroniec M, J. Am. Chem. Soc, 2014, 136, 8839–8842. [PubMed: 24918628]
252. Mishra YK, Modi G, Cretu V, Postica V, Lupan O, Reimer T, Paulowicz I, Hrkac V, Benecke W, Kienle L and Adelung R, ACS Appl. Mater. Interfaces, 2015, 7, 14303–14316. [PubMed: 26050666]
253. Chetia TR, Ansari MS and Qureshi M, ACS Appl. Mater. Interfaces, 2015, 7, 13266–13279. [PubMed: 25966867]
254. Wang L, Liu S, Wang Z, Zhou Y, Qin Y and Wang ZL, ACS Nano, 2016, 10, 2636–2643. [PubMed: 26745209]
255. Pan L, Muhammad T, Ma L, Huang Z-F, Wang S, Wang L, Zou J-J and Zhang X, Appl. Catal., B, 2016, 189, 181–191.
256. Zhou L, Wang W, Xu H, Sun S and Shang M, Chemistry, 2009, 15, 1776–1782. [PubMed: 19115297]

257. Jang NH, Suh JS and Moskovits M, J. Phys. Chem. B, 1997, 101, 8279–8285.
258. Wang P, Huang B, Qin X, Zhang X, Dai Y, Wei J and Whangbo MH, Angew. Chem. Int. Ed, 2008, 47, 7931–7933.
259. Linic S, Christopher P and Ingram DB, Nature Materials, 2011, 10, 911. [PubMed: 22109608]
260. Bi Y, Ouyang S, Umezawa N, Cao J and Ye J, J. Am. Chem. Soc, 2011, 133, 6490–6492. [PubMed: 21486031]
261. Ahmed B, Kumar S, Kumar S and Ojha AK, J. Alloys Compd, 2016, 679, 324–334.
262. Costi R, Saunders AE, Elmalem E, Salant A and Banin U, Nano Lett, 2008, 8, 637–641. [PubMed: 18197720]
263. Debe MK, Nature, 2012, 486, 43. [PubMed: 22678278]
264. Roldan Cuenya B, Acc. Chem. Res, 2013, 46, 1682–1691. [PubMed: 23252675]
265. Chen C, Kang Y, Huo Z, Zhu Z, Huang W, Xin HL, Snyder JD, Li D, Herron JA, Mavrikakis M, Chi M, More KL, Li Y, Markovic NM, Somorjai GA, Yang P and Stamenkovic VR, Science, 2014, 343, 1339–1343. [PubMed: 24578531]
266. Bu L, Zhang N, Guo S, Zhang X, Li J, Yao J, Wu T, Lu G, Ma JY, Su D and Huang X, Science, 2016, 354, 1410–1414. [PubMed: 27980207]
267. Crespo-Quesada M, Andanson JM, Yarulin A, Lim B, Xia Y and Kiwi-Minsker L, Langmuir, 2011, 27, 7909–7916. [PubMed: 21591816]
268. Crespo-Quesada M, Yarulin A, Jin M, Xia Y and Kiwi-Minsker L, J. Am. Chem. Soc, 2011, 133, 12787–12794. [PubMed: 21749155]
269. Shao M, Yu T, Odell JH, Jin M and Xia Y, Chem. Commun, 2011, 47, 6566–6568.
270. Lim B, Kobayashi H, Camargo PHC, Allard LF, Liu J and Xia Y, Nano Res, 2010, 3, 180–188.
271. Liu S, Tao H, Zeng L, Liu Q, Xu Z, Liu Q and Luo JL, J. Am. Chem. Soc, 2017, 139, 2160–2163. [PubMed: 28150946]
272. Xie Y, He W, Li F, Perera TS, Gan L, Han Y, Wang X, Li S and Dai H, ACS Appl. Mater. Interfaces, 2016, 8, 10212–10219. [PubMed: 27043792]
273. Huang X, Song J, Yung BC, Huang X, Xiong Y and Chen X, Chem. Soc. Rev, 2018, 47, 2873–2920. [PubMed: 29568836]
274. Yang Y, Zhao Q, Feng W and Li F, Chem. Rev, 2013, 113, 192–270. [PubMed: 22702347]
275. Liu Z, Qi W and Xu G, Chem. Soc. Rev, 2015, 44, 3117–3142. [PubMed: 25803228]
276. Rosso-Vasic M, Spruijt E, Popović Z, Overgaag K, van Lagen B, Grandidier B, Vanmaekelbergh D, Domínguez-Gutiérrez D, De Cola L and Zuilhof H, J. Mater. Chem, 2009, 19, 5926.
277. von Haartman E, Jiang H, Khomich AA, Zhang J, Burikov SA, Dolenko TA, Ruokolainen J, Gu H, Shenderova OA, Vlasov II and Rosenholm JM, J. Mater. Chem. B, 2013, 1, 2358.
278. Kim J, Kim HS, Lee N, Kim T, Kim H, Yu T, Song IC, Moon WK and Hyeon T, Angew. Chem, 2008, 120, 8566–8569.
279. Pandey S, Thakur M, Mewada A, Anjarlekar D, Mishra N and Sharon M, J. Mater. Chem. B, 2013, 1, 4972.
280. Yu K, Ng P, Ouyang J, Zaman MB, Abulrob A, Baral TN, Fatehi D, Jakubek ZJ, Kingston D, Wu X, Liu X, Hebert C, Leek DM and Whitfield DM, ACS Appl. Mater. Interfaces, 2013, 5, 2870–2880. [PubMed: 23486927]
281. Xu H, Li Q, Wang L, He Y, Shi J, Tang B and Fan C, Chem. Soc. Rev, 2014, 43, 2650–2661. [PubMed: 24394966]
282. Michalet X, Pinaud FF, Bentolila LA, Tsay JM, Doose S, Li JJ, Sundaresan G, Wu AM, Gambhir SS and Weiss S, Science, 2005, 307, 538–544. [PubMed: 15681376]
283. Pinaud F, Clarke S, Sittner A and Dahan M, Nat. Methods, 2010, 7, 275. [PubMed: 20354518]
284. Ha HD, Jang M-H, Liu F, Cho Y-H and Seo TS, Carbon, 2015, 81, 367–375.
285. Li J and Zhu JJ, Analyst, 2013, 138, 2506–2515. [PubMed: 23518695]
286. Yong KT, Ding H, Roy I, Law WC, Bergey EJ, Maitra A and Prasad PN, ACS Nano, 2009, 3, 502–510. [PubMed: 19243145]
287. Chang J-Y, Wang G-Q, Cheng C-Y, Lin W-X and Hsu J-C, J. Mater. Chem, 2012, 22, 10609.
288. Wolfbeis OS, Chem. Soc. Rev, 2015, 44, 4743–4768. [PubMed: 25620543]

289. Yong KT, Hu R, Roy I, Ding H, Vathy LA, Bergey EJ, Mizuma M, Maitra A and Prasad PN, ACS Appl. Mater. Interfaces, 2009, 1, 710–719. [PubMed: 20160901]
290. Kumar R, Ding H, Hu R, Yong K-T, Roy I, Bergey EJ and Prasad PN, Chem. Mater, 2010, 22, 2261–2267.
291. Niu WJ, Shan D, Zhu RH, Deng SY, Cosnier S and Zhang XJ, Carbon, 2016, 96, 1034–1042.
292. Sivun D, Vidal C, Munkhbat B, Arnold N, Klar TA and Hrelescu C, Nano Lett, 2016, 16, 7203–7209. [PubMed: 27700125]
293. Zaman MB, Baral TN, Zhang J, Whitfield D and Yu K, J. Mater. Chem. C, 2008, 113, 496–499.
294. Jung S and Chen X, Adv. Healthcare Mater, 2018, 7, 1800252.
295. Shao A, Xie Y, Zhu S, Guo Z, Zhu S, Guo J, Shi P, James TD, Tian H and Zhu WH, Angew. Chem. Int. Ed, 2015, 54, 7275–7280.
296. Wang M, Xu Y, Liu Y, Gu K, Tan J, Shi P, Yang D, Guo Z, Zhu W, Guo X and Cohen Stuart MA, ACS Appl. Mater. Interfaces, 2018, 10, 25186–25193. [PubMed: 29975045]
297. Tsang MK, Bai G and Hao J, Chem. Soc. Rev, 2015, 44, 1585–1607. [PubMed: 25200182]
298. Zhou J, Liu Q, Feng W, Sun Y and Li F, Chem. Rev, 2015, 115, 395–465. [PubMed: 25492128]
299. Haase M and Schafer H, Angew. Chem. Int. Ed, 2011, 50, 5808–5829.
300. Zhou J, Liu Z and Li F, Chem. Soc. Rev, 2012, 41, 1323–1349. [PubMed: 22008740]
301. Liu C, Wang H, Zhang X and Chen D, J. Mater. Chem, 2009, 19, 489–496.
302. Li Z and Zhang Y, Nanotechnology, 2008, 19, 345606.
303. Zeng S, Wang H, Lu W, Yi Z, Rao L, Liu H and Hao J, Biomaterials, 2014, 35, 2934–2941. [PubMed: 24406214]
304. Liu Q, Chen M, Sun Y, Chen G, Yang T, Gao Y, Zhang X and Li F, Biomaterials, 2011, 32, 8243–8253. [PubMed: 21820170]
305. Sun Y, Yu M, Liang S, Zhang Y, Li C, Mou T, Yang W, Zhang X, Li B, Huang C and Li F, Biomaterials, 2011, 32, 2999–3007. [PubMed: 21295345]
306. Gai S, Yang P, Li C, Wang W, Dai Y, Niu N and Lin J, Adv. Funct. Mater, 2010, 20, 1166–1172.
307. Liu Q, Sun Y, Li C, Zhou J, Li C, Yang T, Zhang X, Yi T, Wu D and Li F, ACS Nano, 2011, 5, 3146–3157. [PubMed: 21384900]
308. Wu L, Mendoza-Garcia A, Li Q and Sun S, Chem. Rev, 2016, 116, 10473–10512. [PubMed: 27355413]
309. Gallo J, Long NJ and Aboagye EO, Chem. Soc. Rev, 2013, 42, 7816–7833. [PubMed: 23788179]
310. Lee N and Hyeon T, Chem. Soc. Rev, 2012, 41, 2575–2589. [PubMed: 22138852]
311. Ho D, Sun X and Sun S, Acc. Chem. Res, 2011, 44, 875–882. [PubMed: 21661754]
312. Reddy LH, Arias JL, Nicolas J and Couvreur P, Chem. Rev, 2012, 112, 5818–5878. [PubMed: 23043508]
313. Angelovski G, Acc. Chem. Res, 2017, 50, 2215–2224. [PubMed: 28841293]
314. Park JY, Baek MJ, Choi ES, Woo S, Kim JH, Kim TJ, Jung JC, Chae KS, Chang Y and Lee GH, ACS Nano, 2009, 3, 3663–3669. [PubMed: 19835389]
315. Na HB, Lee JH, An K, Park YI, Park M, Lee IS, Nam D-H, Kim ST, Kim S-H, Kim S-W, Lim K-H, Kim K-S, Kim S-O and Hyeon T, Angew. Chem, 2007, 119, 5493–5497.
316. Rieter WJ, Taylor KML, An H, Lin W and Lin W, J. Am. Chem. Soc, 2006, 128, 9024–9025. [PubMed: 16834362]
317. Lin LS, Song J, Song L, Ke K, Liu Y, Zhou Z, Shen Z, Li J, Yang Z, Tang W, Niu G, Yang HH and Chen X, Angew. Chem. Int. Ed, 2018, 57, 4902–4906.
318. Shen Z, Song J, Zhou Z, Yung BC, Aronova MA, Li Y, Dai Y, Fan W, Liu Y, Li Z, Ruan H, Leapman RD, Lin L, Niu G, Chen X and Wu A, Adv. Mater, 2018, 30, 1803163.
319. Yang J, Lee CH, Ko HJ, Suh JS, Yoon HG, Lee K, Huh YM and Haam S, Angew. Chem. Int. Ed, 2007, 46, 8836–8839.
320. Huang G, Hu J, Zhang H, Zhou Z, Chi X and Gao J, Nanoscale, 2014, 6, 726–730. [PubMed: 24287667]
321. Johnson NJJ, Oakden W, Stanisz GJ, Scott Prosser R and van Veggel FCJM, Chem. Mater, 2011, 23, 3714–3722.

322. Kim J, Lee JE, Lee SH, Yu JH, Lee JH, Park TG and Hyeon T, Adv. Mater, 2008, 20, 478–483.
323. Yang H, Zhuang Y, Sun Y, Dai A, Shi X, Wu D, Li F, Hu H and Yang S, Biomaterials, 2011, 32, 4584–4593. [PubMed: 21458063]
324. Yang L, Zhou Z, Liu H, Wu C, Zhang H, Huang G, Ai H and Gao J, Nanoscale, 2015, 7, 6843–6850. [PubMed: 25806860]
325. Zhou Z, Huang D, Bao J, Chen Q, Liu G, Chen Z, Chen X and Gao J, Adv. Mater, 2012, 24, 6223–6228. [PubMed: 22972529]
326. Smith BR and Gambhir SS, Chem. Rev, 2017, 117, 901–986. [PubMed: 28045253]
327. Lee N, Yoo D, Ling D, Cho MH, Hyeon T and Cheon J, Chem. Rev, 2015, 115, 10637–10689. [PubMed: 26250431]
328. Zhou Z, Yang L, Gao J and Chen X, Adv. Mater, 2019, 31, 1804567.
329. Na HB, Song IC and Hyeon T, Adv. Mater, 2009, 21, 2133–2148.
330. Kim BH, Lee N, Kim H, An K, Park YI, Choi Y, Shin K, Lee Y, Kwon SG, Na HB, Park JG, Ahn TY, Kim YW, Moon WK, Choi SH and Hyeon T, J. Am. Chem. Soc, 2011, 133, 12624–12631. [PubMed: 21744804]
331. Manus LM, Mastarone DJ, Waters EA, Zhang XQ, Schultz-Sikma EA, Macrenaris KW, Ho D and Meade TJ, Nano Lett, 2010, 10, 484–489. [PubMed: 20038088]
332. Park M, Lee N, Choi SH, An K, Yu S-H, Kim JH, Kwon S-H, Kim D, Kim H, Baek S-I, Ahn T-Y, Park OK, Son JS, Sung Y-E, Kim Y-W, Wang Z, Pinna N and Hyeon T, Chem. Mater, 2011, 23, 3318–3324.
333. Lei M, Fu C, Cheng X, Fu B, Wu N, Zhang Q, Fu A, Cheng J, Gao J and Zhao Z, Adv. Funct. Mater, 2017, 27, 1700978.
334. Zhao Z, Bao J, Fu C, Lei M and Cheng J, Chem. Mater, 2017, 29, 10455–10468.
335. Zhou Z, Zhao Z, Zhang H, Wang Z, Chen X, Wang R, Chen Z and Gao J, ACS Nano, 2014, 8, 7976–7985. [PubMed: 25093532]
336. Zhou Z, Wu C, Liu H, Zhu X, Zhao Z, Wang L, Xu Y, Ai H and Gao J, ACS Nano, 2015, 9, 3012–3022. [PubMed: 25670480]
337. Yang L, Wang Z, Ma L, Li A, Xin J, Wei R, Lin H, Wang R, Chen Z and Gao J, ACS Nano, 2018, 12, 4605–4614. [PubMed: 29672022]
338. Huang G, Li H, Chen J, Zhao Z, Yang L, Chi X, Chen Z, Wang X and Gao J, Nanoscale, 2014, 6, 10404–10412. [PubMed: 25079966]
339. Jang JT, Nah H, Lee JH, Moon SH, Kim MG and Cheon J, Angew. Chem. Int. Ed, 2009, 48, 1234–1238.
340. Lee J-H, Huh Y-M, Jun Y.-w., Seo J.-w., Jang J.-t., Song H-T, Kim S, Cho E-J, Yoon H-G, Suh J-S and Cheon J, Nat. Med, 2006, 13, 95. [PubMed: 17187073]
341. Yang L, Ma L, Xin J, Li A, Sun C, Wei R, Ren BW, Chen Z, Lin H and Gao J, Chem. Mater, 2017, 29, 3038–3047.
342. Zhou Z, Tian R, Wang Z, Yang Z, Liu Y, Liu G, Wang R, Gao J, Song J, Nie L and Chen X, Nat. Commun, 2017, 8, 15468. [PubMed: 28516947]
343. Zhao Z, Chi X, Yang L, Yang R, Ren BW, Zhu X, Zhang P and Gao J, Chem. Mater, 2016, 28, 3497–3506.
344. Yang L, Sun C, Lin H, Gong X, Zhou T, Deng W-T, Chen Z and Gao J, Chem. Mater, 2019, 31, 1381–1390.
345. Sathya A, Guardia P, Brescia R, Silvestri N, Pugliese G, Nitti S, Manna L and Pellegrino T, Chem. Mater, 2016, 28, 1769–1780.
346. Qiu L, Chen T, Ocsoy I, Yasun E, Wu C, Zhu G, You M, Han D, Jiang J, Yu R and Tan W, Nano Lett, 2015, 15, 457–463. [PubMed: 25479133]
347. Yu G, Yu S, Saha ML, Zhou J, Cook TR, Yung BC, Chen J, Mao Z, Zhang F, Zhou Z, Liu Y, Shao L, Wang S, Gao C, Huang F, Stang PJ and Chen X, Nat. Commun, 2018, 9, 4335. [PubMed: 30337535]
348. Cheng L, Wang C, Feng L, Yang K and Liu Z, Chem. Rev, 2014, 114, 10869–10939. [PubMed: 25260098]

349. Rengan AK, Bukhari AB, Pradhan A, Malhotra R, Banerjee R, Srivastava R and De A, Nano Lett, 2015, 15, 842–848. [PubMed: 25554860]
350. Dreaden EC, Alkilany AM, Huang X, Murphy CJ and El-Sayed MA, Chem. Soc. Rev, 2012, 41, 2740–2779. [PubMed: 22109657]
351. Loo C, Lowery A, Halas N, West J and Drezek R, Nano Lett, 2005, 5, 709–711. [PubMed: 15826113]
352. Lu W, Xiong C, Zhang G, Huang Q, Zhang R, Zhang JZ and Li C, Clin. Cancer. Res, 2009, 15, 876–886. [PubMed: 19188158]
353. Song J, Yang X, Jacobson O, Huang P, Sun X, Lin L, Yan X, Niu G, Ma Q and Chen X, Adv. Mater, 2015, 27, 4910–4917. [PubMed: 26198622]
354. Liu Y, Yang Z, Huang X, Yu G, Wang S, Zhou Z, Shen Z, Fan W, Liu Y, Davisson M, Kalish H, Niu G, Nie Z and Chen X, ACS Nano, 2018, 12, 8129–8137. [PubMed: 30001110]
355. Kim J-W, Galanzha EI, Shashkov EV, Moon H-M and Zharov VP, Nat. Nanotechnol, 2009, 4, 688. [PubMed: 19809462]
356. Li W, Zamani R, Rivera Gil P, Pelaz B, Ibanez M, Cadavid D, Shavel A, Alvarez-Puebla RA, Parak WJ, Arbiol J and Cabot A, J. Am. Chem. Soc, 2013, 135, 7098–7101. [PubMed: 23647089]
357. Nel AE, Mädler L, Velegol D, Xia T, Hoek EMV, Somasundaran P, Klaessig F, Castranova V and Thompson M, Nat. Mater, 2009, 8, 543. [PubMed: 19525947]
358. Manshian BB, Himmelreich U and Soenen SJ, Chem. Res. Toxicol, 2017, 30, 595–603. [PubMed: 27982583]
359. Bhamidipati M and Fabris L, Bioconj. Chem, 2017, 28, 449–460.
360. Wang S, Lu W, Tovmachenko O, Rai US, Yu H and Ray PC, Chem. Phys. Lett, 2008, 463, 145–149. [PubMed: 24068836]
361. Yu T, Malugin A and Ghandehari H, ACS Nano, 2011, 5, 5717–5728. [PubMed: 21630682]
362. Hamilton RF, Wu N, Porter D, Buford M, Wolfarth M and Holian A, Part. Fibre. Toxicol, 2009, 6, 35. [PubMed: 20043844]
363. Stoehr LC, Gonzalez E, Stampfl A, Casals E, Duschl A, Puntes V and Oostingh GJ, Part. Fibre. Toxicol, 2011, 8, 36. [PubMed: 22208550]
364. Brown DM, Kinloch IA, Bangert U, Windle AH, Walter DM, Walker GS, Scotchford CA, Donaldson K and Stone V, Carbon, 2007, 45, 1743–1756.
365. Tay CY, Cai P, Setyawati MI, Fang W, Tan LP, Hong CH, Chen X and Leong DT, Nano Lett, 2014, 14, 83–88. [PubMed: 24313755]
366. Garcia-Hevia L, Valiente R, Fernandez-Luna JL, Flahaut E, Rodriguez-Fernandez L, Villegas JC, Gonzalez J and Fanarraga ML, Adv. Healthcare Mater, 2015, 4, 1640–1644.
367. Gonzalez L, De Santis Puzzonia M, Ricci R, Aureli F, Guarguaglini G, Cubadda F, Leyns L, Cundari E and Kirsch-Volders M, Nanotoxicology, 2015, 9, 729–736. [PubMed: 25325157]
368. Huang X, Teng X, Chen D, Tang F and He J, Biomaterials, 2010, 31, 438–448. [PubMed: 19800115]
369. Xie X, Liao J, Shao X, Li Q and Lin Y, Sci. Rep, 2017, 7, 3827. [PubMed: 28630477]
370. Chithrani BD, Ghazani AA and Chan WCW, Nano Lett, 2006, 6, 662–668. [PubMed: 16608261]
371. Wang Z, Zhang J, Ekman JM, Kenis PJA and Lu Y, Nano Lett, 2010, 10, 1886–1891. [PubMed: 20405820]
372. Donaldson K, Poland CA, Murphy FA, MacFarlane M, Chernova T and Schinwald A, Adv. Drug Deliv. Rev, 2013, 65, 2078–2086. [PubMed: 23899865]
373. C. A. Poland, R. Duffin, I. Kinloch, A. Maynard, Wallace WAH, Seaton A, Stone V, Brown S, MacNee W and Donaldson K, Nat. Nanotechnol, 2008, 3, 423. [PubMed: 18654567]
374. Liu Z, Cai W, He L, Nakayama N, Chen K, Sun X, Chen X and Dai H, Nat. Nanotechnol, 2006, 2, 47. [PubMed: 18654207]
375. Moore TL, Pitzer JE, Podila R, Wang X, Lewis RL, Grimes SW, Wilson JR, Skjervold E, Brown JM, Rao A and Alexis F, Part. Part. Syst. Charact, 2013, 30, 365–373. [PubMed: 27642231]

376. Liu Z, Davis C, Cai W, He L, Chen X and Dai H, Proc. Natl. Acad. Sci. U. S. A, 2008, 105, 1410–1415. [PubMed: 18230737]

377. Schipper ML, Nakayama-Ratchford N, Davis CR, Kam NWS, Chu P, Liu Z, Sun X, Dai H and Gambhir SS, Nat. Nanotechnol, 2008, 3, 216. [PubMed: 18654506]

378. Peer D, Karp JM, Hong S, Farokhzad OC, Margalit R and Langer R, Nat. Nanotechnol, 2007, 2, 751. [PubMed: 18654426]

379. Prabhakar U, Maeda H, Jain RK, Sevick-Muraca EM, Zamboni W, Farokhzad OC, Barry ST, Gabizon A, Grodzinski P and Blakey DC, Cancer Res, 2013, 73, 2412–2417. [PubMed: 23423979]

380. Huynh E and Zheng G, Nanomedicine, 2015, 10, 1993–1995. [PubMed: 26096565]

381. Kolhar P, Anselmo AC, Gupta V, Pant K, Prabhakarpandian B, Ruoslahti E and Mitragotri S, Proc. Natl. Acad. Sci. U. S. A, 2013, 110, 10753–10758. [PubMed: 23754411]

382. Anselmo AC, Modery-Pawlowski CL, Menegatti S, Kumar S, Vogus DR, Tian LL, Chen M, Squires TM, Sen Gupta A and Mitragotri S, ACS Nano, 2014, 8, 11243–11253. [PubMed: 25318048]

383. Niikura K, Matsunaga T, Suzuki T, Kobayashi S, Yamaguchi H, Orba Y, Kawaguchi A, Hasegawa H, Kajino K, Ninomiya T, Ijiro K and Sawa H, ACS Nano, 2013, 7, 3926–3938. [PubMed: 23631767]

384. Chauhan VP, Popovic Z, Chen O, Cui J, Fukumura D, Bawendi MG and Jain RK, Angew. Chem. Int. Ed, 2011, 50, 11417–11420.

385. Christian DA, Cai S, Garbuzenko OB, Harada T, Zajac AL, Minko T and Discher DE, Mol. Pharm, 2009, 6, 1343–1352. [PubMed: 19249859]

386. Huang C, Butler PJ, Tong S, Muddana HS, Bao G and Zhang S, Nano Lett, 2013, 13, 1611–1615. [PubMed: 23484640]

387. Yu M, Wang J, Yang Y, Zhu C, Su Q, Guo S, Sun J, Gan Y, Shi X and Gao H, Nano Lett, 2016, 16, 7176–7182. [PubMed: 27700115]

388. Decuzzi P, Godin B, Tanaka T, Lee SY, Chiappini C, Liu X and Ferrari M, J. Control. Release, 2010, 141, 320–327. [PubMed: 19874859]

389. Black KC, Wang Y, Luehmann HP, Cai X, Xing W, Pang B, Zhao Y, Cutler CS, Wang LV, Liu Y and Xia Y, ACS Nano, 2014, 8, 4385–4394. [PubMed: 24766522]

390. Godin B, Chiappini C, Srinivasan S, Alexander JF, Yokoi K, Ferrari M, Decuzzi P and Liu X, Adv. Funct. Mater, 2012, 22, 4225–4235. [PubMed: 23227000]

391. Mittal A, Schulze K, Ebensen T, Weissmann S, Hansen S, Guzman CA and Lehr CM, J. Control Release, 2015, 206, 140–152. [PubMed: 25795506]

392. Mittal A, Schulze K, Ebensen T, Weissmann S, Hansen S, Lehr CM and Guzman CA, Nanomedicine, 2015, 11, 147–154. [PubMed: 25200611]

393. Mittal A, Raber AS, Schaefer UF, Weissmann S, Ebensen T, Schulze K, Guzman CA, Lehr CM and Hansen S, Vaccine, 2013, 31, 3442–3451. [PubMed: 23290836]

394. Geng Y, Dalhaimer P, Cai S, Tsai R, Tewari M, Minko T and Discher DE, Nat. Nanotechnol, 2007, 2, 249. [PubMed: 18654271]

395. Huang X, Li L, Liu T, Hao N, Liu H, Chen D and Tang F, ACS Nano, 2011, 5, 5390–5399. [PubMed: 21634407]

396. Arnida M. Janat-Amsbury M, Ray A, Peterson CM and Ghandehari H, Eur. J. Pharm. Biopharm, 2011, 77, 417–423. [PubMed: 21093587]

397. Lee T-R, Choi M, Kopacz AM, Yun S-H, Liu WK and Decuzzi P, Sci. Rep, 2013, 3, 2079. [PubMed: 23801070]

398. Park JH, von Maltzahn G, Zhang L, Schwartz MP, Ruoslahti E, Bhatia SN and Sailor MJ, Adv. Mater, 2008, 20, 1630–1635. [PubMed: 21687830]

399. Akiyama Y, Mori T, Katayama Y and Niidome T, Nanoscale Res. Lett, 2012, 7, 565. [PubMed: 23050635]

400. Shukla S, Wen AM, Ayat NR, Commandeur U, Gopalkrishnan R, Broome AM, Lozada KW, Keri RA and Steinmetz NF, Nanomedicine, 2014, 9, 221–235. [PubMed: 23834501]

401. Pombo Garcia K, Zarschler K, Barbaro L, Barreto JA, O'Malley W, Spiccia L, Stephan H and Graham B, Small, 2014, 10, 2516–2529. [PubMed: 24687857]

402. Perez-Campana C, Gomez-Vallejo V, Puigivila M, Martin A, Calvo-Fernandez T, Moya SE, Ziolo RF, Reese T and Llop J, ACS Nano, 2013, 7, 3498–3505. [PubMed: 23473535]

403. De Jong WH, Hagens WI, Krystek P, Burger MC, Sips AJ and Geertsma RE, Biomaterials, 2008, 29, 1912–1919. [PubMed: 18242692]

404. Soo Choi H, Liu W, Misra P, Tanaka E, Zimmer JP, Itty Ipe B, Bawendi MG and Frangioni JV, Nat. Biotechnol, 2007, 25, 1165. [PubMed: 17891134]

405. Ruggiero A, Villa CH, Bander E, Rey DA, Bergkvist M, Batt CA, Manova-Todorova K, Deen WM, Scheinberg DA and McDevitt MR, Proc. Natl. Acad. Sci. U. S. A, 2010, 107, 12369–12374. [PubMed: 20566862]

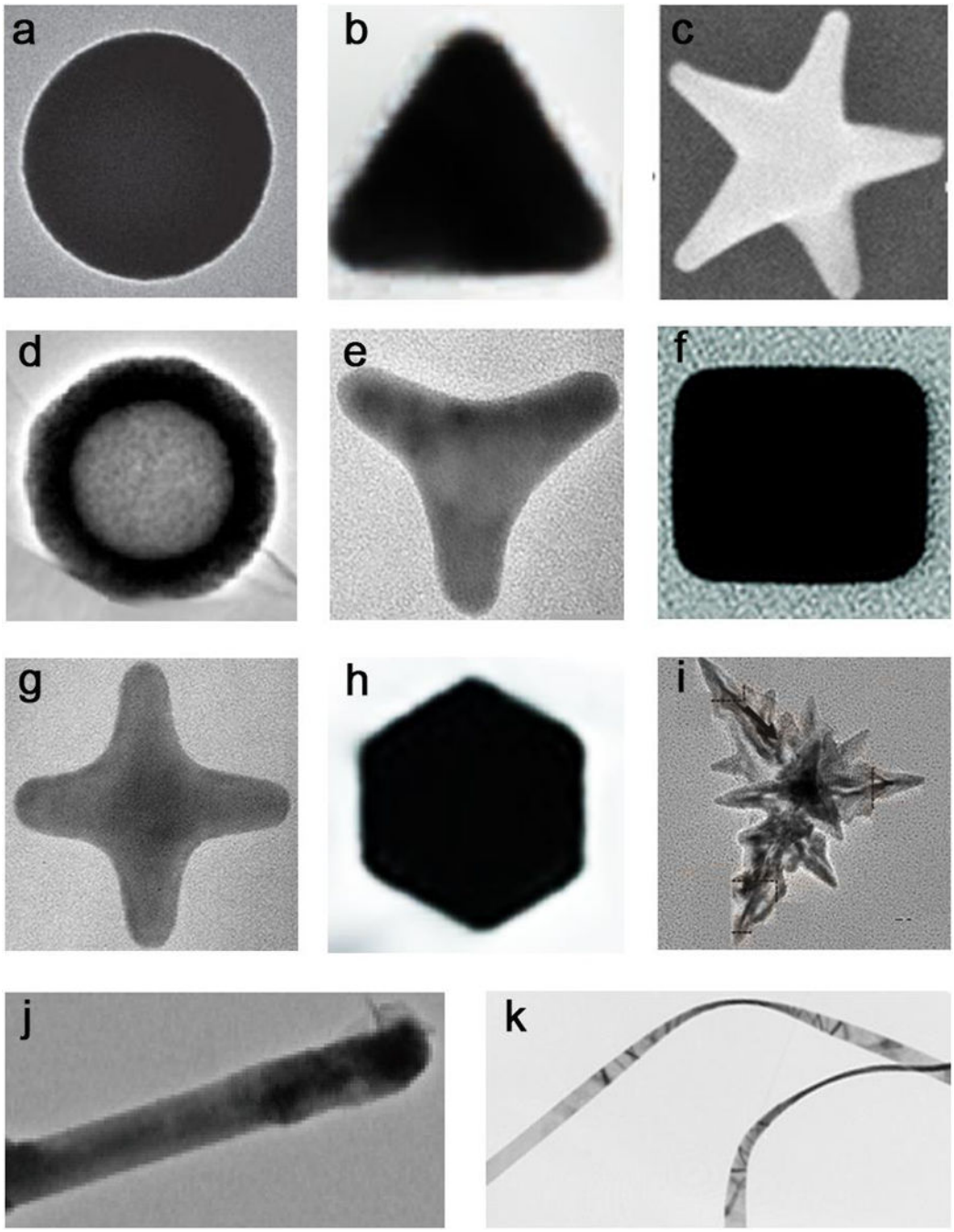

Figure 1.

(a) NiCo sphere, (b) Au triangle, (c) Au star, (d) hollow TiO_2/GC, (e) Au tripod, (f) Ag cube, (g) Au tetrapod, (h) PtPb hexagon, (i) Fe_3O_4 branches, (j) MoS_2/CdS rod, (k) Au belt. Reproduced with permission from refs 4–13. (a) Reprinted with permission from ref 4, copyright 2015 Nature Publishing Group. (b, c) Adapted by permission from refs 5 and 6, copyright 2017 and 2008 Wiley-VCH. (d, e, f, g, i, j, m, and k) Reproduced with permission from refs 7, 8, 9, 11, 12, and 13, copyright 2015, 2003, 2010, 2015, 2016, and 2008 American Chemical Society, respectively. (h) Adapted with permission from ref 10,

copyright 2016 American Association for the Advancement of Science. The backgrounds of some figures are removed for clarity, details for original images and scale bars please see the relevant references.

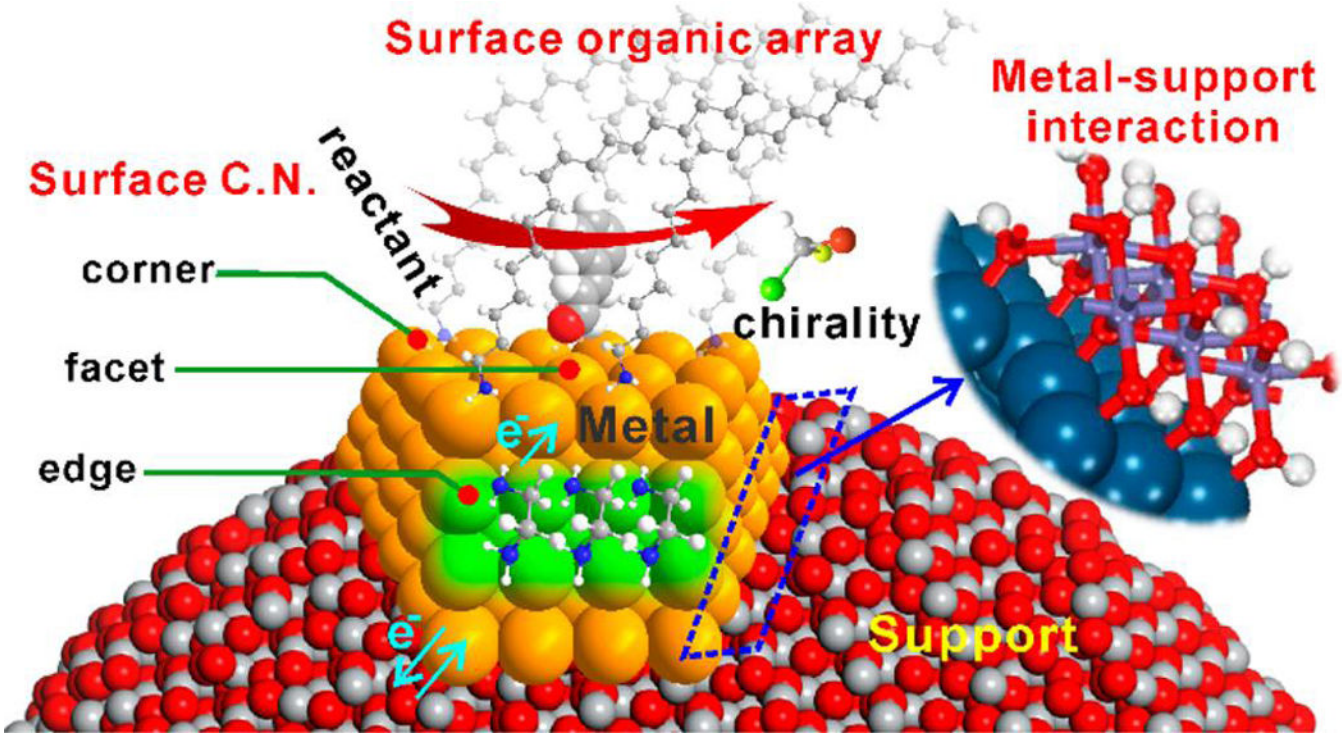

Figure 2.

Coordination chemistry on the surface or interface of metal NPs: surface coordination number, surface organic array, metal-support interaction, electronic effect, and so on. The distribution of these coordination sites on the surface is often dependent on NP shape which can tailor the overall catalysis, especially selectivity. Reprinted with permission from ref 54, copyright 2017 American Chemical Society.

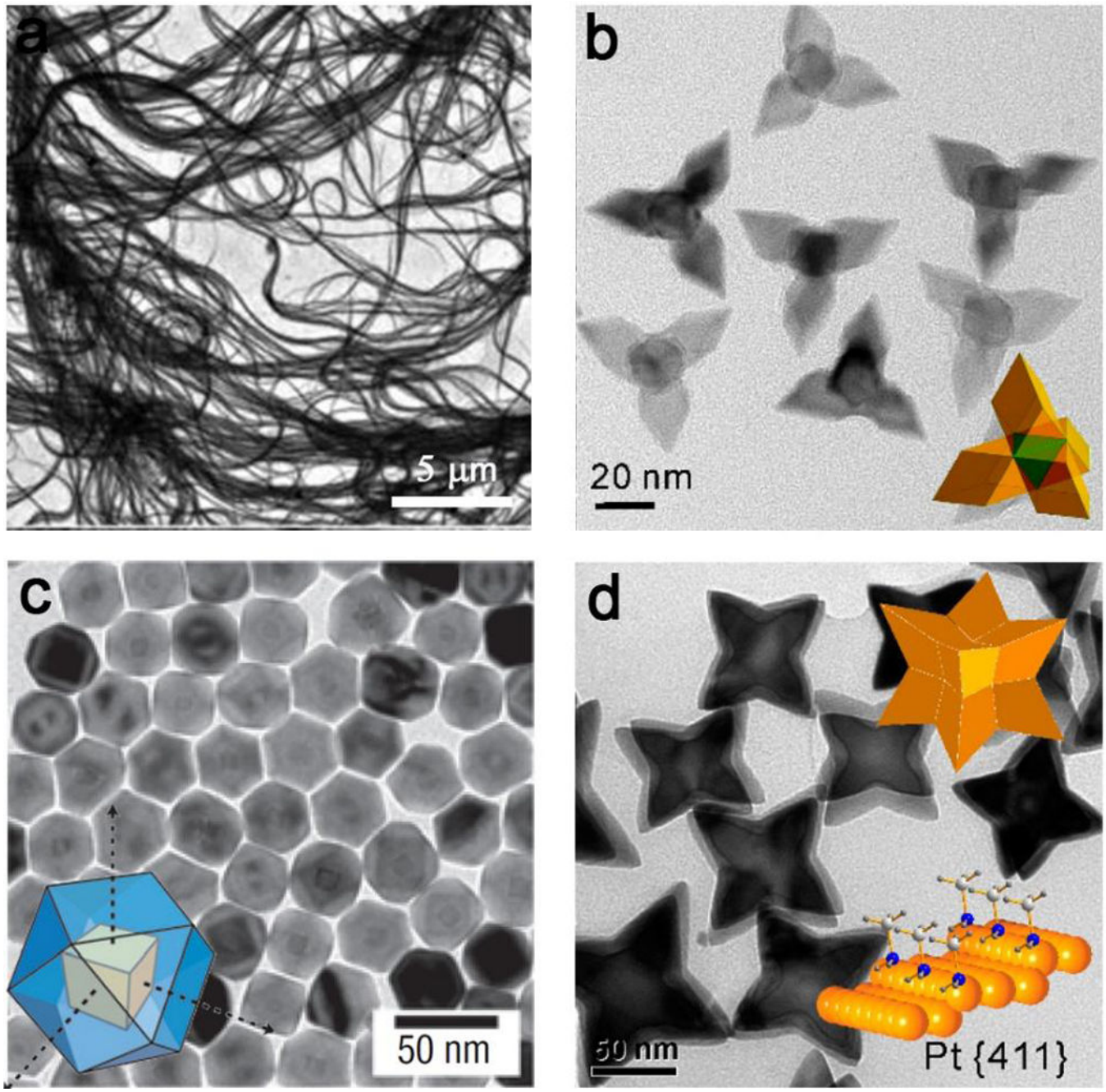

Figure 3.

The effect of surface coordination of small ligands on the shape-controlled synthesis of metal nanocrystals. (a) Au nanowires made by the bonding of CO. (b) Pd tetrapods formed by the use of CO and H_2; (c) Pt/Pd core–shell cuboctahedra by direct growth of Pd on Pt nanocubes achieved with the addition of NO_2. (d) Amine-assisted formation of Pt octapods enclosed by high-index {411} facets. The scale bars in (a-d) are 5 μm, 20 nm, 50 nm and 50 nm, respectively. (a) Reprinted with permission from ref 77, copyright 2010 Royal Society of Chemistry. (b) and (d) Reproduced with permission from refs 78 and 80, copyright 2012

and 2011 American Chemical Society. (c) Reproduced with permission from ref 79, copyright 2007 Nature Publishing Group.

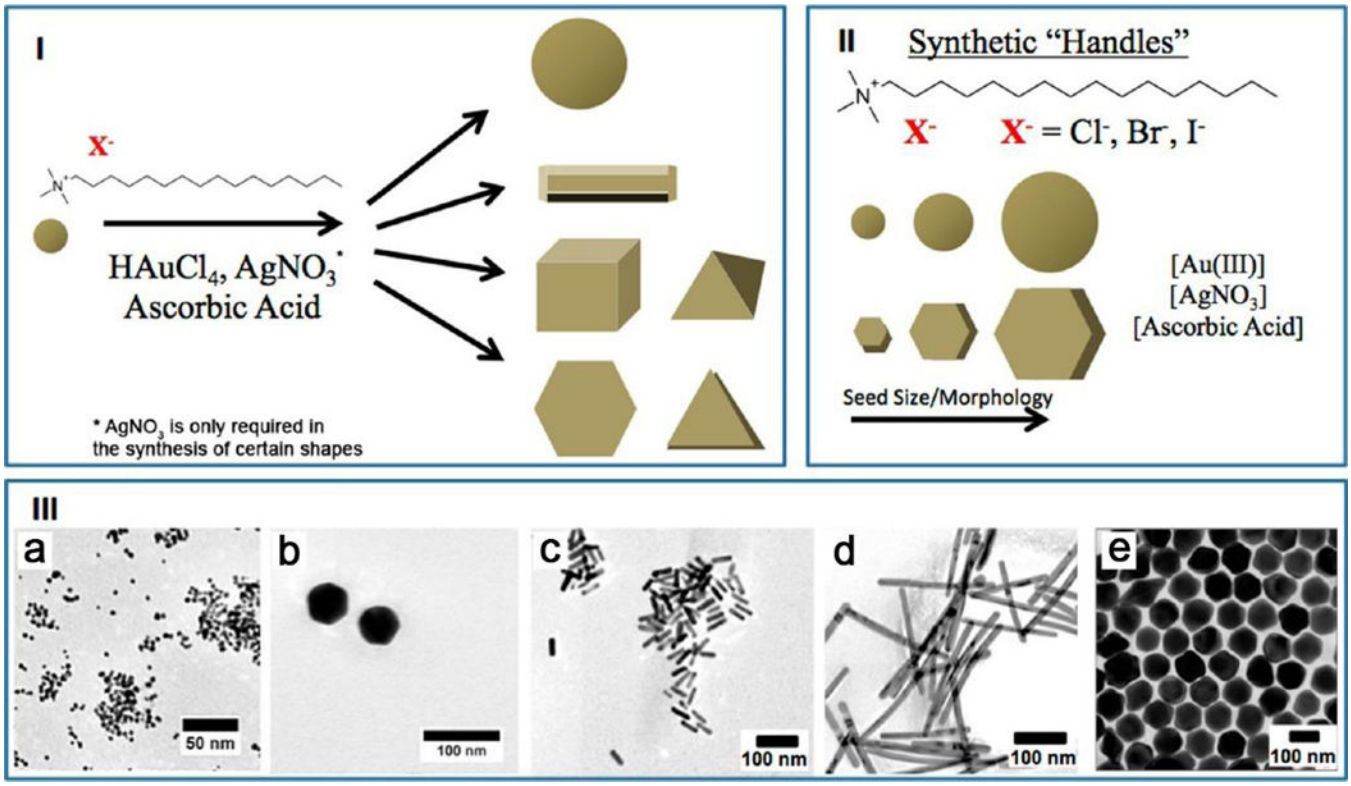

Figure 4.

Several capping agents used to prepare Au NPs with a wide variety of shapes. (I) The general conditions for synthesizing anisotropic Au NPs. (II) A variety of reagents can be employed to change the shape of Au NPs, which provide synthetic handles to control the shape, including the corresponding halide counterion, the concentration of the surfactant and Au salt, silver nitrate, and ascorbic acid. (III) TEM images of Au NPs with different shapes: (a) 3.0 nm Au nanospheres, (b) 40.0 nm Au nanospheres, (c) Au nanorods, (d) pentagonal twinned Au nanorods, and (e) trisoctahedral Au NPs. Reprinted with permission from ref 89, copyright 2014 American Chemical Society.

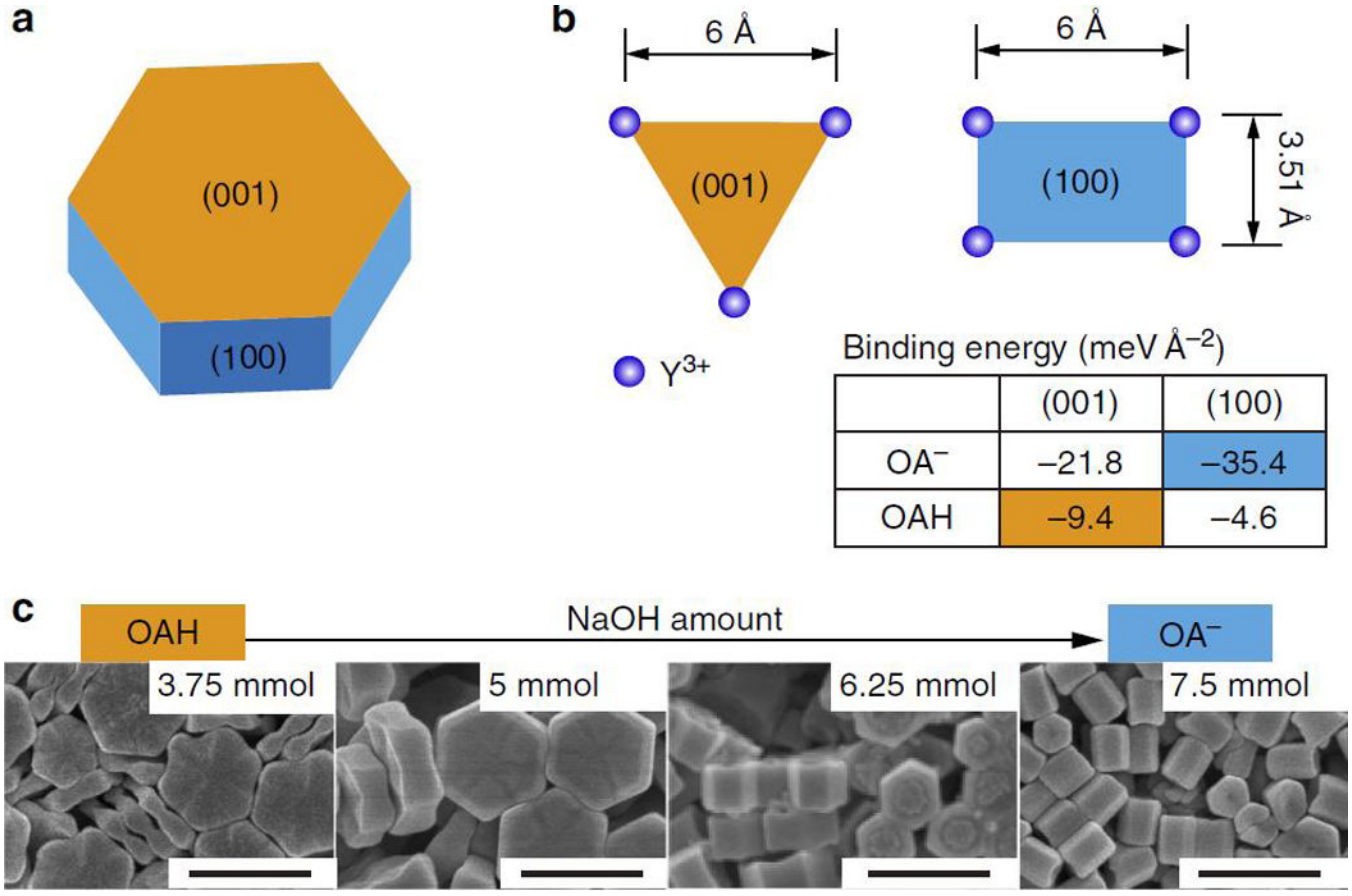

Figure 5.

Favored molecular capping or bonding models of OA^- and OAH of β-$NaYF_4$ nanocrystals. (a) The schematic shape chosen as the core for directional epitaxial growth. The hexagonal plate consists of the (001) facets at the ends, and identical (100) and (010) facets around the sides. (b) The Y^{3+} arrangements and binding energies of OAH and OA^- on the most stable (001) and (100) facets. (c) SEM images of nanocrystals synthesized using varied ratios of capping agents (scale bar, 500 nm). Reprinted with permission from ref 96, copyright 2016 Nature Publishing Group.

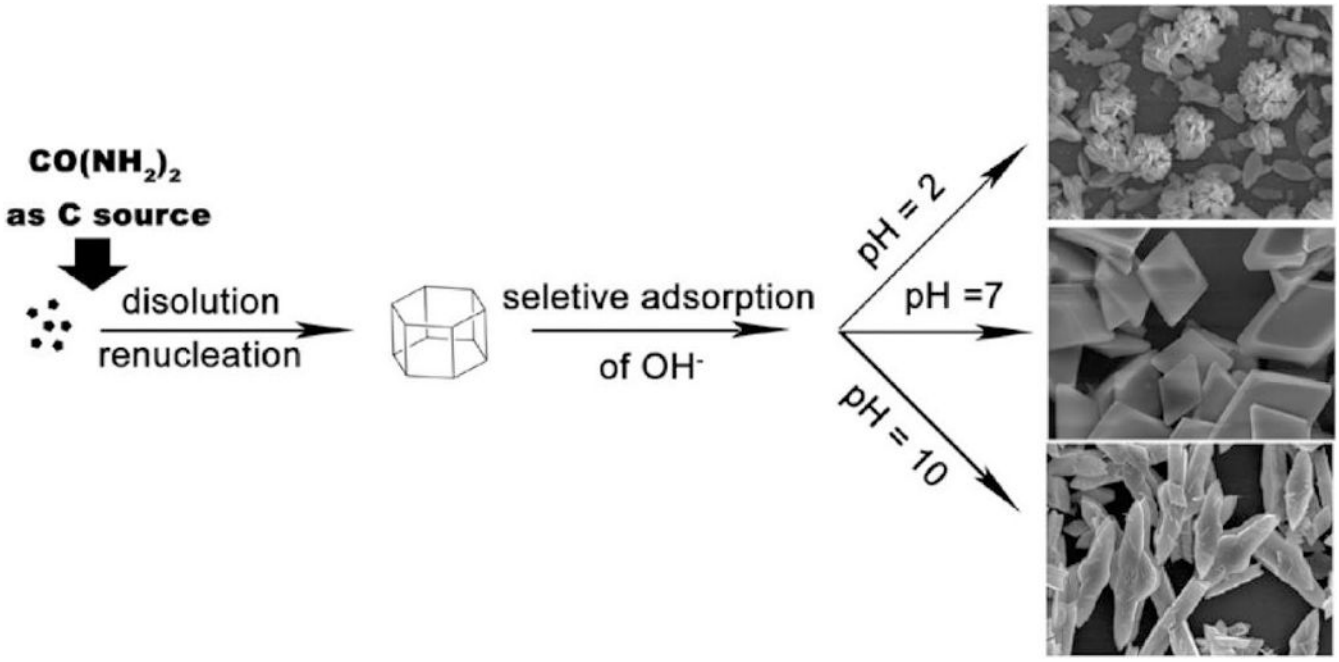

Figure 6.
Schematic illustration of the possible growth process of $LaCO_3OH$ microcrystals with various shapes at different pH values (2, 7, and 10). Reprinted with permission from ref 103, copyright 2010 American Chemical Society.

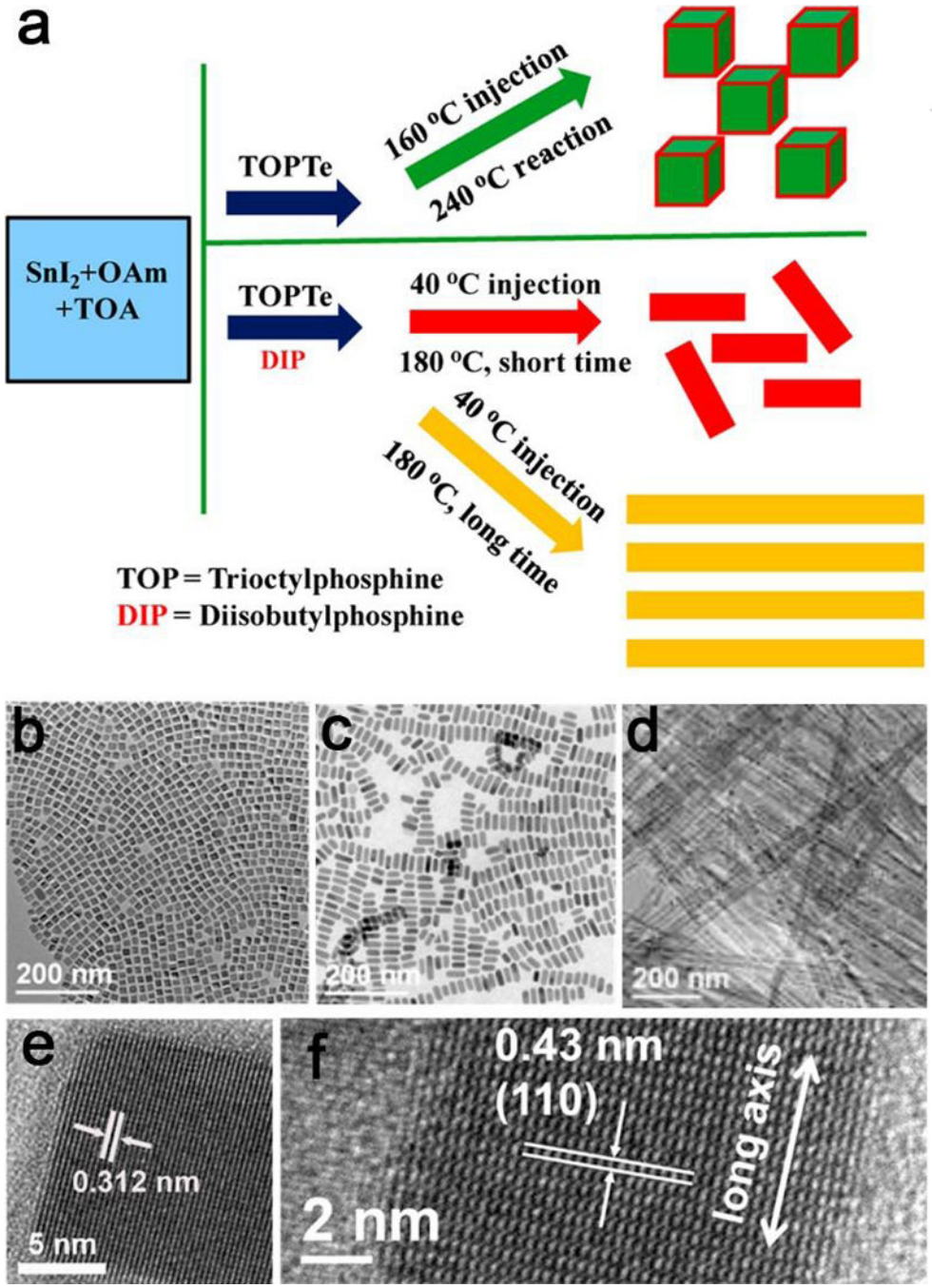

Figure 7.

(a) Schematic illustration of controlled syntheses of SnTe nanocubes and nanorods with various aspect ratios. (b,c) TEM and (e,f) corresponding HRTEM images of SnTe nanocubes and nanorods. (d) TEM images of SnTe nanowires prepared with T_{inj} = 40 °C, T_r = 180 °C, and t_r = 8 h. Adapted with permission from ref 109, copyright 2015 American Chemical Society.

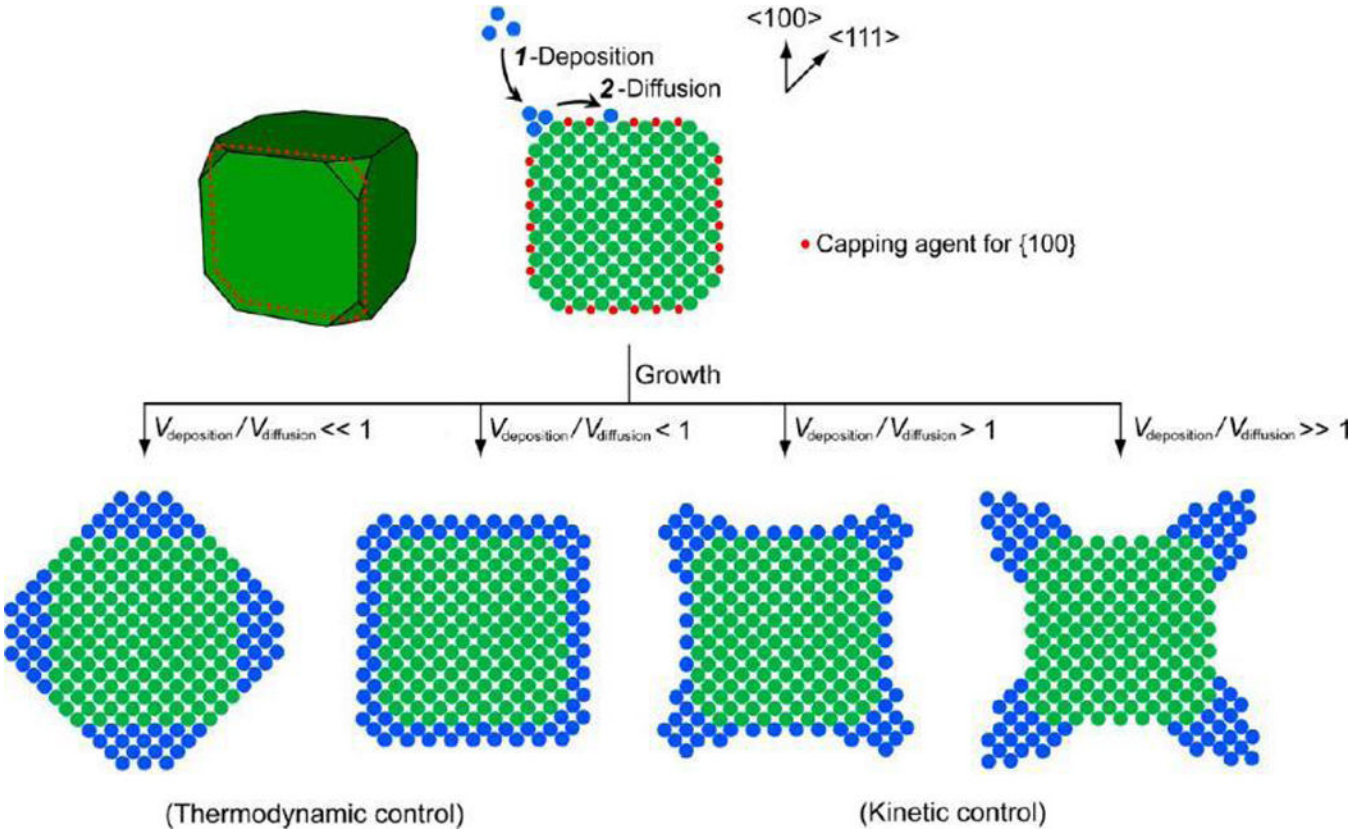

Figure 8.

The schematic illustration of the shape evolution of a cubic seed under different conditions. The side faces of the seed are covered by a capping agent to show the difference, and the anisotropy and shape could be totally different by the thermodynamic and kinetic control. The 2-D atomic models in this figure correspond to the cross-section of the 3-D model. Reprinted with permission from ref 110, copyright 2015 American Chemical Society.

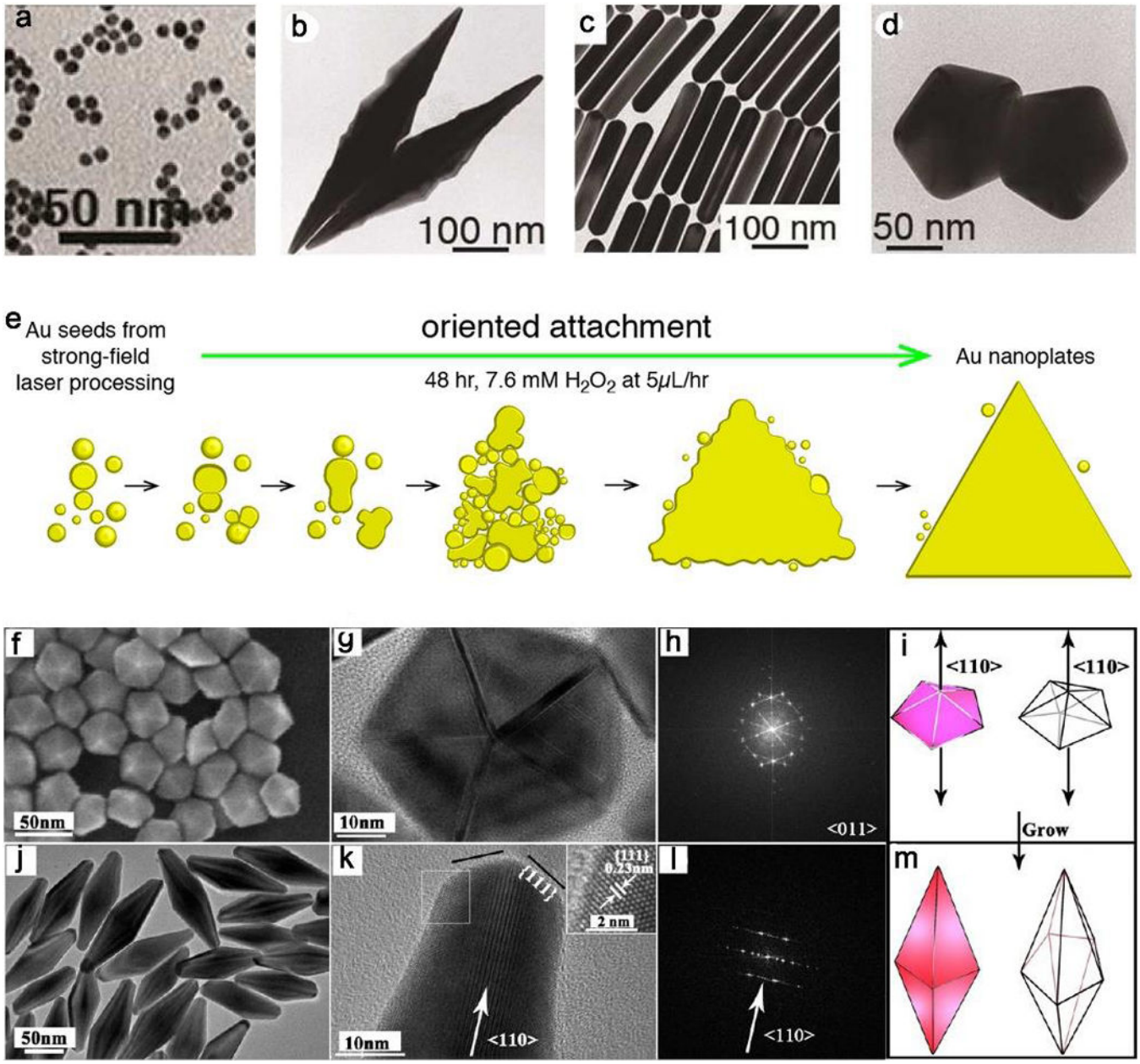

Figure 9.

(a) Representative TEM image of the gold seeds with thermally-induced twinning for 90 min at 80 ºC. TEM images of NPs with (b) bipyramids, (c) nanorods and (d) decahedra shapes, showing the effect of seed concentration on the formation of NP in a single growth step. (e) Schematic illustration of the sequential steps leading to triangular Au nanoplate from spherical Au seeds with a strong field laser processing. (f) SEM image of decahedral seeds with a 30 nm edge, (g) HRTEM image, (h) corresponding FFT pattern and (i) sketch of one decahedron. (j) TEM image of nanobipyramids, (k) HRTEM image (inset, HRTEM image of area marked by the box), (l) corresponding FFT pattern and (i) sketch of one bipyramid. (a-d), (e) and (f-m) are adapted with permission from refs 119, 120 and 121, copyright 2017, 2015 and 2013 American Chemical Society, respectively.

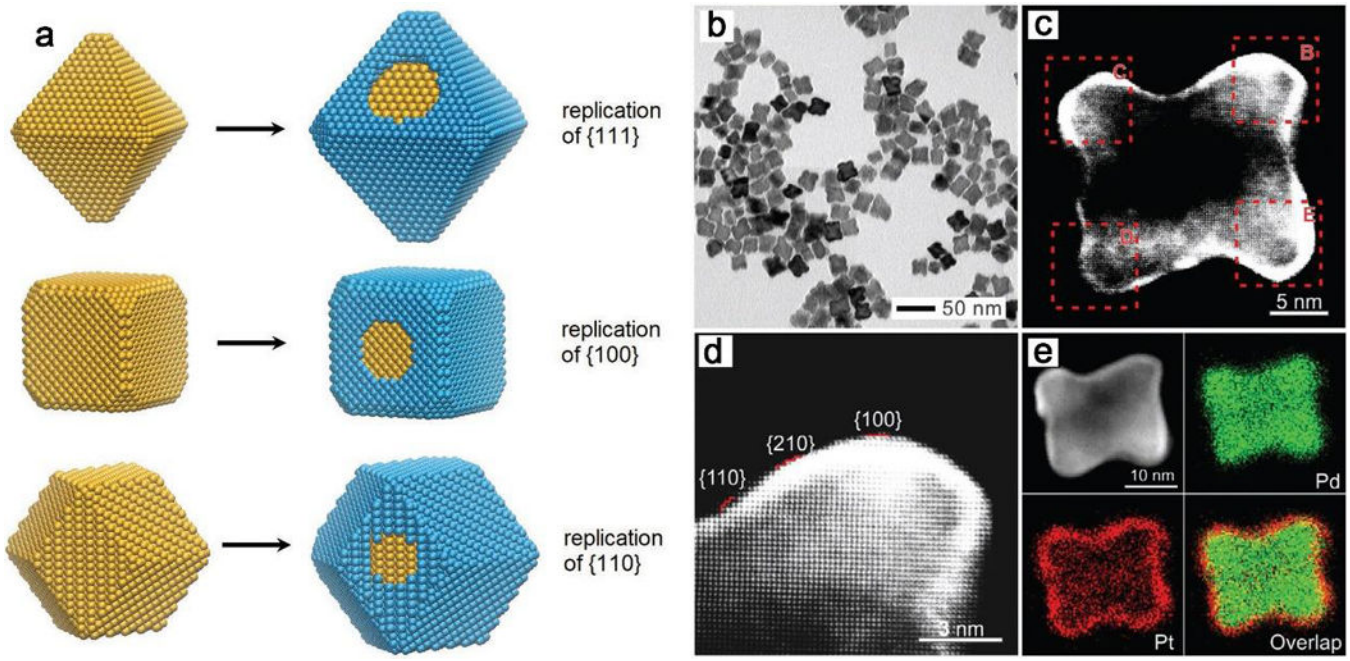

Figure 10.

(a) Schematic illustration of the approach employed to control the growth of nanocrystals. Replication of surface structure, ultrathin layers formed on the surface of seed in a layer-by-layer fashion. (b) TEM image of Pd@Pt core–shell concave nanocubes, and (c) corresponding HAADF-STEM image and (d) high-magnification image, showing replication of the high-index faceting and the Z-contrast between the Pd seed and the Pt shell. (e) Elemental mapping of an individual Pd@Pt concave nanocube, showing the distribution of Pd and Pt atoms, which confirmed the deposition of ultrathin Pt shells on Pd concave nanocubes. (a) and (b-e) Adapted with permission of ref 122 and ref 124, copyright 2018 and 2016 Wiley-VCH.

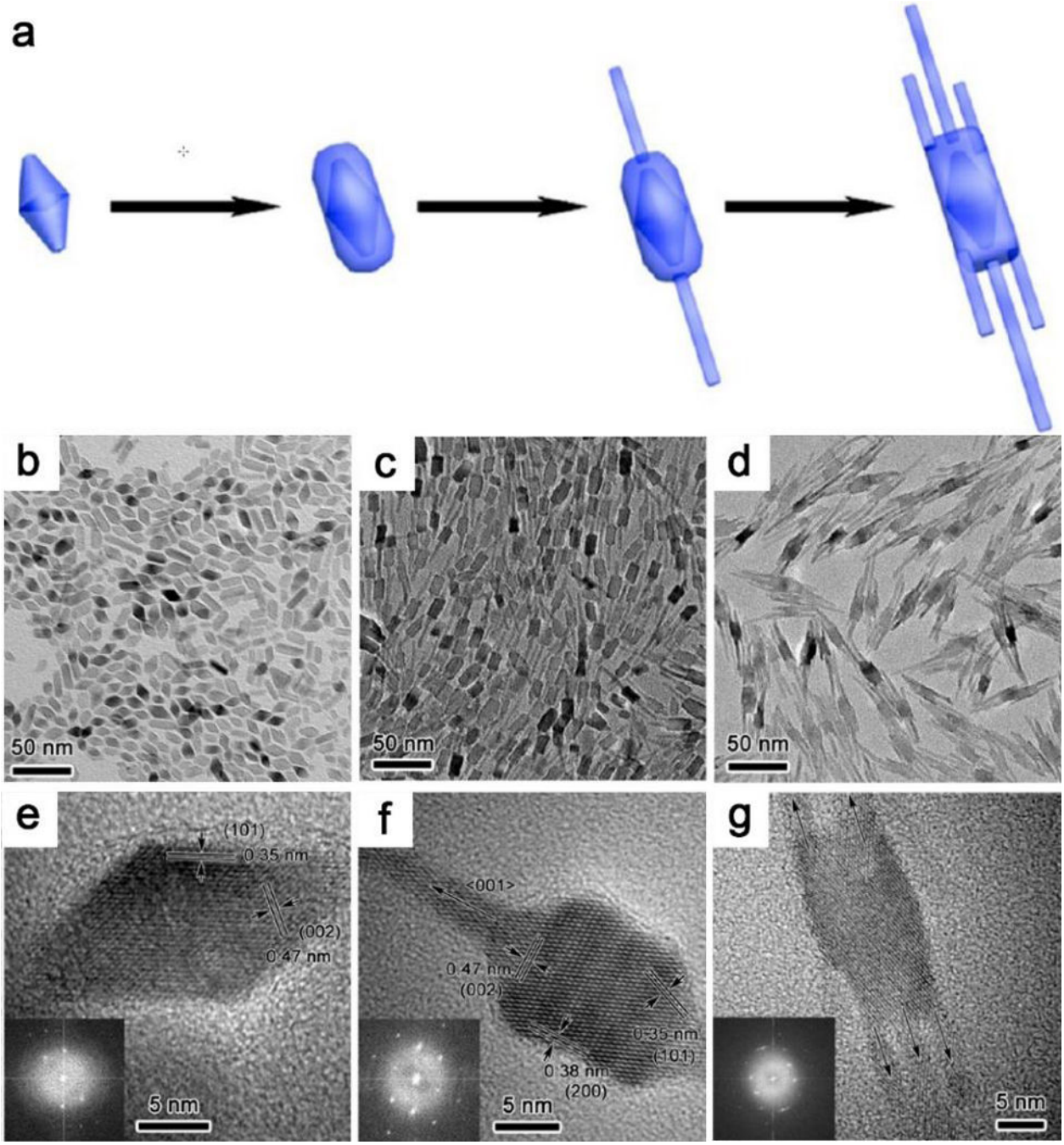

Figure 11.

Structural characterization of truncated octahedral bipyramidal nanocrystals seeds and core-antenna nanocrystals after seed-mediated growth. (a) Schematic illustration of the growth pathway of core-antenna nanostructures from seeds. (b) Low magnification TEM image of seed and (c, d) resultant nanorods and core-antenna nanocrystals after seeded growth. (e-g) Typical HRTEM images of the up TEM images, insets are FFT patterns (along the [100] zone axis). Reproduced with permission from ref 129, copyright 2015 American Chemical Society.

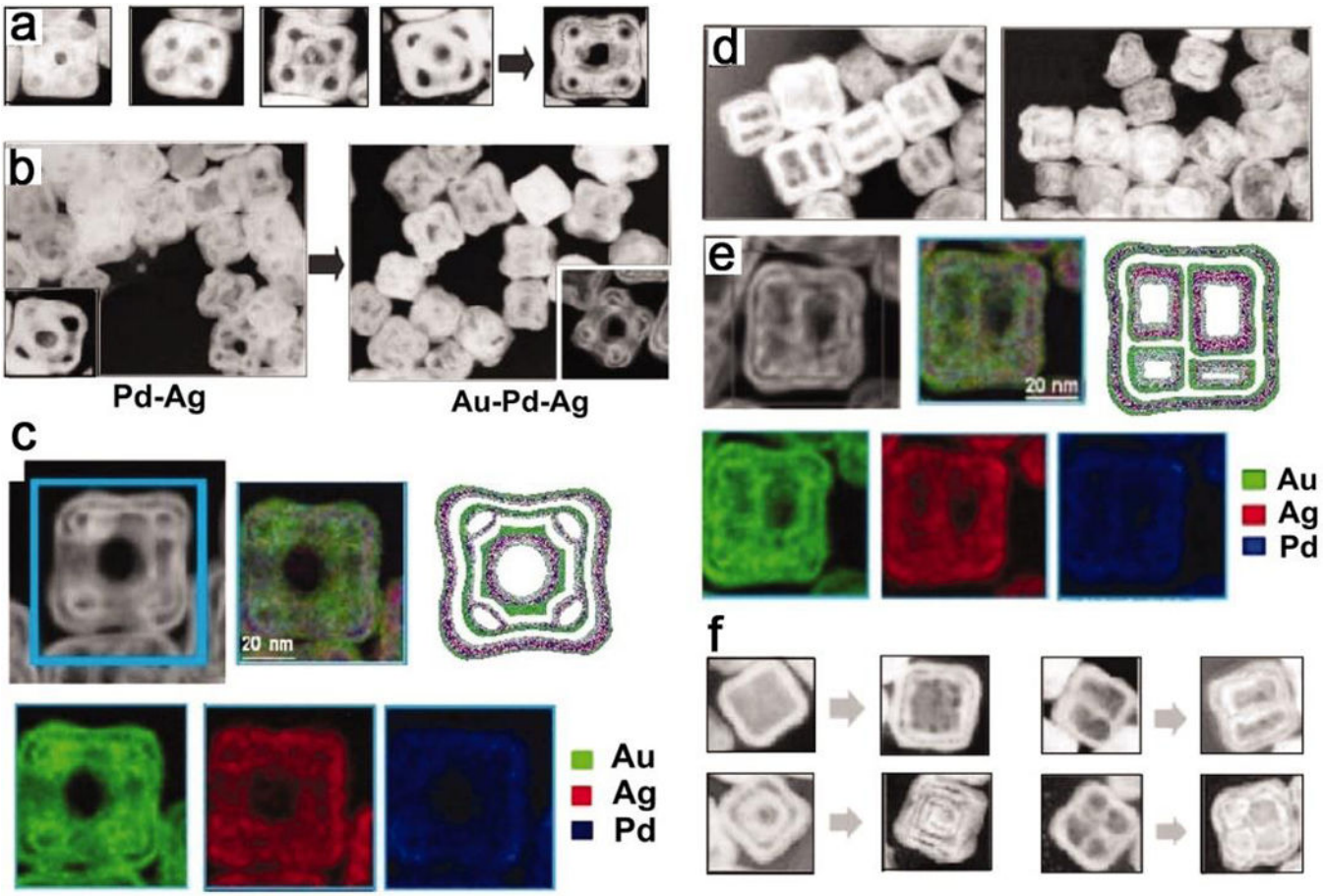

Figure 12.

(a) The illustration of the formation of hollow nanostructures *via* sequential galvanic replacement and Kirkendall effect and (b) the nanostructures dominated by galvanic replacement by Kirkendall effect, and (d) multichambered NPs, all showed in TEM images. (c) and (e) HAADF-STEM images and their corresponding EDX elemental maps. (f) TEM images of different structures synthesized by sequential galvanic replacement or Kirkendall effect. Reprinted with permission from ref 153, copyright 2011 American Association for the Advancement of Science.

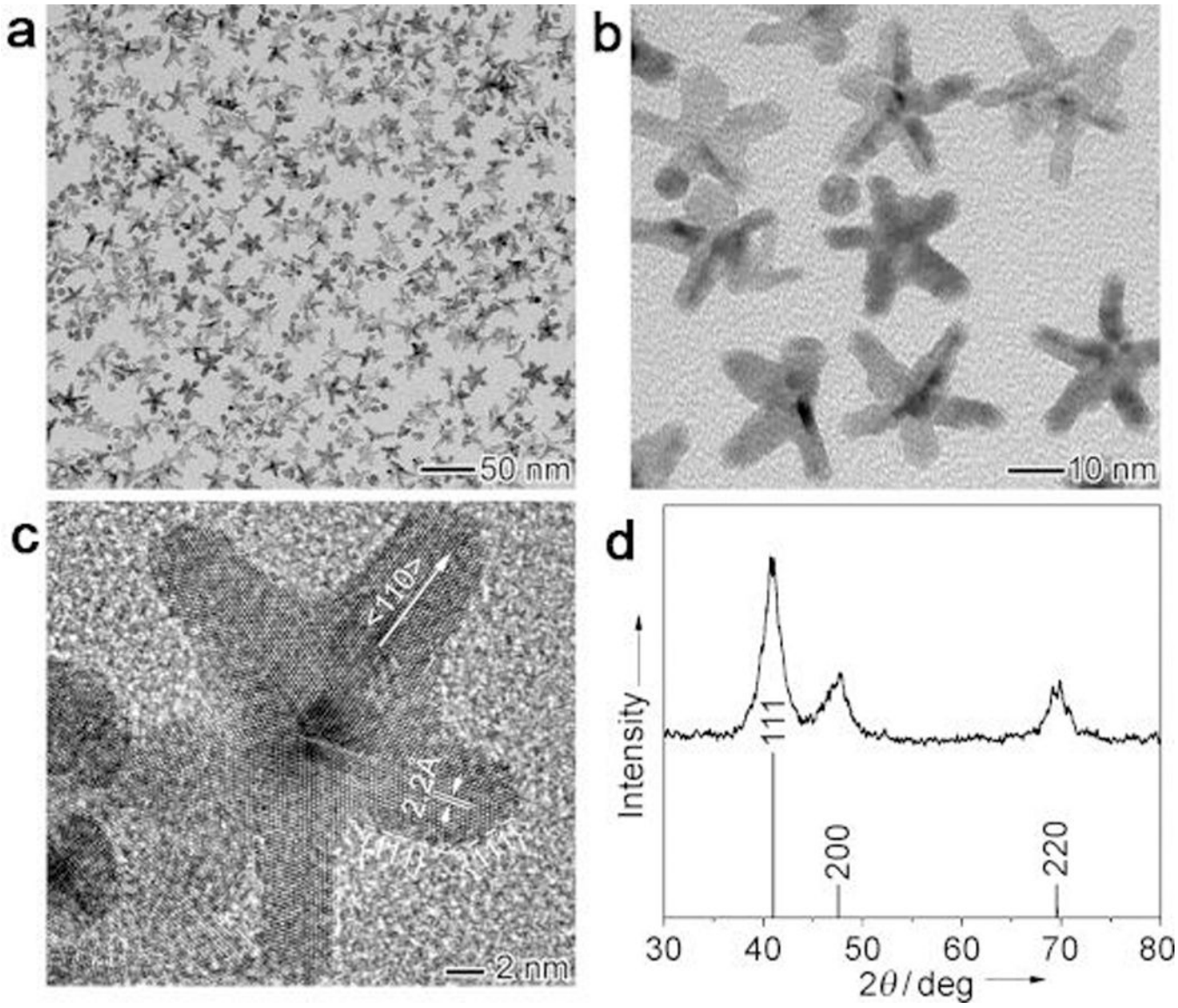

Figure 13.

TEM images of starfish-like Rh nanocrystals with five branched arms obtained using polyol reduction at 180 °C for 6 h, at (a) low and (b) high magnifications. (c) A representative high-resolution TEM image and (d) the XRD pattern. Adapted with permission from ref 172, copyright 2010 Wiley-VCH.

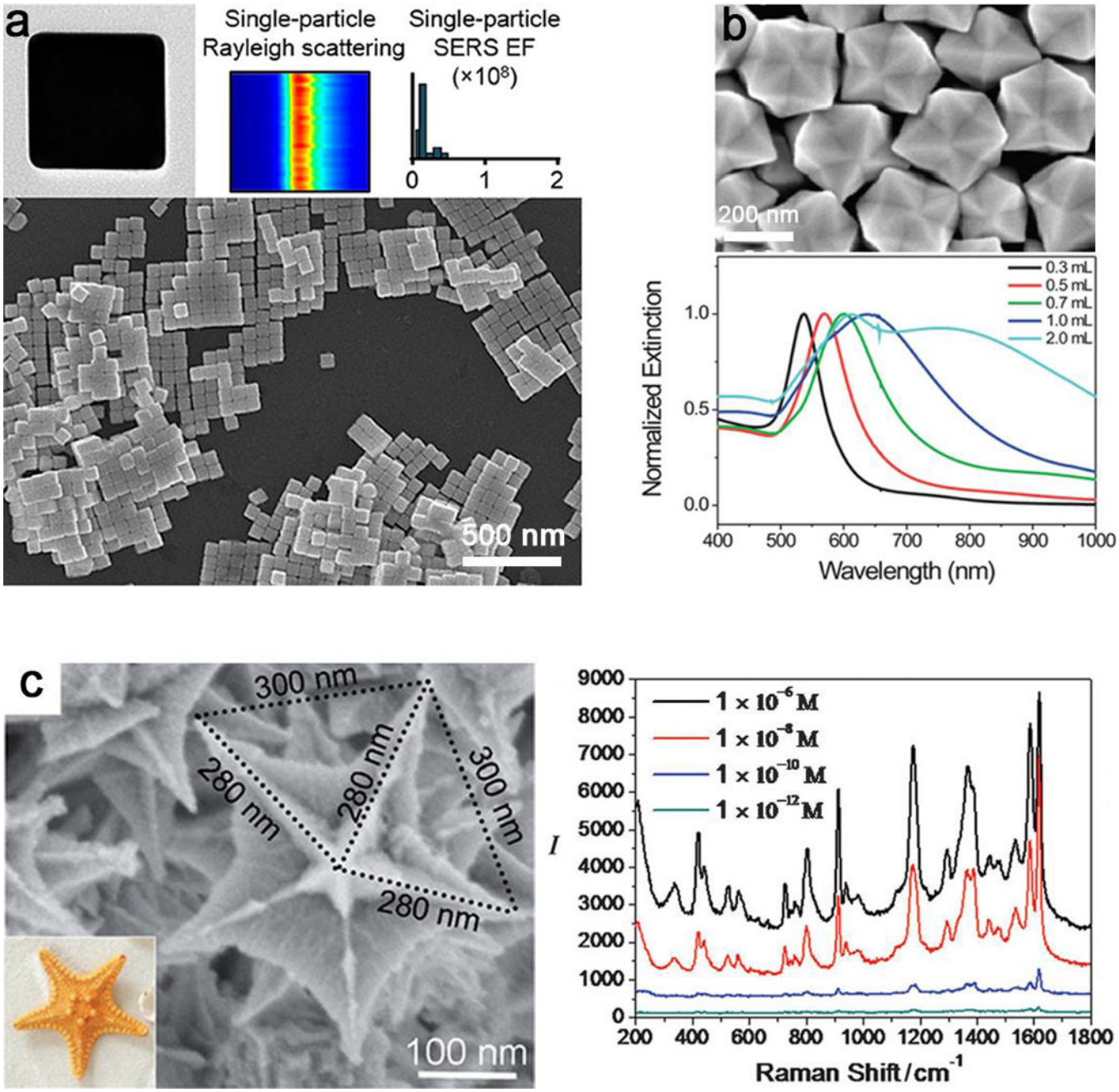

Figure 14.

Characterization of anisotropic NPs and their optical properties. (a) Representative TEM image, Rayleigh scattering and the quantitative surface-enhanced Raman scattering (SERS) enhancement factor (EF) of a single-particle, and SEM image of Au nanocubes with sharp cornered shapes. (b) SEM image of the hexoctahedral Au NPs and their normalized UV-vis extinction spectra prepared with different amounts of $HAuCl_4$. (c) High-magnification SEM images and SERS spectra of crystal violet adsorbed on the concave branched Au/Pd bimetallic nanocrystals. The scale bars of (a), (b) and (c) are 500 nm, 200 nm and 100 nm, respectively. The SERS spectra were obtained with lex = 514 nm excitation, Plaser = 1 mW,

and t = 20 s. (a, b) Reprinted by permission from refs 188 and 189, copyright 2018 and 2012 American Chemical Society. (c) Adapt with permission from ref 190, copyright 2015 Wiley-VCH.

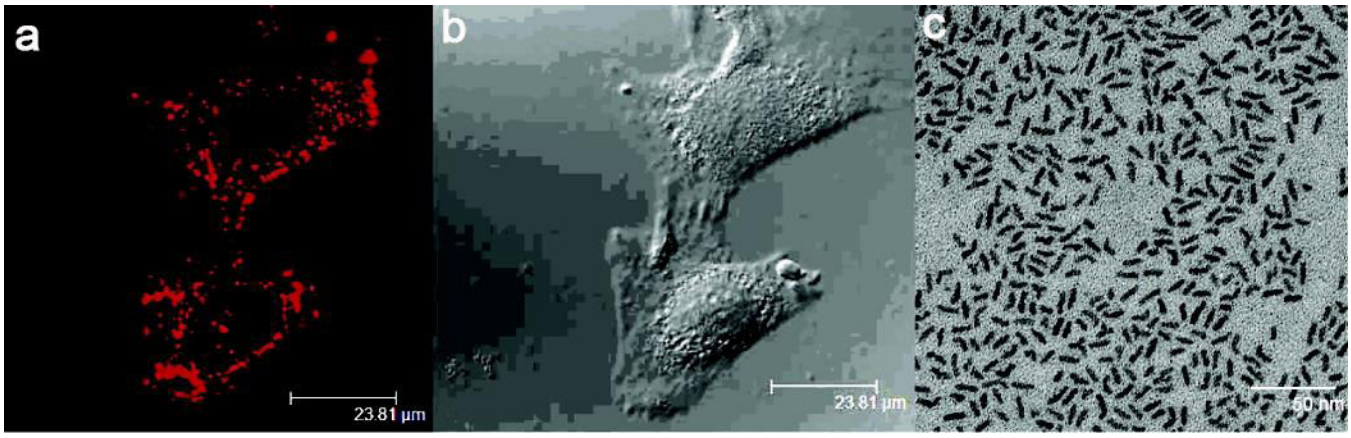

Figure 15.

Confocal microscopic images of HeLa cells, (a) the florescence image and (b) their corresponding transmission image, treated with transferrin-conjugated CdSe/CdS/ZnS quantum rods. Confocal microscopy images were obtained with laser excitation at 442 nm. (c) TEM image of CdSe/CdS/ZnS quantum rods casts from nonpolar organic solvent. The average diameter and length of the nanorods are 14 and 4 nm with an aspect ratio of 3.5. The scale bars of (a) and (b) are 23.81 nm, (c) is 50 nm. Adapt with permission from ref 217, copyright 2007 American Chemical Society.

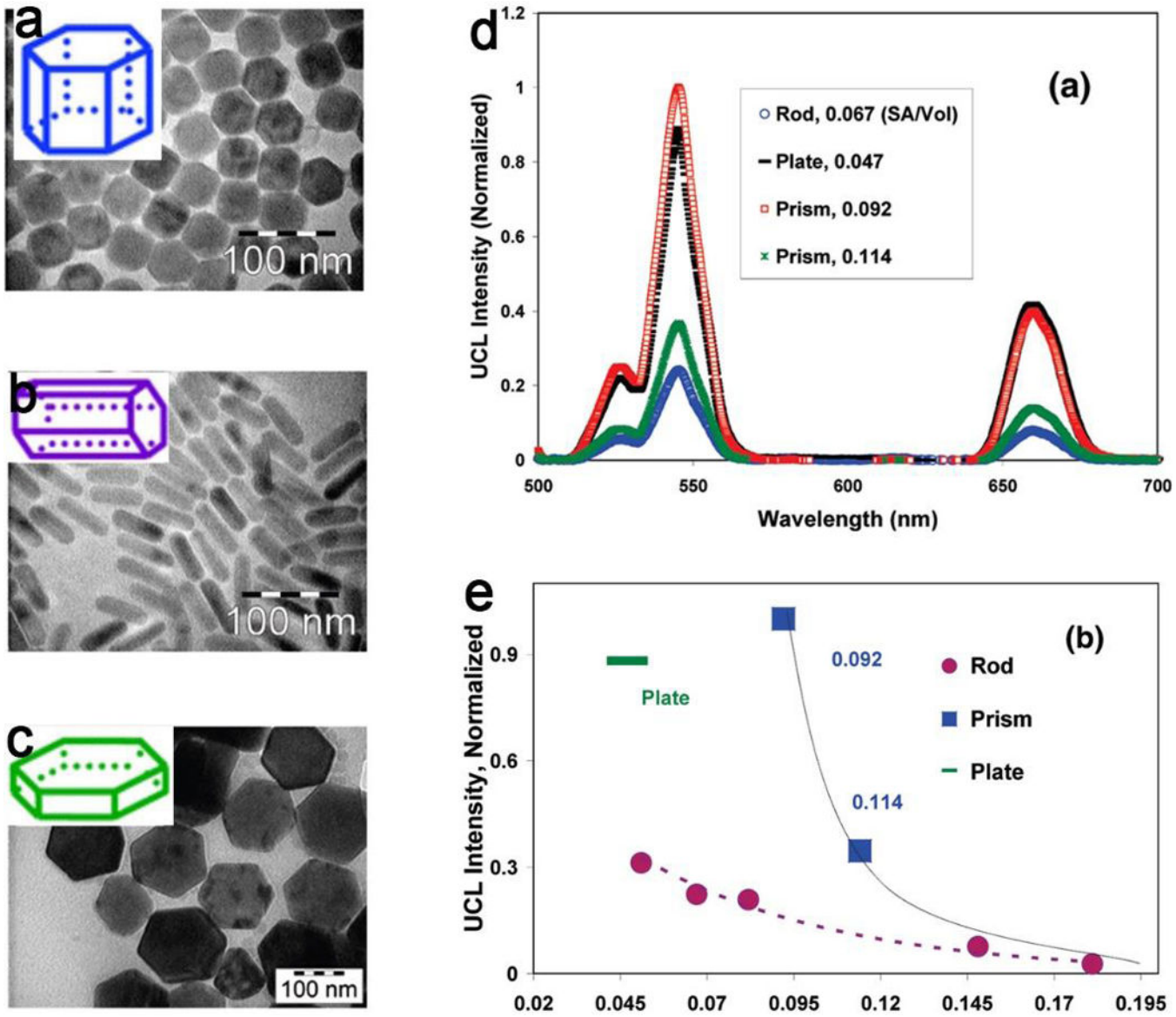

Figure 16.

TEM images of the upconversion NPs in three shapes (a) nanoprism, (b) nanorod, (c) nanoplate, insert is the geometrical description of the shape. (d) The upconversion emission spectra and (e) surface to volume ratios vs upconversion luminescence intensity for three upconversion NPs with three shapes. Adapt with permission from ref 225, copyright 2016 American Chemical Society.

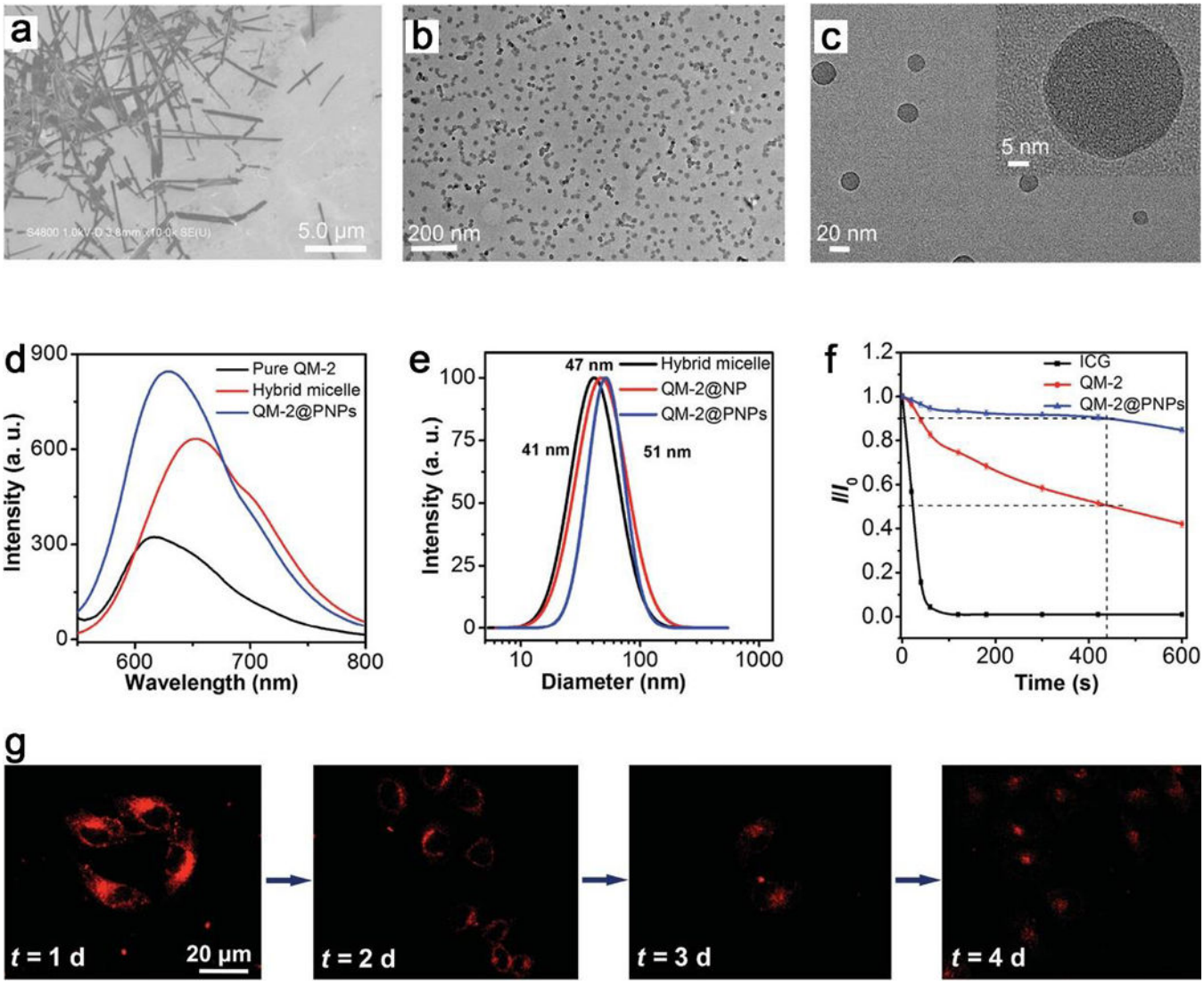

Figure 17.

(a) The SEM image of QM-2 in water/THF mixture with f_w = 70 vol%. TEM images of QM-2@PNPs at (b) low and (c) high magnifications. (d) Emission spectra of pure QM-2 in water/THF mixture at f_w = 70 vol%, hybrid micelles before shell cross-linking, and QM-2@PNPs in water. (e) Size distributions of hybrid micelle, QM-2@NP and QM-2@PNPs in water by dynamic light scattering. (f) Fluorescence stability of ICG (indocyanine green, a FDA-approved NIR imaging agent in clinic), QM-2, and QM-2@PNPs under continuous illumination (0, 10, 20, 40, 60, 120, 180, 300, 420, and 600 s). (g) Fluorescence images of MCF-7 cells stained by QM-2@PNPs at different cell passages. The scale bar (20 μm) is the same for all images. Reproduced with permission from ref 235, copyright 2016 Wiley-VCH.

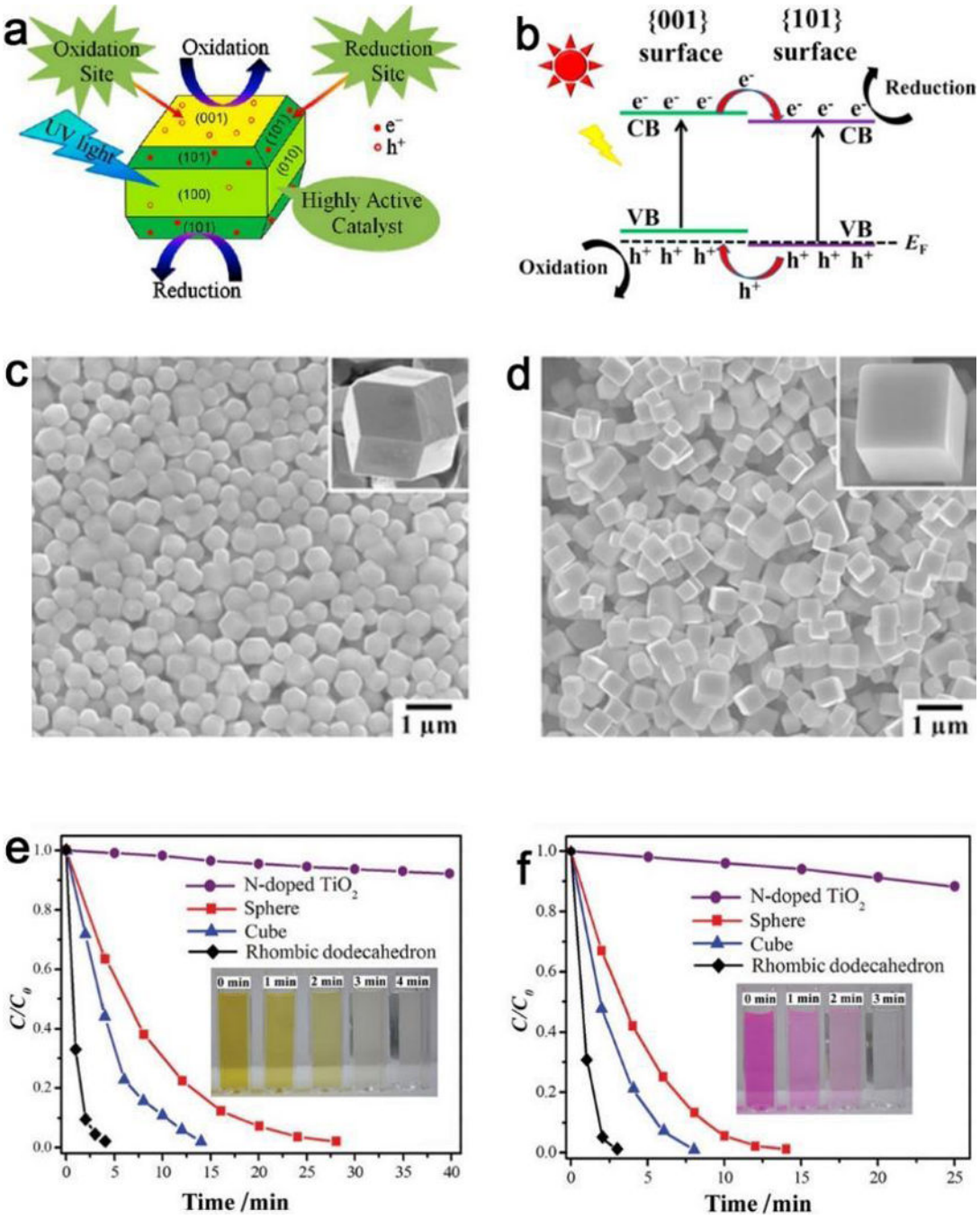

Figure 18.

Shape & facet effect of photocatalysis. (a) Synergy of low-energy {101} and high-energy {001} TiO_2 crystal facets for enhanced photocatalysis. (b) {001} and {101} surface heterojunction of TiO_2. SEM images of (c) rhombic dodecahedrons and (d) cubic Ag_3PO_4 with different morphologies. The photocatalytic activities of Ag_3PO_4 rhombic dodecahedrons, cubes, spheres, and N-doped TiO_2 are shown for the degradation of (e) MO and (f) RhB under visible light irradiation ($\lambda > 400$ nm). (a, b, c-f) Adapted with permission

from refs 250, 251 and 260, copyright 2013, 2014 and 2011 American Chemical Society, respectively.

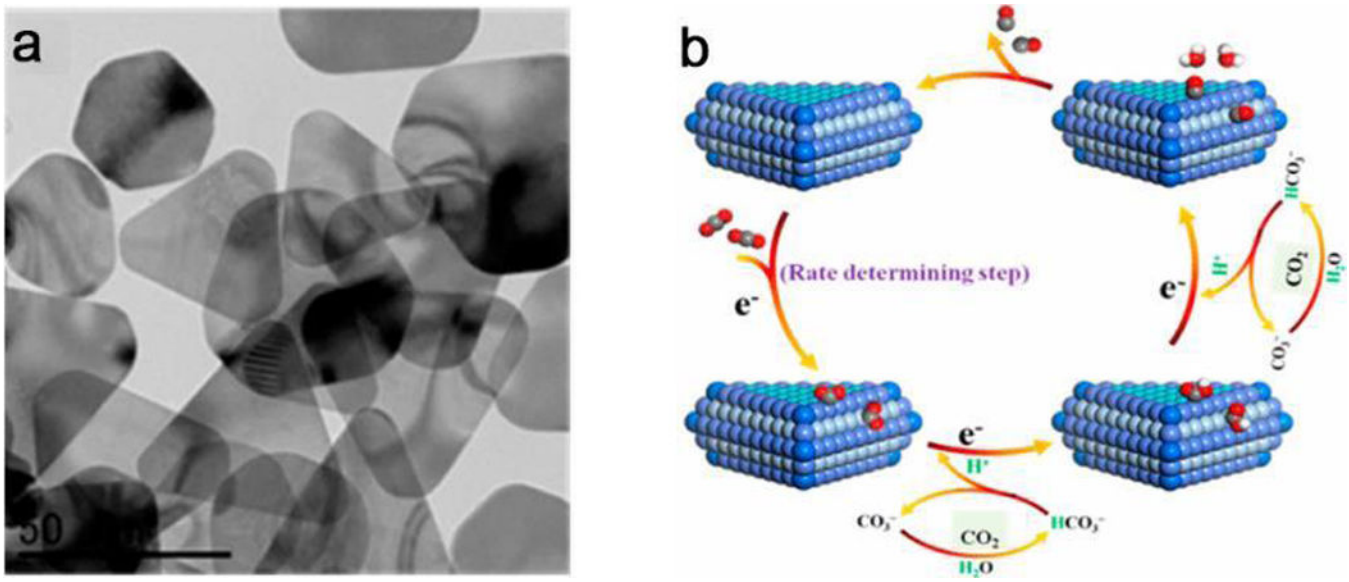

Figure 19.

Shape-dependent electrocatalytic reduction of CO_2 to CO on triangular silver nanoplates. (a) TEM image of triangular silver nanoplates (Tri-Ag-NPs), and (b) proposed mechanism for CO_2RR to CO on Tri-Ag-NPs. Adapted with permission from ref 271, copyright 2017 American Chemical Society.

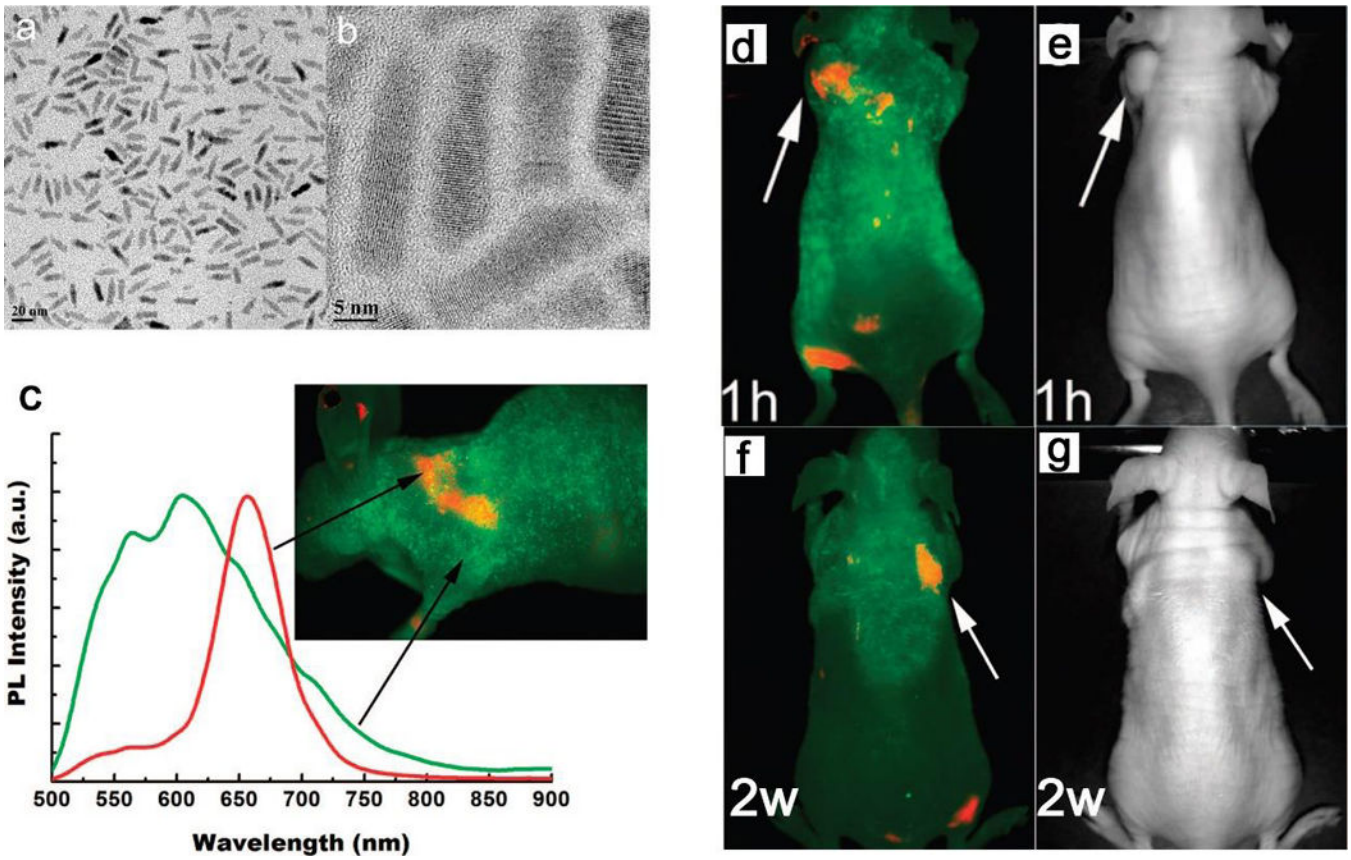

Figure 20.

TEM images of CdSe/CdS/ZnS quantum rods (QRs) at a (a) low and (b) high magnification. The average length and width are 20.5 and 4.5 nm with an aspect ratio of 4.5. (c) The spectra of autofluorescence (green) and QR (red) of a nude mouse bearing tumor with QR bioconjugates. The signal of QR was obtained by subtracting the autofluorescence from the mixture. (d) *In vivo* luminescence imaging of Panc-1 tumor-bearing mice injected with cRGD-peptide-conjugated QRs of (d, e) 1 mg at 1 h and (f, g) 0.5 mg at 2 weeks, TEM images (right) corresponds to luminescence images (left), the tumor is indicated by white arrows. The autofluorescence of tumor-bearing mice is shown in green, and the unmixed QR signal in red. All images were acquired in the same experimental conditions. Reproduced with permission from ref 289, copyright 2009 American Chemical Society.

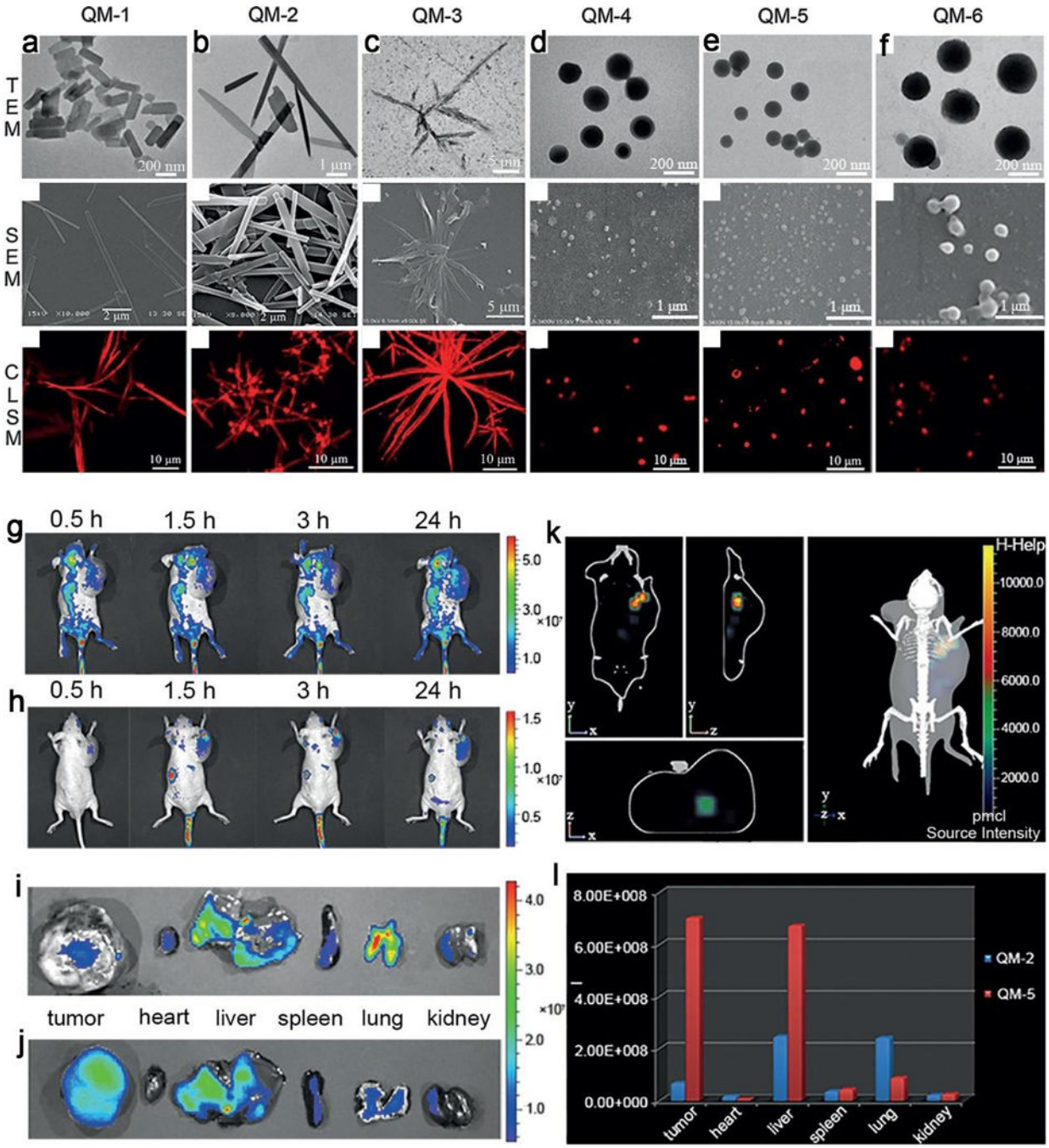

Figure 21.

Multiple morphologies fabricated from quinoline–malononitrile (QM) derivatives. The TEM, SEM, and confocal laser scanning microscope images (from up to down) of (a) QM-1, (b) QM-2, (c) QM-3, (d) QM-4, (e) QM-5 and (f) QM-6, respectively. *In vivo* non-invasive imaging of mice bearing tumor after intravenous injection of (g) QM-2, (h) QM-5 at different time points (0.5, 1.5, 3 and 24 h), and fluorescence images of the organs of mice sacrificed at 24 h post-injection with (i) QM-2 and (j) QM-5. (k) The 3D fluorescence imaging of a tumor-bearing mice after intravenous injection of QM-5 for 24 h. (l) The

distribution of average fluorescence intensity for tumor and internal organs from mice sacrificed at 24 h post-injection with QM-2 and QM-5 ($n = 3$). Adapted with permission from ref 295, copyright 2015 Wiley-VCH.

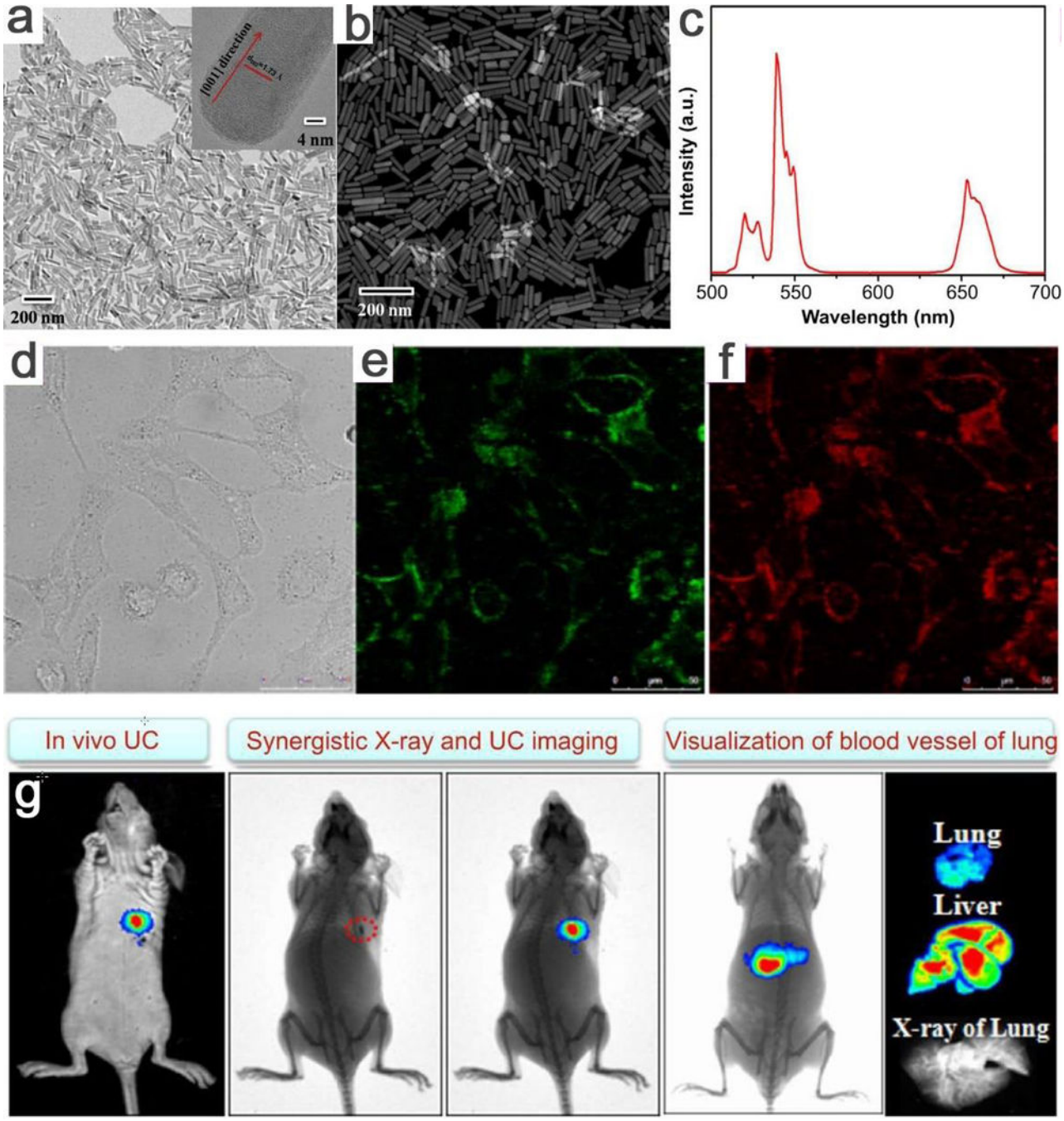

Figure 22.

(a) The TEM image (insert: a corresponding HRTEM image of single nanorod) and (b) STEM image of $NaLuF_4$:Gd/Yb/Er. (b) The upconversion spectra of OA-coated $NaLuF_4$:Gd/Yb/Er nanorods under the excitation of 980 nm. (c) *In vitro* optical imaging of HeLa cells treated with $NaLuF_4$:Gd/Yb/Er nanorods under 980 nm excitation, (d) bright field image, corresponding (e) green and (f) red upconversion fluorescent image. (g) Synergistical *in vivo* dual-modal X-ray and upconversion bioimaging of a nude mouse with subcutaneous injection of $NaLuF_4$:Gd/Yb/Er nanorods. The ex-*vivo* upconversion

bioimaging of lung, liver and X-ray imaging of lung of scarified nude mouse after 0.5 h intravenous injection with $NaLuF_4$:Gd/Yb/Er nanorods. Adapted with permission from ref 303, copyright 2014 Elsevier Science.

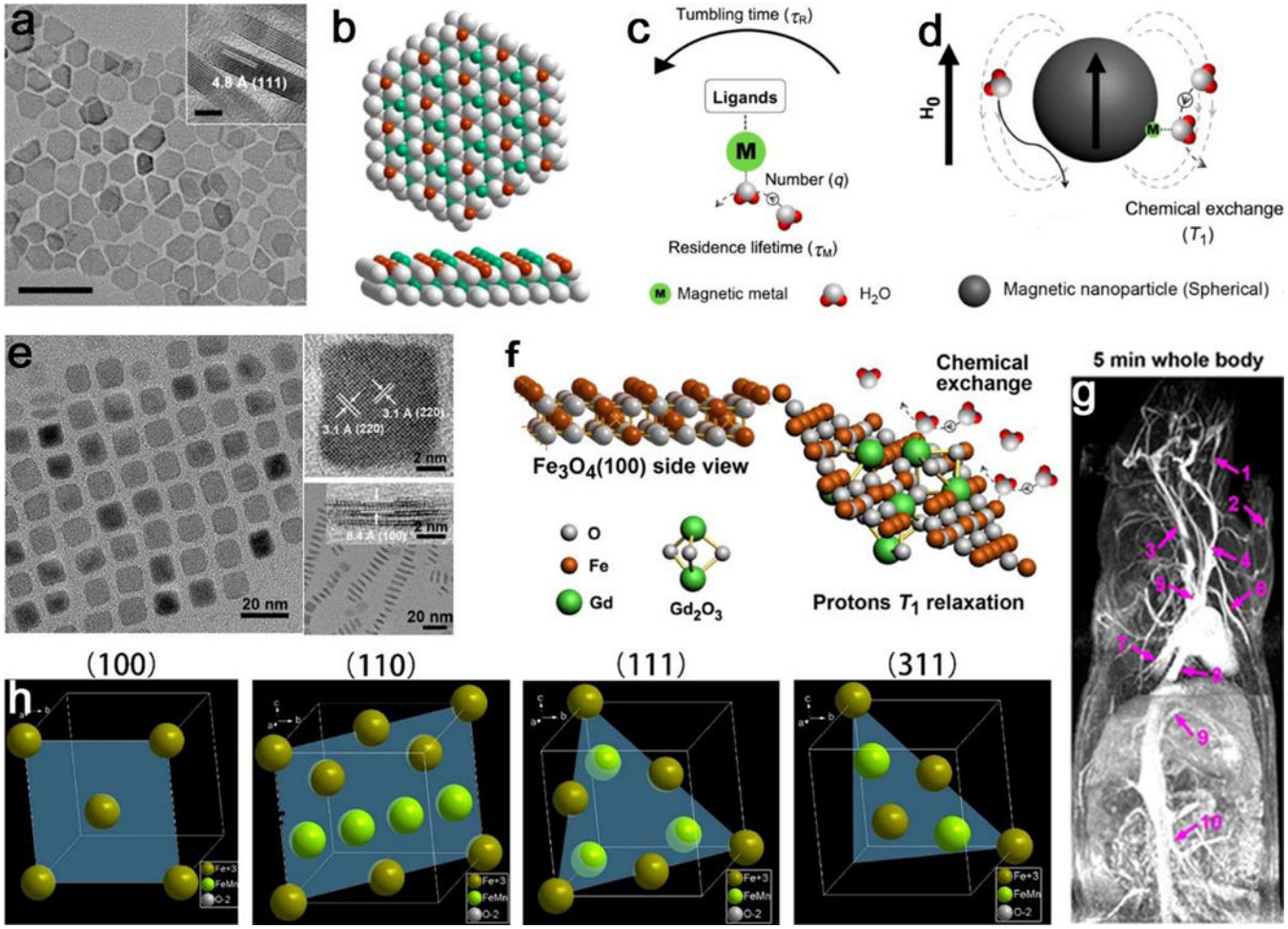

Figure 23.

The effect of surface structure with different shapes on T_1 contrast performance for NPs in T_1 imaging. For IO plates, (a) TEM image of IO nanoplates with a thickness of 4.8 nm, (b) the distribution of atoms on the exposed Fe_3O_4 (111) facet, (c) main key parameters to T_1 relaxation of protons, and (d) the proton interaction in a spherical magnetic NP system. For GdIOP nanoplates, (e) TEM and HRTEM images of vertically aligned GdIOP, (f) atomic side views of Fe_3O_4 (100) plane and Gd_2O_3 decorated surface for chemical exchange, and (g) the contrast-enhanced T_1 MRA imaging of rats at 5 min after injection of GdIOP at 3.0 T with a dose of 0.2 mmol (Fe + Gd)/kg. (h) The exposed faces of (100), (110), (111), and (311) of MnIO NPs, showing different occupancy rates of metal ions on the surfaces. (a-d), (e-g) and (h) Reproduced with permission from ref 335, 336 and 337, copyright 2014, 2015 and 2018 American Chemical Society, respectively.

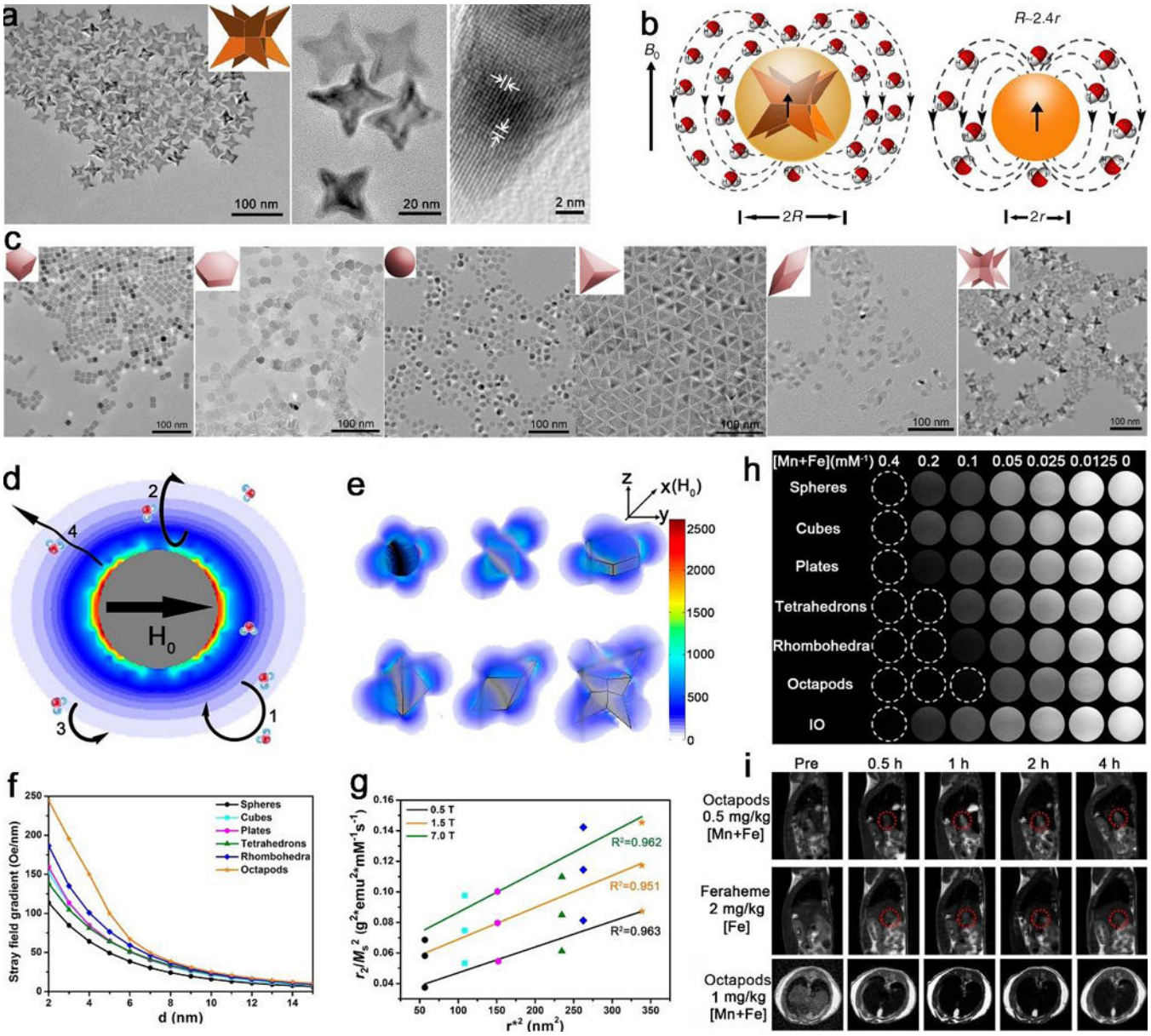

Figure 24.

The effect of morphology on T_2 contrast performance for NPs in T_2 imaging. For pure IO octapods, (a) TEM images in low and high magnifications and HRTEM image of a trigonal pyramidal arm with IO Octapod-30, (b) schematic illustration shows the effective radius of octapod is 2.4 times of spheres with the same geometric volume under an external magnetic field of B_0. For ferrite oxides, (c) TEM images of ferrite oxides of different morphologies with the same geometric volume, (d) scheme of water molecular diffusion and proton relaxation process around spherical magnetic NPs, (e) spatial distributions of stray fields of different shapes along the longest diagonal at an external magnetic field H_0, (f) changes of stray field gradients with different shapes, (g) the linear relationship of the ratio of r_2 value to the square of saturated magnetization (r_2/M_s^2) and the square of effective radius (r*), (h) T_2-weighted phantom images of ferrite oxides with multiple shapes measured at 1.5 T MRI,

and (h) *in vivo* T_2-weighted MRI of liver tumor in sagittal plane and liver in transverse plane of mice at 7.0 T. The scale bars in (a) are 100 nm, 20 nm and 2 nm, respectively. All scale bars in (c) is 100 nm. (a-b) Adapted with permission from ref 88, copyright 2013 Nature Publishing Group. (c-i) Reproduced with permission from ref 337, copyright 2018 American Chemical Society.

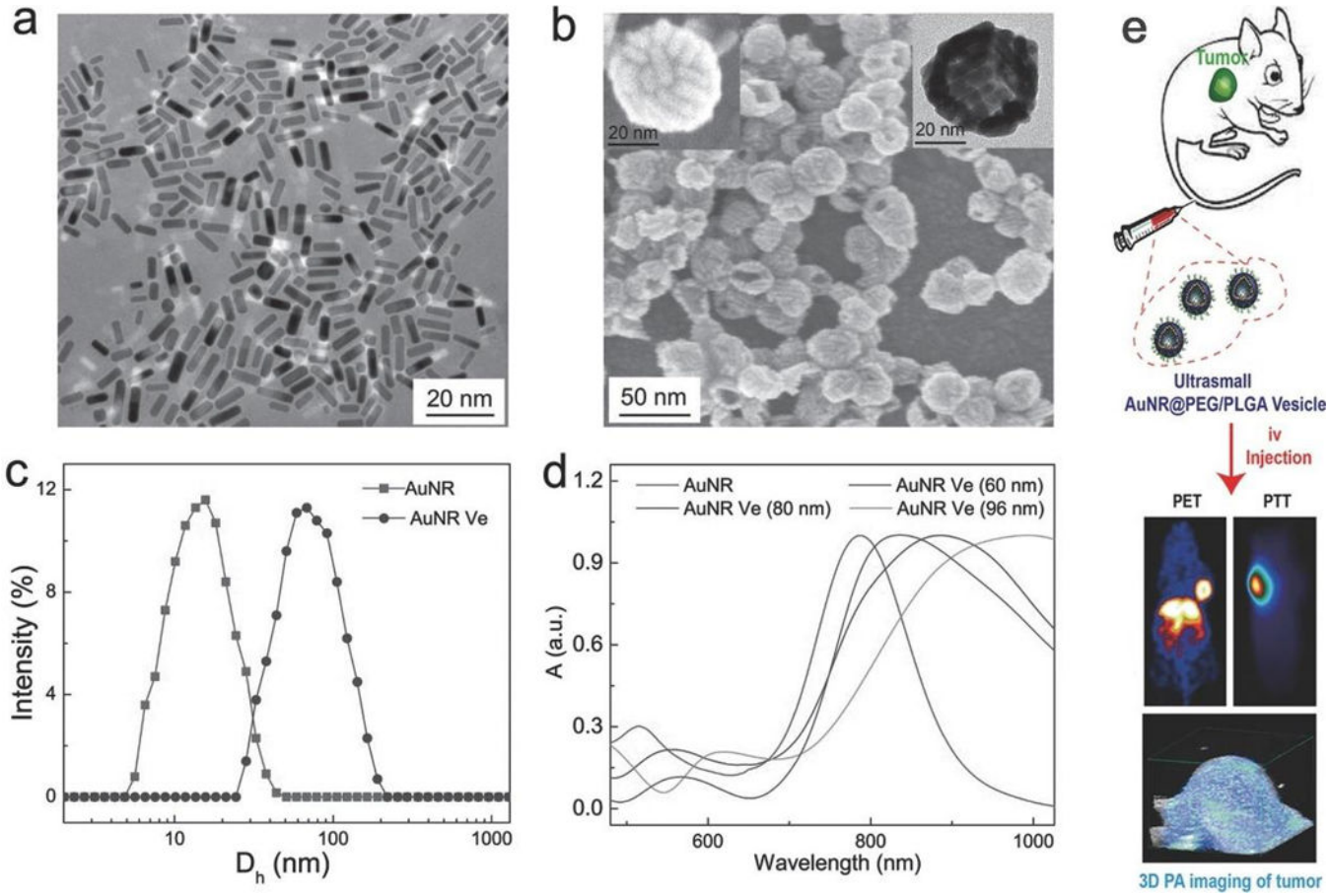

Figure 25.

(a) The TEM image of small Au nanorods (about 8 nm × 2 nm). (b) The SEM image of small plasmonic Au NR@PEG/PLGA vesicles, insets are SEM and TEM images of Au vesicle at a large magnification. (c) The hydrodynamic diameter distribution of Au NR and Au NR vesicles. (d) The UV–vis spectra of Au NR and Au NR vesicles with different sizes (60, 80, and 96 nm) in water. (e) The schematic illustration of Au vesicles with prominent tumor accumulation and enhanced photoacoustic and photothermal cancer therapy efficacy. Adapted by permission from ref 353, copyright 2015 Wiley-VCH.

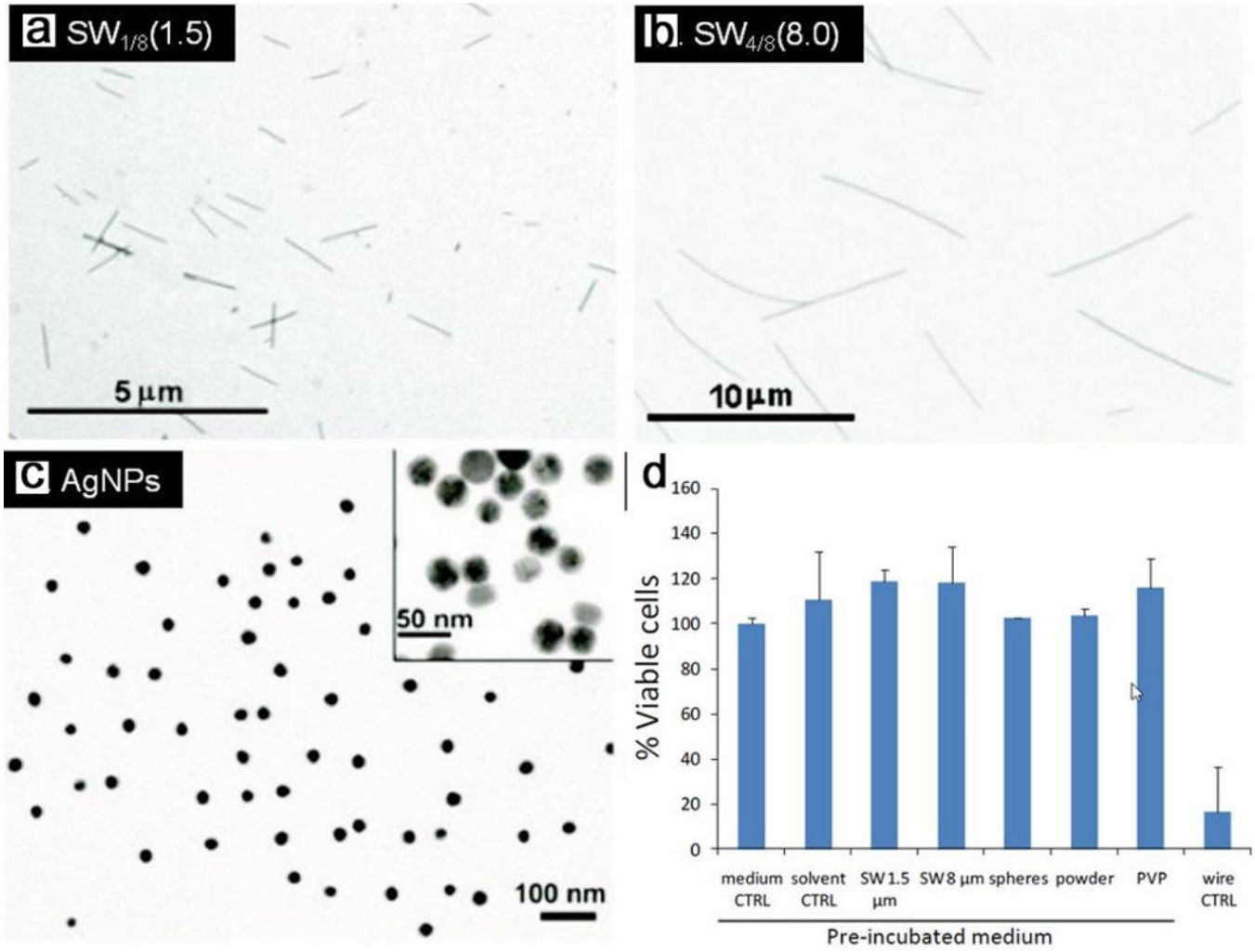

Figure 26.

(a) The TEM image of silver nanowires with lengths of (a) 1.5 μm and (b) 8.0 μm, and (c) spherical Ag NPs of 30 nm. (d) Cell viability and cytotoxic effects of A549 cells using CellTiter Blue®. NPs were incubated in cell culture medium for 48 hours at 37 °C and 5% CO_2. After centrifugation the supernatants were added onto A549 cells and incubated for another 48 hours. Adapted by permission from ref 363, copyright 2011 Springer Nature.

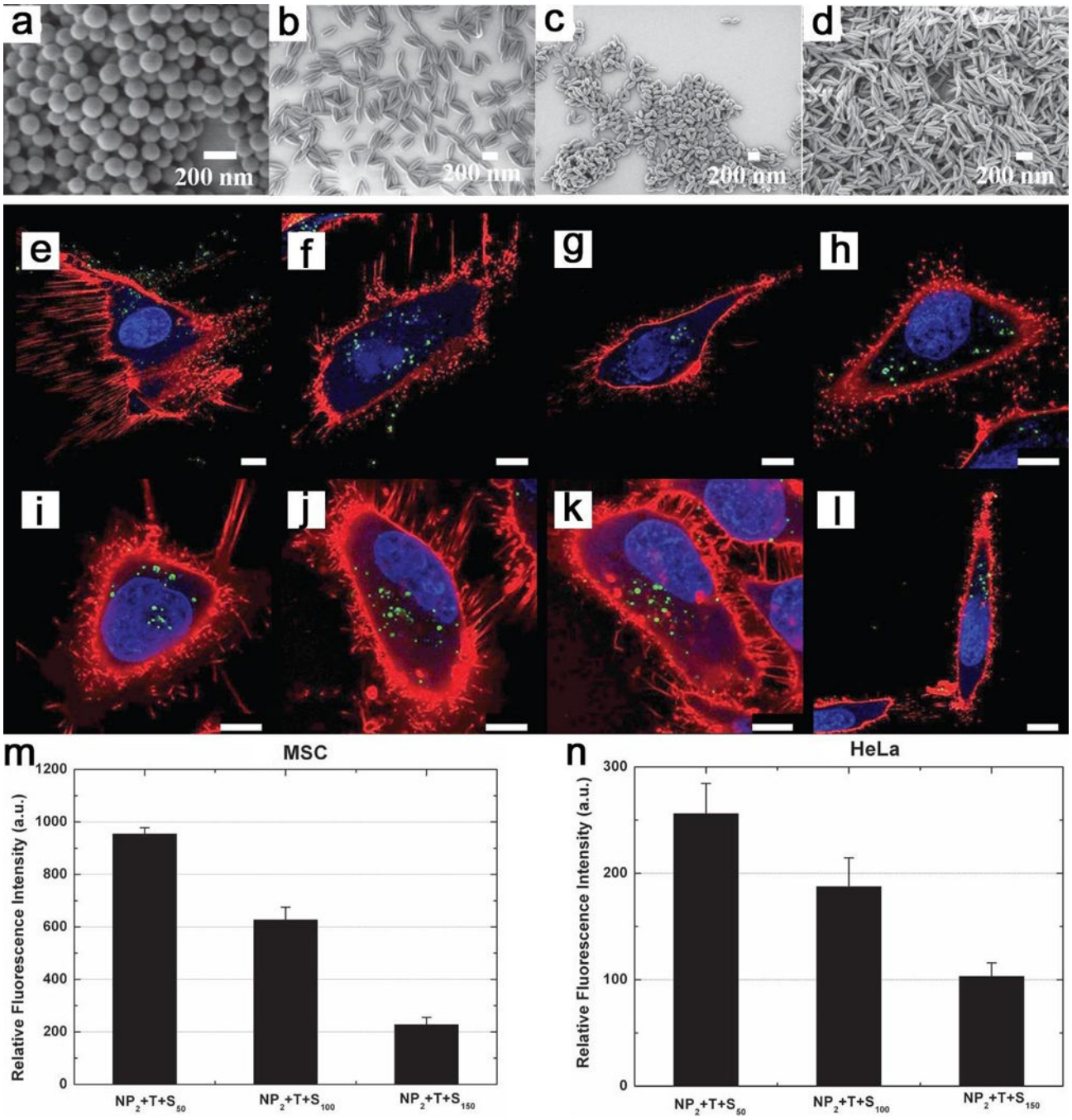

Figure 27.

SEM micrographs of (a) NP_2+T-S_0, (b) NP_2+T+S_{50}, (c) NP_2+T+S_{100} and (d) NP_2+T+S_{150}. NP_i, NP_i+T+S (NPs with temperature treatment and stretching) and NP_i+T-S (NPs with temperature treatment and without stretching). Corresponding uptake of (a-d) into (e–h) MSC-cells and (i–l) HeLa-cells after 20 h of incubation at a concentration of 75 μg mL^{-1}. Particles (in green), cell membrane (in red), and cell nuclei (in blue). Scale bar is 10 μm. Uptake of NPs with different aspect ratios in (m) MSC and (n) HeLa cells of NP_2+T+S_{50},

NP_2+T+S_{100} and NP_2+T+S_{150}. Adapted by permission from ref 25, copyright 2012 Wiley-VCH.

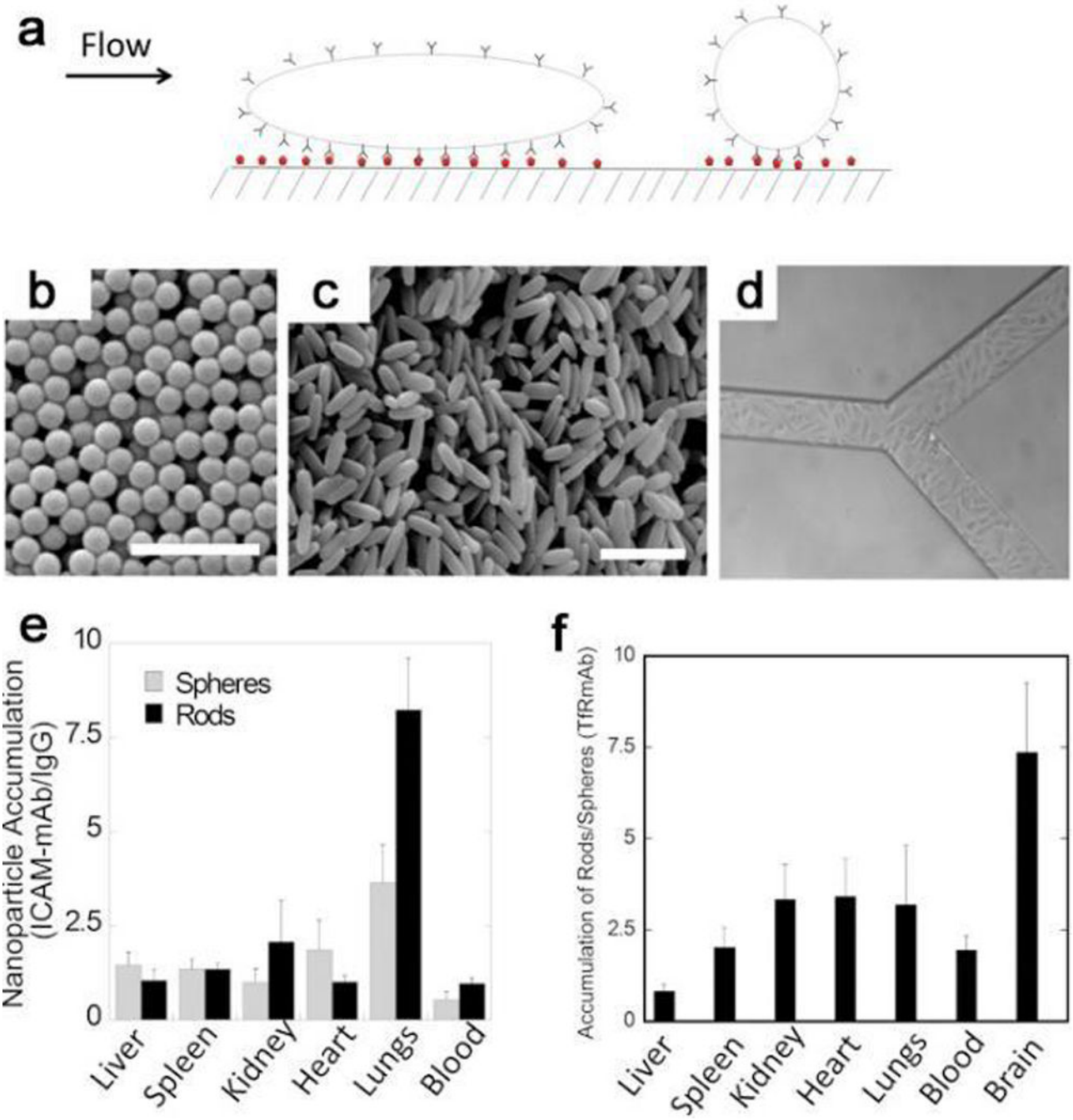

Figure 28.

Shape–effects on targeting and biodistribution of NPs under flow. (a) Schematic of NPs with different shapes interacting with a wall under flow. (b) SEM images of (b) polystyrene spheres and (c) elongated particles stretched from (a). Scale bar is 1 μm. (d) RBE4 cells-laden synthetic microvascular networks. Ratio of (e) ICAM-mAb–coated NPs to IgG–coated NPs for rods (in black) and spheres (in gray) and (f) TfR-mAb–coated rods to spheres (n = 3–5). Adapted with permission from ref 381, copyright 2013 National Academy of Sciences.

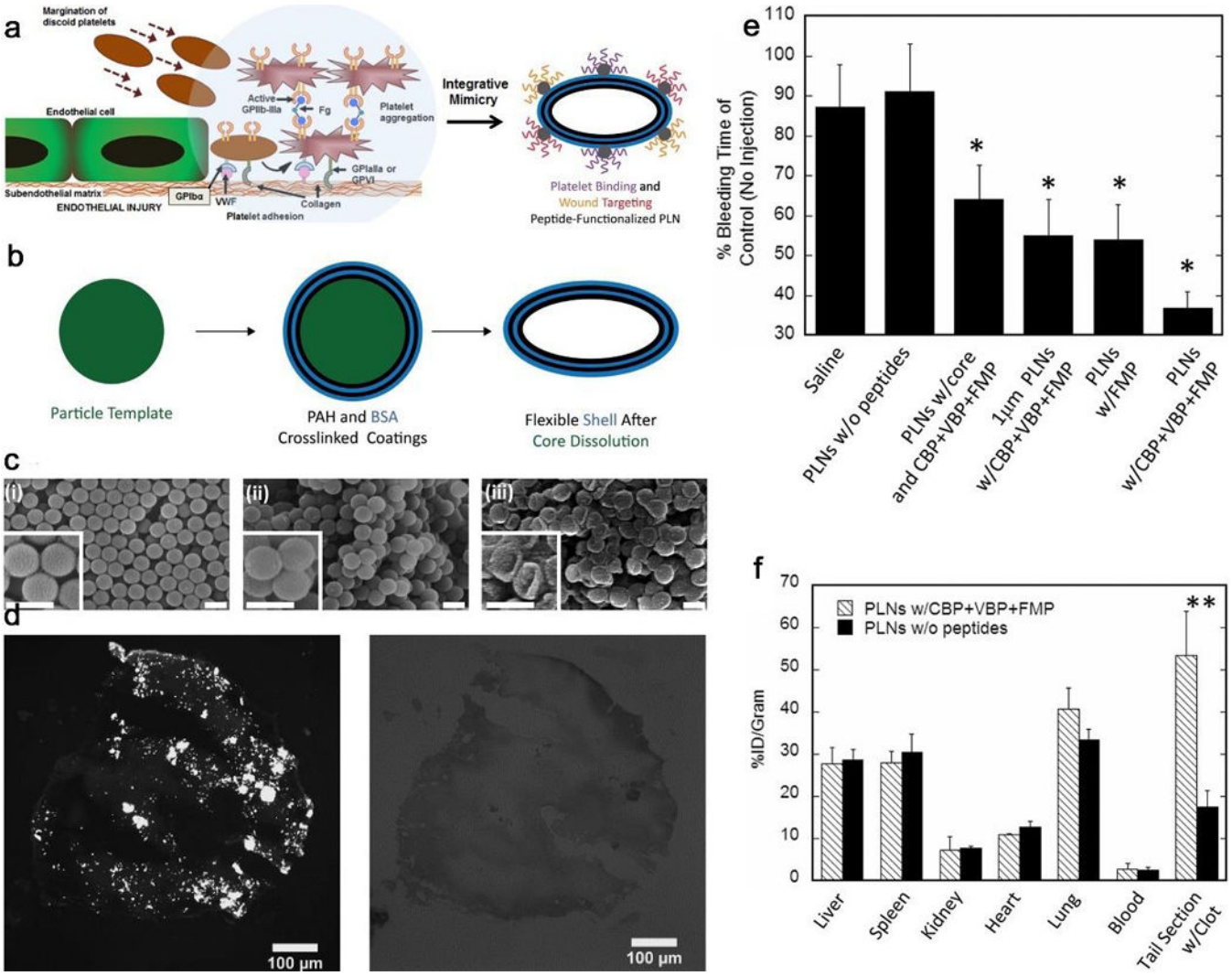

Figure 29.

(a) Schematic showing platelet interactions in hemostasis and corresponding platelet-inspired design. (b) Illustration of the platelet-like NPs (PLNs) synthesis to two bilayers of PAH/BSA. (c) SEM of (i) sacrificial 200 nm spherical and (ii) (PAH/BSA)4-coated polystyrene templates, (iii) final PLNs. Scale bar is 200 nm. (d) Brightfield and fluorescent images of tail section clot. (e) Hemostatic effect of PLNs in a tail amputation model in mice. (f) Biodistributions in organ with plain PLNs or PLNs functionalized with CBP+VBP+FMP at 1 h after tail amputation. Adapted with permission from ref 382, copyright 2014 American Chemical Society.

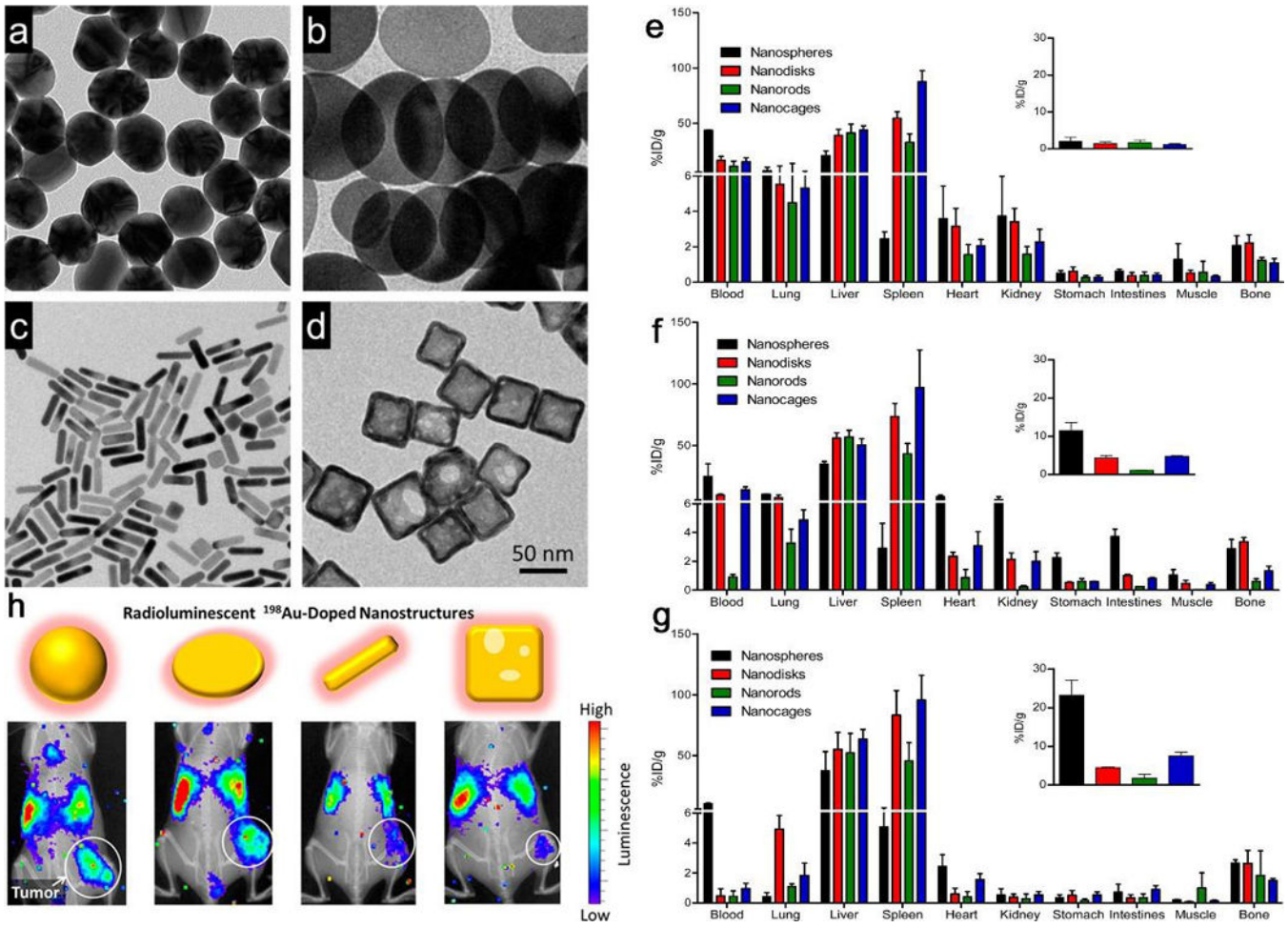

Figure 30.

TEM images of (a) nanospheres, (b) nanodisks, (c) nanorods, and (d) cubic nanocages Au NPs. The scale bar applies to all images. Biodistribution of the different types of ^{198}Au-doped Au NPs at (e) 1 h, (f) 6 h, and (g) 24 h after injection, insets are the tumor uptake data. (h) Co-registered X-ray and *in vivo* luminescence images of the tumor-bearing mice at 24 h post-injection of different types of ^{198}Au-incorporated NPs. From left to right is nanospheres, nanodisks, nanorods, and cubic nanocages, respectively. Reproduced with permission from ref 389, copyright 2014 American Chemical Society.